Personalized musculoskeletal modeling of the knee joint

Marco Antonio Marra

Personalized musculoskeletal modeling of the knee joint

Marco Antonio Marra

Design and layout
Marco A. Marra

Cover art
Wolfgang Claussen on Pixabay.com

Printing
Ipskamp Printing

ISBN
978-94-028-1436-1

Personalized musculoskeletal modeling
of the knee joint

Proefschrift ter verkrijging van de graad van doctor
aan de Radboud Universiteit Nijmegen
op gezag van de rector magnificus prof. dr. J.H.J.M. van Krieken,
volgens besluit van het college van decanen
in het openbaar te verdedigen op

dinsdag 16 april 2019
om 12:30 uur precies

door

Marco Antonio Marra

geboren op 13 juni 1989
te Galatina (Italië)

CONTENTS

Introduction

RESEARCH FRAMEWORK AND THE BIOMECHTOOLS PROJECT

After mental health disorders, musculoskeletal disorders are the second most common cause of disability worldwide[1]. The increasing demand for healthcare, along with the ageing and increasing obesity of the world's population, will increase the social and economic burden of musculoskeletal conditions in the near future. Therefore, current diagnostic methods need to be improved, and the costs of treatment need to be reduced.

The present research work was conducted within the project *BioMechTools* (Biomechanical diagnostic, pre-planning and outcome tools to improve musculoskeletal surgery) funded by the European Research Council under the European Union's Seventh Framework Programme (FP/2007-2013, Grant Agreement no. 323091 awarded to Prof. Dr. Ir. Nico Verdonschot). This project aims at generating versatile, accurate and objective methods to quantify the (pathological) musculoskeletal condition of the lower extremity, by consolidating innovations related to imaging, sensor technology and biomechanical modeling. The advanced tools produced in this project will allow clinicians and researchers to have detailed biomechanical information about abnormal tissue deformations, pathological loading of the joints, aberrant joint kinematics and abnormal stress and strain distributions within the hard and soft tissues. This platform will aid clinicians and researchers to improve the quality of patient care, and opens new research fields that address musculoskeletal pathologies with a strong biomechanical approach.

Typically, musculoskeletal diseases manifest through some sort of biomechanical dysfunction. Within the framework of this thesis, two distinct musculoskeletal conditions were addressed: total knee replacement (TKR), as the main treatment option for arthritis of the knee joint, and facioscapulohumeral muscular dystrophy (FSHD). Key objectives of the BioMechTools project that were specifically addressed in this thesis include: creation and validation of a new computational approach for personalized biomechanical modeling of the lower extremity, and demonstration of the clinical applicability of the personalized diagnostic and pre-planning platform.

Arthritis and total knee replacement

Arthritis encompasses many disorders of the joints, which cause pain and limitations in movement. Osteoarthritis and rheumatoid arthritis are the two most common forms of arthritis. Arthritis is highly prevalent, affecting more than 50 million adults in the United States aged 17 years and older. The incidence and prevalence of arthritis increase with age. Therefore, owing to the ageing of the worldwide population, arthritis has become the leading cause of disability in adults[2]. End-stage arthritis is effectively treated by joint replacement (or arthroplasty).

Total knee replacement (TKR) is a successful surgical treatment for end-stage arthritis of the knee joint. In TKR, the affected articulating surfaces of the knee joint are resurfaced and replaced by artificial implants, in order to relieve pain and restore function. In The Netherlands, 138 knee replacement surgeries per 100,000 population were performed in 2015, which is slightly above the worldwide average of 126 per 100,000 population[3]. Since 2000 the rate of TKRs has nearly doubled worldwide, and it has increased in the majority of the countries, in line with the ageing population. Recent projections see a net increase of TKR procedures, especially in the 80- and 90-year and older groups, which constitutes an important socio-economic burden[4].

Despite the fact that TKR is currently the best treatment option for end-stage arthritis, about 14% of TKR patients are dissatisfied[5]. Many factors play a role in the success of TKR, including patient variability and own expectations, surgeon expertise, and surgical technique. For the planning of surgical procedures, orthopedic surgeons have access to a set of diagnostic tools, such as X-ray, computed tomography (CT) and/or magnetic resonance images (MRI). These routine medical images provide only a static picture, such as the disease progression of arthritis, or the presence of joint deformities, and tell very little about joint function under dynamic loading conditions of daily activities. Furthermore, the current clinical assessment is highly subjective, as it involves manual procedures to assess joint laxity and range of motion. The pre-operative planning and surgery are also largely affected by personal experience and they are typically not targeted to patient-specific needs. Hence, in orthopedic surgery, there is a lack of diagnostic, pre-planning and outcome tools to more objectively quantify the status of musculoskeletal

conditions such as knee arthritis, and to aid in the formulation of more optimal and targeted treatments.

Facioscapulohumeral muscular dystrophy

Muscular dystrophies are a type of rare diseases, as they affect fewer than 5 people in 10,000 in Europe[6], to the detriment of muscle tissue. Their effects on patients' lives are devastating, which include a shorter life expectancy, profound disabilities in everyday activities, wheelchair dependency, and death. The etiology of many dystrophies is still scarcely understood and no cures are currently available.

Facioscapulohumeral muscular dystrophy (FSHD) is a type of muscular dystrophy characterized by an onset in the facial and shoulder girdle muscles, which then progresses to the trunk and leg muscles[7]. Its estimated prevalence is 12 per 100,000 population[8]. Common signs of all muscular dystrophies are a variable muscle fiber size, fiber death and fatty infiltration within the muscles. In FSHD, inflammation is also present. There is, currently, no definitive cure for muscular dystrophies[9].

The underlying cause of muscle weakness in FSHD is yet not completely known, though a thorough understanding of the mechanisms of weakness would be essential to pursue possible therapeutic interventions[10]. Image-based techniques and quantitative assessment of muscle strength are currently being investigated to characterize disease progression and its relation to muscles weakness[11]. Atrophy and fatty infiltration are typical signs in muscles of FSHD patients[12], and a reduction in contractile strength in type II FSHD muscle fibers is also found *in vitro*[10]. Although all these factors may contribute to muscle weakness *in vivo*, their individual contribution has not yet been fully elucidated. Specifically, it remains unclear whether the specific muscle strength (maximal force per unit area of contractile tissue) is reduced in muscles of patients with FSHD.

MODELING THE MUSCULOSKELETAL SYSTEM

Musculoskeletal models are mathematical representations of the musculoskeletal system, and represent a promising tool for the study of human movement and for the understanding of musculoskeletal

(patho-)physiology. Through musculoskeletal modeling and simulation, it is possible to obtain insights into joint loadings, muscle forces and coordination, which would otherwise be unpractical (and often impossible) to assess *in vivo* using experimental techniques. Musculoskeletal models have been used in a variety of fields, from ergonomics[13,14] and occupational health[15], to rehabilitation[16] and sports biomechanics[17,18], for both clinical applications and more fundamental research.

Key elements of any musculoskeletal models are: the segmental model representation, that is the arrangement and properties of the skeletal system parts (*segments*), and its actuation (muscles). Of these two elements, an overview is provided in Figure 1.1, according to the current state of the art. The skeletal and muscular representations form a coupled mechanical system that is described, mathematically, by governing equations, following from the laws of classical mechanics. In this thesis, the *multi-rigid-body system dynamics* (abbreviated as *multibody dynamics*) framework was used as a foundation for the biomechanical analysis of the musculoskeletal system, of which a general introduction is provided hereafter.

Segments, joints and degrees of freedom

In multibody dynamics models, the musculoskeletal system is subdivided into multiple segments, each of which assumed rigid (not deformable), linked together at the joints by means of kinematic constraint equations. In 3-dimensional (3-D) space, each segment introduces six unknowns, corresponding to the coordinates (three translations and three rotations) of the degrees of freedom (DoFs). Each joint subtracts from the system as many DoFs as kinematic constraint equations it introduces. Typically, models with a larger number of DoFs are also employed to describe more complex types of motion.

Each segment is characterized by its inertial properties (mass and inertia tensor) and a number of points describing the joints and muscles locations. Common types of joints used in musculoskeletal models are the idealized mechanical joints, such as the ball-and-socket (or spherical) joint and the hinged (or revolute) joint. A spherical joint is typically used to represent the hip joint, as it allows three rotations, and constrains all three translations. A revolute joint is commonly used for the knee and ankle joints, as it only allows
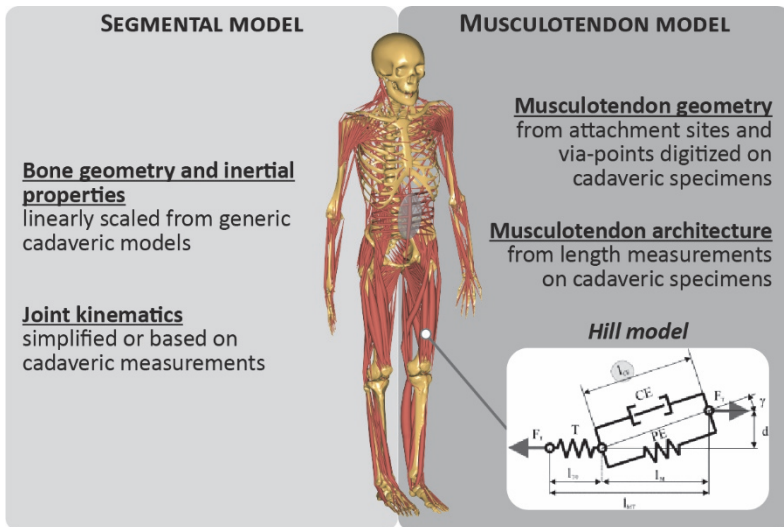
Figure 1.1 Aspects of musculoskeletal model generation according to the current state of the art. The segmental representation (bone geometry and inertial properties) is obtained by scaling existing cadaveric model datasets, and the joint kinematics are either simplified or prescribed based on measurements on cadavers (left panel). The musculotendon model is based on existing cadaveric model datasets and length measurements (right panel). Muscletendon units are represented using 3-element Hill muscle models, consisting of an active contractile element (CE) and a parallel elastic element (PE), in series with an elastic tendon element (T). The total length of the musculotendon unit, l_{MT}, is given by the sum of tendon length, l_T, and of muscle length, l_M. Because muscle fibers may, in general, not be aligned with the direction of the musculotendon unit as a whole, muscle length can be obtained from the actual muscle fiber length, l_{CE}, correcting it for the fiber pennation angle, γ.

a rotation about a fixed axis. Idealized joints may be a reasonable choice for studying the overall body-level motion coordination and net joint moments during gait. However, they also bring important simplifications to segmental motion, and whether these are acceptable or not must be assessed for each specific application. For instance, to study differences in the amount of femoral roll-back between two knee prosthetic designs, idealizing the knee joint as a hinge would be a poor modeling choice.

Multibody dynamics

Once a segmental and joint representation is established, multibody dynamics techniques can be used to solve the dynamics of the musculoskeletal system, that is simulating how the motion (kinematics) and forces (dynamics) evolve under specific conditions. From a mathematical point of view, a musculoskeletal model is a system of second-order differential equations, in coordinates of choice, relating the forces acting on the system to the motion (acceleration) of its DoFs, subject to constraint equations. For that reason, such equations are commonly referred to as *equations of motion*.

There are mainly two distinct approaches to solve for the dynamics of a musculoskeletal model: *direct* (or *forward*) *dynamics* and *inverse dynamics*. In forward dynamics, the motion of the segments is predicted based on known muscle forces and external forces. Because muscle forces are typically not known *a priori*, the input to forward-dynamics models can be in the form of muscle excitations (e.g., obtained from electromyography), so that muscle forces can be calculated as part of the solution process. The solution consists of integrating numerically the equations of motion twice, provided the relevant initial conditions, which can be computationally intensive. Alternatively, forward dynamics can also be used to track known input kinematics, which is also known as *forward dynamics assisted data tracking*[19]. This process involves a control system that varies the muscle excitations so that the desired kinematics are obtained. In this way, muscle forces and excitations are estimated.

In inverse dynamics, an inverse problem is solved: with knowledge of segmental kinematics (*effect*), the forces that *caused* that motion can be calculated, following the classic laws of dynamics. Typically, input is in the form of segmental positions and orientation, as well as external forces (e.g., foot-ground interactions). Muscle forces, as well as joint reactions are calculated as output. Inverse dynamics analyses do not require integration of the equations of motion, thus it is computationally less intensive, but requires the segmental accelerations, which can be obtained by differentiation of the position data (whenever accelerations were not available directly). Inverse dynamics can be combined with optimization techniques to find optimal combinations of forces and movements, according to some predefined performance criteria (*motion optimization*). This process requires iterations

through specified kinematic parameters until performance criteria are met, and can also be computationally very intensive.

Recently, a novel technique for the analysis of non-conforming joints was proposed, called *force-dependent kinematics* (FDK)[20,21]. Force-dependent kinematics enhances a traditional inverse dynamics analysis by circumventing the limitations of the idealized joint constraints. In FDK, 'small' motions in the joint are allowed and governed by the concomitant effects of muscle forces, ligament forces, and joint contact forces. This is possible under an assumption of quasi-static[1] equilibrium between the forces in the joint.

Musculotendon models

To account for the effect of musculotendon forces on joint loading and kinematics, and on the overall dynamics of the musculoskeletal system, muscles and tendons forces should also be accounted for in a musculoskeletal model. A widely used approach in multibody dynamics is to represent musculotendon units using 1-dimensional (1-D) lines between their origin and insertion sites on the bones. Possibly, these lines may be split into multiple bundles, to account for wide attachment areas, and their path may be further defined using via-points and wrapping objects, to account for specific musculotendon paths and to prevent bone penetration. Such a 1-D representation of muscles and tendons is relatively inexpensive, when compared to the computational cost of a fully 3-D representation[22], which remains currently prohibitive.

With regard to the force produced by musculotendon actuators, a widely adopted model is a phenomenological lumped-element model, originally proposed by Hill[23] and later extended by Zajac[24]. This model comprises three elements (Figure 1.1): one active element, representing the contractile part of the muscle, one passive element in parallel, representing the passive elasticity of muscle fibers and connective tissue, and one passive element in series, representing the elastic properties of the tendon. The force in the active

---

[1] In a quasi-static approximation, a simplified set of governing equations are solved, in which the time derivatives of the coordinates are neglected and assumed to be identically zero. Inertial effects are, thus, ignored and the system is thought as being in static equilibrium at each instant of time.

element depends on four parameters (peak isometric muscle force, optimal muscle-fiber length, optimal muscle-fiber pennation angle, and a scaling factor accounting for the maximum shortening velocity of the muscle). The force in the (passive) series elastic tendon element is controlled by another parameter (tendon slack length).

A complication of muscle-actuated models resides in the mathematical indeterminacy associated with the muscle recruitment problem: in other words, there are, in general, more unknown musculotendon forces than the system has equations. For such an indeterminate system, infinite solutions exist; namely, there are infinite combinations of muscle forces able to solve the equations of motion. To overcome this problem, the number of muscle actuators can be *reduced* to the number of available equations, which, however, oversimplifies the musculotendon representation[25]. Alternatively, the muscle redundancy can be addressed by posing an *optimization* problem, which leads to a unique combination of muscle forces. This approach is often referred to as *static optimization*, meaning that an optimization problem is solved independently at each time instant, in contrast to *dynamic optimization*, where the current state of the musculoskeletal system also depends on previous ones, and a solution for the motion must be found implicitly. In static optimization, a cost function depending on all muscle forces is minimized according to some assumed optimality criteria (e.g., minimum energy, minimum stress, minimum fatigue). The underlying idea of minimizing a cost function attempts to capture the goal of our central nervous system when it recruits motor units in muscles. From a strictly mathematical point of view, every combination of muscle forces that solves the optimization problem is admissible. However, different criteria may result in more or less physiological distributions of muscle forces[26], and it is the modeler's responsibility to make appropriate choices based on the goals of the simulation.

Model validation

One very important aspect of any model is validation, that is assessing whether model predictions conform to experimental measurements from the physical reality. In musculotendon-actuated musculoskeletal models, typical output variables are muscle and joint reaction forces estimated during real-life movements. Therefore, an ideal validation process would seek to validate

these variables against experimental measurements of the same physical quantities (*direct* validation)[27].

In the case of muscle forces, this approach becomes unfeasible, as there are no direct means of measuring muscle forces *in vivo*. An alternative is provided by electromyography (EMG), which records the electrical signal coming from the muscles, and can provide a means for *indirect* validation. However, muscle forces and EMG signals represent different physical quantities, and the comparison is further complicated by their highly nonlinear relationship during dynamic measurements[27]. Unless musculoskeletal models are developed that can also predict the EMG signal[28], the applicability of EMG for validation purposes remains limited.

An interesting opportunity for direct validation is provided by experimental measurements of *in vivo* joint contact forces in patients fitted with force-sensing telemetric prostheses during activities of daily living[29–33]. Experimental measurements obtained with such prostheses were made freely available to the research community in the form of open-access datasets, and gave rise to initiatives such as *Orthoload*[34] and the *Grand challenge competition to predict in vivo knee loads*[29], which incentivized and stimulated the musculoskeletal research community to validate musculoskeletal models for the prediction of TKR joint mechanics.

MUSCULOSKELETAL MODELS FOR THE STUDY OF TKR MECHANICS

The study of knee mechanics in TKR has been pursued using both experimental and theoretical approaches. The former rely on experimental techniques, such as telemetry, fluoroscopy, CT, MRI, and motion analysis, whereas the latter involve mathematical models of various complexity. Mathematical approaches and, particularly, musculoskeletal models are very interesting because of their predictive capabilities. For instance, by using a musculoskeletal model of TKR, one could predict changes in knee loads and kinematics due to changes in implant design, alignment and/or patient anatomy.

Previous recent models of TKR utilized a variety of mathematical approaches. The finite-element (FE) method was employed for the study of articular

contact pressure distribution and contact area[35–37]. Rigid body spring contact models were used to estimate knee contact forces during gait[38,39]. In combination with rigid multibody dynamics, elastic-foundation (EF) models[40,41] and nonlinear contact models with viscous damping[42–44] were employed to solve for contact mechanics during the analysis of several activities, or applied for the study of polyethylene wear[45]. Surrogate modeling techniques were also proposed to accelerate the computation of contact mechanics[46–48].

Unlike deformable FE models, EF models estimate contact forces based on the interpenetration between the contacting bodies and the definition of a pressure-overclosure relationship[49]. In general, EF models have shown excellent kinematic agreement with more computationally expensive deformable FE models, and overall good estimations of contact area and pressure distribution[50,51]. Whilst FE models are the standard *de facto* for accurate computational dynamics analyses, EF models are much more efficient, as they enable dynamic simulations of joint mechanics within minutes, rather than hours[50]. For these reasons, EF models are well suited for repeated dynamic analyses, parametric and optimization studies.

AIMS AND OUTLINE OF THE THESIS

This thesis aims at a) developing and validating a computational framework for personalized musculoskeletal modeling that allows the estimation of internal knee loads and kinematics; b) proving the feasibility of addressing sagittal alignment positioning problems in TKR by means of personalized musculoskeletal modeling; and c) investigating whether specific muscle strength is reduced in FSHD patients compared to healthy controls using image-based musculoskeletal models. These aims are reflected by the chapter subdivision of the present thesis, which is articulated as follows:

Development of a personalized and efficient musculoskeletal modeling framework

In Chapter 2, a personalized musculoskeletal modeling framework for the analysis of knee biomechanics of TKR is presented, along with its validation. The presented methodology enables kinematic analysis, based on *in vivo* measurements, and allows concurrent estimation of muscle forces, joint

contact forces, ligament forces, and tibiofemoral and patellofemoral kinematics.

Chapter 3 proposes a solution to accelerate the calculation of joint contact forces in the TKR model presented in Chapter 2, based on surrogate modeling techniques. The gain in terms of computational efficiency is discussed and the accuracy is evaluated in the context of analysis of activities of daily living with simultaneous estimation of muscle, ligament and joint contact forces and kinematics.

Feasibility of personalized musculoskeletal models to address clinically relevant research questions

In Chapter 4, the sagittal alignment of the tibial component in cruciate-retaining (CR) TKR is investigated. The patient-specific musculoskeletal model presented in Chapter 2 is used to analyze the effect of variations of tibial slope on knee biomechanics and related surgical techniques. The results of the analysis are discussed in the context of surgical choices in TKR.

Chapter 5, focuses on the sagittal alignment of the femoral component in CR-TKR, and shows how the size and flexion of the femoral component can be optimized in CR-TKR to provide a good biomechanical reconstruction of the knee extensor mechanism.

Chapter 6 investigates causes of muscle weakness in FSHD and elucidates whether specific muscle strength is lower in FSHD patients than in healthy controls. A multidisciplinary approach is used, combining medical imaging and image processing, muscle strength assessment, and musculoskeletal modeling.

General discussion

Chapter 7 provides a general discussion about the main findings and topics presented in this thesis. It reflects on the potentials of personalized musculoskeletal modeling as a tool to improve the diagnosis and treatment of musculoskeletal conditions, and outlines weaknesses and remaining problems that need to be addressed in future research.

REFERENCES

1. Vos, T. *et al.* Years lived with disability (YLDs) for 1160 sequelae of 289 diseases and injuries 1990-2010: A systematic analysis for the Global Burden of Disease Study 2010. *Lancet* **380**, 2163–2196 (2012).

2. Ma, V. Y., Chan, L. & Carruthers, K. J. Incidence, prevalence, costs, and impact on disability of common conditions requiring rehabilitation in the United States: stroke, spinal cord injury, traumatic brain injury, multiple sclerosis, osteoarthritis, rheumatoid arthritis, limb loss, and back pa. *Arch. Phys. Med. Rehabil.* **95**, 986–995.e1 (2014).

3. OECD. Hip and knee replacement. in *Health at a Glance 2017: OECD Indicators* 178–179 (OECD Publishing, 2017). doi:10.1787/health_glance-2017-65-en

4. Hitzl, W., Sattler, M., Eckstein, F. & Cotofana, S. The projected numbers of total knee replacement in Austria – from 2010 to 2075. *Osteoarthr. Cartil.* **22**, S216–S217 (2014).

5. Noble, P. C., Conditt, M. A., Cook, K. F. & Mathis, K. B. The John Insall Award: Patient Expectations Affect Satisfaction with Total Knee Arthroplasty. *Clin. Orthop. Relat. Res.* **452**, 35–43 (2006).

6. Humphreys, G. Coming together to combat rare diseases. *Bulletin of the World Health Organization* **90**, 406–407 (2012).

7. Mul, K. *et al.* What's in a name? The clinical features of facioscapulohumeral muscular dystrophy. *Pract. Neurol.* **16**, 201–207 (2016).

8. Deenen, J. C. W. *et al.* Population-based incidence and prevalence of facioscapulohumeral dystrophy. *Neurology* **83**, 1056–9 (2014).

9. Emery, A. E. H. The muscular dystrophies. *Lancet (London, England)* **359**, 687–95 (2002).

10. Lassche, S. *et al.* Sarcomeric dysfunction contributes to muscle weakness in facioscapulohumeral muscular dystrophy. *Neurology* **80**, 733–7 (2013).

11. Kan, H. E. *et al.* Quantitative MR imaging of individual muscle involvement in facioscapulohumeral muscular dystrophy. *Neuromuscul. Disord.* **19**, 357–62 (2009).

12. Janssen, B. H. *et al.* Distinct disease phases in muscles of facioscapulohumeral dystrophy patients identified by MR detected fat infiltration. *PLoS One* **9**, e85416 (2014).

13. Grujicic, M. *et al.* Musculoskeletal computational analysis of the influence of car-seat design/adjustments on long-distance driving fatigue. *Int. J. Ind. Ergon.* **40**, 345–355 (2010).

14. Rasmussen, J., Tørholm, S. & de Zee, M. Computational analysis of the influence of seat pan inclination and friction on muscle activity and spinal joint forces. *Int. J. Ind. Ergon.* **39**, 52–57 (2009).

15. Mirakhorlo, M., Azghani, M. R. & Kahrizi, S. Validation of a musculoskeletal model of lifting and its application for biomechanical evaluation of lifting techniques. *J. Res. Health Sci.* **14**, 23–8 (2014).

16. Shelburne, K. B. & Pandy, M. G. Determinants of cruciate-ligament loading during rehabilitation exercise. *Clin. Biomech.* **13**, 403–413 (1998).

17.   Ali, N., Andersen, M. S., Rasmussen, J., Robertson, D. G. E. & Rouhi, G. The application of musculoskeletal modeling to investigate gender bias in non-contact ACL injury rate during single-leg landings. *Comput. Methods Biomech. Biomed. Engin.* **17**, 1602–16 (2014).

18.   Farahani, S. D., Bertucci, W., Andersen, M. S., Zee, M. De & Rasmussen, J. Prediction of crank torque and pedal angle profiles during pedaling movements by biomechanical optimization. *Struct. Multidiscip. Optim.* (2014). doi:10.1007/s00158-014-1135-6

19.   Erdemir, A., McLean, S., Herzog, W. & van den Bogert, A. J. Model-based estimation of muscle forces exerted during movements. *Clin. Biomech. (Bristol, Avon)* **22**, 131–54 (2007).

20.   Andersen, M. S., Damsgaard, M. & Rasmussen, J. Force-dependent kinematics: a new analysis method for non-conforming joints. in *XIII International Symposium on Computer Simulation in Biomechanics* (2011).

21.   Skipper Andersen, M., de Zee, M., Damsgaard, M., Nolte, D. & Rasmussen, J. Introduction to Force-Dependent Kinematics: Theory and Application to Mandible Modeling. *J. Biomech. Eng.* **139**, 091001 (2017).

22.   Webb, J. D., Blemker, S. S. & Delp, S. L. 3D finite element models of shoulder muscles for computing lines of actions and moment arms. *Comput. Methods Biomech. Biomed. Engin.* **17**, 829–37 (2014).

23.   Hill, a. V. The Heat of Shortening and the Dynamic Constants of Muscle. *Proc. R. Soc. B Biol. Sci.* **126**, 136–195 (1938).

24.   Zajac, F. E. Muscle and tendon: properties, models, scaling, and application to biomechanics and motor control. *Crit. Rev. Biomed. Eng.* **17**, 359–411 (1989).

25.   Schipplein, O. D. & Andriacchi, T. P. Interaction between active and passive knee stabilizers during level walking. *J. Orthop. Res.* **9**, 113–119 (1991).

26.   Rasmussen, J., Damsgaard, M. & Voigt, M. Muscle recruitment by the min/max criterion — a comparative numerical study. *J. Biomech.* **34**, 409–415 (2001).

27.   Lund, M. E., de Zee, M., Andersen, M. S. & Rasmussen, J. On validation of multibody musculoskeletal models. *Proc. Inst. Mech. Eng. H.* **226**, 82–94 (2012).

28.   Mordhorst, M., Heidlauf, T. & Röhrle, O. Predicting electromyographic signals under realistic conditions using a multiscale chemo–electro–mechanical finite element model. *Interface Focus* **5**, 20140076 (2015).

29.   Fregly, B. J. *et al.* Grand challenge competition to predict in vivo knee loads. *J. Orthop. Res.* **30**, 503–13 (2012).

30.   Bergmann, G. *et al.* In vivo glenohumeral contact forces-Measurements in the first patient 7 months postoperatively. *J. Biomech.* **40**, 2139–2149 (2007).

31.   Kutzner, I. *et al.* Loading of the knee joint during activities of daily living measured in vivo in five subjects. *J. Biomech.* **43**, 2164–2173 (2010).

32.   Heinlein, B. *et al.* ESB clinical biomechanics award 2008: Complete data of total knee replacement loading for level walking and stair climbing measured in vivo with a follow-up of 6-10 months. *Clin. Biomech.* **24**, 315–326 (2009).

33.   D'Lima, D. D., Patil, S., Steklov, N., Slamin, J. E. & Colwell, C. W. Tibial forces measured in vivo after total knee arthroplasty. *J. Arthroplasty* **21**, 255–262 (2006).

34.   Bergmann, G. Orthoload.com. *Charité Universitaetsmedizin Berlin* (2008). Available at: http://www.orthoload.com/?page_id=7. (Accessed: 25th January 2018)

35.   Halloran, J. P., Petrella, A. J. & Rullkoetter, P. J. Explicit finite element modeling of total knee replacement mechanics. *J. Biomech.* **38**, 323–31 (2005).

36.   Heegaard, J. H., Leyvraz, P. F. & Hovey, C. B. A computer model to simulate patellar biomechanics following total knee replacement: the effects of femoral component alignment. *Clin. Biomech. (Bristol, Avon)* **16**, 415–23 (2001).

37.   Godest, a C., Beaugonin, M., Haug, E., Taylor, M. & Gregson, P. J. Simulation of a knee joint replacement during a gait cycle using explicit finite element analysis. **35**, 267–275 (2002).

38.   Piazza, S. J. & Delp, S. L. Three-dimensional dynamic simulation of total knee replacement motion during a step-up task. *J. Biomech. Eng.* **123**, 599–606 (2001).

39.   Hast, M. W. & Piazza, S. J. Dual-joint modeling for estimation of total knee replacement contact forces during locomotion. *J. Biomech. Eng.* **135**, 021013 (2013).

40.   Bei, Y. & Fregly, B. J. Multibody dynamic simulation of knee contact mechanics. *Med. Eng. Phys.* **26**, 777–89 (2004).

41.   Thelen, D. G., Won Choi, K. & Schmitz, A. M. Co-simulation of neuromuscular dynamics and knee mechanics during human walking. *J. Biomech. Eng.* **136**, 021033 (2014).

42.   Kia, M., Stylianou, A. P. & Guess, T. M. Evaluation of a musculoskeletal model with prosthetic knee through six experimental gait trials. *Med. Eng. Phys.* **36**, 335–44 (2014).

43.   Guess, T. M., Stylianou, A. P. & Kia, M. Concurrent prediction of muscle and tibiofemoral contact forces during treadmill gait. *J. Biomech. Eng.* **136**, 021032 (2014).

44.   Stylianou, A. P., Guess, T. M. & Kia, M. Multibody muscle driven model of an instrumented prosthetic knee during squat and toe rise motions. *J. Biomech. Eng.* **135**, 041008 (2013).

45.   Fregly, B. J., Sawyer, W. G., Harman, M. K. & Banks, S. A. Computational wear prediction of a total knee replacement from in vivo kinematics. *J. Biomech.* **38**, 305–14 (2005).

46.   Lin, Y.-C., Walter, J. P., Banks, S. A., Pandy, M. G. & Fregly, B. J. Simultaneous prediction of muscle and contact forces in the knee during gait. *J. Biomech.* **43**, 945–52 (2010).

47.   Lin, Y.-C., Haftka, R. T., Queipo, N. V & Fregly, B. J. Surrogate articular contact models for computationally efficient multibody dynamic simulations. *Med. Eng. Phys.* **32**, 584–94 (2010).

48.   Eskinazi, I. & Fregly, B. J. Surrogate modeling of deformable joint contact using artificial neural networks. *Med. Eng. Phys.* **37**, 885–91 (2015).

49.   Blankevoort, L., Kuiper, J. H., Huiskes, R. & Grootenboer, H. J. Articular contact in a three-dimensional model of the knee. *J. Biomech.* **24**, 1019–31 (1991).

50.   Halloran, J. P., Easley, S. K., Petrella, A. J. & Rullkoetter, P. J. Comparison of Deformable and Elastic Foundation Finite Element Simulations for Predicting Knee Replacement Mechanics. *J. Biomech. Eng.* **127**, 813 (2005).

51.   Pérez-González, A. *et al.* A modified elastic foundation contact model for application in 3D models of the prosthetic knee. *Med. Eng. Phys.* **30**, 387–398 (2008).

Chapter 2

A subject-specific musculoskeletal modeling framework to predict *in vivo* mechanics of total knee arthroplasty

Marco A. Marra, Valentine Vanheule, René Fluit, Bart F.J.M. Koopman, John Rasmussen, Nico Verdonschot, and Michael S. Andersen.

ABSTRACT

Musculoskeletal (MS) models should be able to integrate patient-specific MS architecture and undergo thorough validation prior to their introduction into clinical practice. We present a methodology to develop subject-specific models able to simultaneously predict muscle, ligament, and knee joint contact forces along with secondary knee kinematics. The MS architecture of a generic cadaver-based model was scaled using an advanced morphing technique to the subject-specific morphology of a patient implanted with an instrumented total knee arthroplasty available in the fifth "Grand Challenge Competition to Predict In Vivo Knee Loads" dataset. We implemented two separate knee models, one employing traditional hinge constraints, which was solved using an inverse dynamics technique, and one using an 11-degree-of-freedom representation of the tibio-femoral (TF) and patello-femoral (PF) joints, which was solved using a combined inverse dynamic and quasi-static analysis, called Force Dependent Kinematics (FDK). Tibio-femoral joint forces for one gait and one right-turn trial, and secondary knee kinematics for one unloaded leg-swing trial were predicted and evaluated using experimental data available in the Grand Challenge dataset. Total compressive TF contact forces were predicted by both hinge and FDK knee models with a root-mean-square error (RMSE) and a coefficient of determination (R^2) smaller than 0.3 BW and equal to 0.9 in the gait trial simulation, and smaller than 0.4 BW and larger than 0.8 in the right-turn trial simulation, respectively. Total, medial and lateral TF joint contact force predictions were highly similar, regardless of the type of knee model used. Medial (respectively lateral) TF forces were over- (respectively under-) predicted with a magnitude error of M < 0.2 (respectively > -0.4) in the gait trial, and under- (respectively over-) predicted with a magnitude error of M > -0.4 (respectively < 0.3). Secondary knee kinematics from the unloaded leg-swing trial were overall better approximated using the FDK model (average Sprague and Geers' combined error C = 0.06) than when using a hinged knee model (C = 0.34). The proposed modeling approach allows detailed subject-specific scaling and personalization, and does not contain any non-physiological parameters. This modeling framework has potential applications in aiding the clinical decision-making in orthopedics procedures, and as a tool for virtual implant design.

INTRODUCTION

Movements and loads of musculoskeletal (MS) systems are governed by complex interactions between the forces of muscles, ligaments, bones and a variety of other soft tissues, and the surrounding environment. Muscle, ligament, and joint contact forces acting within the body are, however, very difficult to measure *in vivo* since invasive procedures would be required. A number of studies on patients with instrumented prostheses have recently made available internal joint load measurements *in vivo*[1–4]. In a few cases, such procedures led to the release of extensive databases containing joint forces recorded *in vivo* in patients who received a telemetric prosthesis[5,6]. Remarkable examples of such procedures are the OrthoLoad project[7], providing hip, shoulder, knee, vertebral body and spine fixator forces of implanted patients, and the "Grand Challenge Competition to Predict *in Vivo* Knee Loads"[8], based on the most comprehensive dataset currently available for subjects implanted with a telemetric total knee arthroplasty (TKA). The experimental material provided by these initiatives has stimulated the MS modeling community to improve the clinical utility of their computational models through extensive validation. Unfortunately, such valuable data are only available for a limited number of selected patients, and provide insight into the functioning of a particular type of prosthesis under specific conditions.

Although these datasets provide highly valuable information, they do not include any information on forces generated by the muscles or transmitted through the ligaments. Knowledge of muscle, ligament, and joint contact forces would be highly beneficial from a clinical perspective, but their direct measurement is not feasible in a clinical setting and patients with an instrumented prosthesis are rare. Predictive capabilities of computational MS models are, therefore, being considered to gain dynamic and objective information on the condition of individual patients[9]. This in turn would aid the formulation of quantitative and patient-specific indications for an optimal treatment[10–15]. Such an approach can potentially overcome the limitations of current practice, in which treatments are based on subjective, static and mostly qualitative assessment[8]. Although MS models have been extensively used in many fields including ergonomics[16,17], occupational health[18], gait analysis and training[19], evaluation of prosthetic design[20–22], the lack of proper

validation has delayed the introduction of MS models into clinical practice[23]. Muscle, ligament and joint forces are generally the outputs of a MS model and a common practice is to evaluate model-predicted muscle activities using surface electromyographic (EMG) signals recorded from the main muscles, as an indirect validation of muscle forces[9]. However, this approach proves unsuccessful for validating dynamic tasks, in which the relationship between individual muscle forces and their EMG signals is complex[24,25]. On the other hand, muscle forces are the main determinants of internal joint forces[26], so if the latter are being predicted correctly, it is likely that muscle force predictions are also reasonably accurate.

A few works appeared in the recent literature that dealt with prediction of knee joint mechanics and evaluation of musculoskeletal model predictions using experimental data. Thelen et al. developed a modeling framework for the concurrent simulation of body-level dynamics and joint mechanics during gait[27]. Their method was based on forward-dynamics coupled with computed muscle control (CMC), and could predict muscle activations and tibiofemoral (TF) forces in an elastic foundation model of TKA. Guess et al. employed a similar approach to study the knee joint mechanics during gait using a 12-degree of freedom (DOF) knee model with deformable contact for the estimation of TF forces during treadmill and normal gait[28,29]. Both models used proportional-integrative-derivative (PID) feedback control gains to calculate muscle forces. Although these PID gains were modulated by the physiological cross sectional area (PCSA) of each muscle, global gain values still needed to be set, for which no physiological tuning was available. A sensitivity analysis on the effect of the global control gains was performed by Guess et al. and more accurate predictions were reported for smaller values of these gains[28]. Hast and Piazza proposed a "dual-joint" modeling approach consisting of an idealized knee joint-based inverse dynamics analysis for the estimation of muscle forces, followed by a forward dynamics analysis using a 12-DOF knee model with which contact forces were predicted using a rigid-body spring contact model[30]. Despite the complexity of their model, no effort was made to scale the MS architecture to the patient. The reader is referred to the review paper by Erdemir et al. for an extensive review on MS modeling and optimization techniques for estimation of muscle forces *in vivo*[9].

Andersen and Rasmussen have proposed an enhanced inverse dynamics-like approach, called Force-Dependent Kinematics (FDK), which simultaneously

computes the internal forces and secondary joint kinematics[31]. This is accomplished by assuming that the secondary knee DOFs are not influenced by the global model dynamics, and can, therefore, be solved assuming quasi-static equilibrium between ligament, muscle, and contact forces and external loads. Hence, the application of this FDK technique enables the simulation of the knee joint mechanics in a much more realistic manner than simulating the knee joint with idealized constraints.

Accurate representation of the MS model architecture is also essential for obtaining reliable subject-specific model predictions[32,33]. New advanced scaling techniques, such as morphing, have emerged that allow better scaling of MS models to the subject-specific anatomy than techniques based on linear scaling laws[34,35]. However, none of the recent MS modeling methodologies have made an effort to integrate a subject-specific anatomical representation of the MS architecture together with a detailed representation of the knee joint.

The specific aims of the present study, hence, are: (a) to develop a musculoskeletal modeling framework based on subject-specific CT images, motion capture data, and force plate data that is capable of estimating *in vivo* ligament and muscle forces, TF contact forces and knee joint kinematics; (b) to evaluate the validity of the tibiofemoral joint force and secondary knee kinematic predictions based on the experimental data available in the fifth Grand Challenge Competition dataset; (c) to assess the influence of knee modeling approach (idealized hinge *versus* FDK representation) on the knee model on the predicted outcome variables.

MATERIALS AND METHODS

Experimental data

The data used in this study were part of the fifth "Grand Challenge" dataset for the 7th World Congress of Biomechanics (July 6-11 2014, Boston, Massachusetts)[8], publicly accessible at https://simtk.org/home/kneeloads. The data were obtained from one male subject (age 86, height 180 cm, body weight 75 kg) who received a posterior cruciate-retaining (PCR) total knee replacement (TKR) of his left knee. The tibial implant, a Generation II tray design (eTibia), was equipped with a telemetric force-measuring sensor that

measured the six load components transferred through the prosthesis[6,36]. The competition data included eTibia loads, trajectories of motion capture markers, force plate data, electromyography (EMG) for a series of gait trials, joint calibration trials and fluoroscopy trials, and pre- and post-operative computed tomography (CT) data. Geometric stereolithography (STL) 3-D geometries of the prostheses were provided for the femoral component, tibial tray and insert, patellar button, along with post-operative bone geometries of partial pelvis, femur, patella, tibia, fibula, partial talus and partial calcaneus.

Musculoskeletal model

Full-body model

A subject-specific musculoskeletal model was developed using the AnyBody Modelling System (AMS) v. 6.0.2 (Anybody Technology A/S, Aalborg, Denmark), a software for the simulation and analysis of the musculoskeletal system[37]. The generic human body model from the AnyBody Managed Model Repository (AMMR) v. 1.6 was the basis for the subsequent personalization with the subject-specific data. It comprises head, two arms, trunk, pelvis and two legs. The leg model was updated to the newly collected Twente Lower Extremity Model v. 2.0 (TLEM 2.0) dataset[38] based on clinical images, and comprises thigh, shank, patella, talus and foot segments, together with coordinates of all muscle attachments and wrapping shapes. Segments were connected to each other by means of hinge joints at the neck, ankle, subtalar, TF and patellofemoral (PF) joints, and by means of spherical joints at the glenohumeral and hip joint, and between the vertebrae of the lumber spine in addition to a spinal rhythm that leaves three DOFs between pelvis and thorax. A more complex representation of the TF and PF joints was also used in this study, in which the constraints of the hinge joints were released, leaving additional DOFs to be controlled. We will describe this in more detail in the following sections. Fifty-five muscle-tendon (MT) units were represented using 166 Hill-type one-dimensional string elements spanning from origin to insertion through via-points, and wrapping over analytical surfaces fitted to the bone geometries.
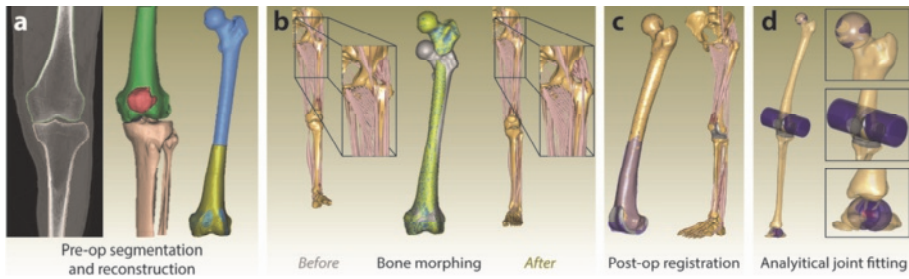
Figure 2.1 Steps for obtaining a subject-specific MS model. (a) Pre-operative bone segmentation from CT images. Partial bones were merged with post-operative bone geometries to generate complete 3-D pre-operative bone models; (b) morphing of the generic TLEM 2.0 bone meshes to the patient-specific pre-operative bones (note the variation in muscle insertion sites); (c) registration of post-operative bone geometries to the morphed pre-operative bones; (d) analytical joint fitting of post-operative bone geometries to obtain patient-specific hip joint center, tibiofemoral, patellofemoral, ankle and subtalar joint axes.

Model scaling

To scale the TLEM 2.0 generic model to the subject-specific bone geometries, we segmented the subject's pre-operative bone CT images in Mimics v. 14 (Materialise NV, Leuven, Belgium), and 3-D bone geometries were exported in the STL format (Figure 2.1a). Only the distal femur and proximal tibia-fibula were available in the pre-operative CT images. Thus, these partial 3-D bone models were combined with post-operative full-leg 3-D bone models provided in the dataset to obtain complete pre-operative bone models. An advanced morphing method, based on the 3-D reconstruction system of Redert et al.[34], developed by Materialise NV (Leuven, Belgium) and evaluated by Pellikaan et al.[35], morphed the topology of the TLEM 2.0 atlas bones to the corresponding subject-specific pre-operative bones (Figure 2.1b). These morphed bone meshes were used to scale the muscle attachment sites defined on the given segment using a Radial Basis Function (RBF) interpolation scheme: firstly, an affine transformation was defined to roughly scale the original TLEM 2.0 generic bone (source) to the subject-specifically morphed TLEM 2.0 bone (target) based on selected bony landmarks; secondly, a tri-harmonic RBF scaling function was defined based on the vertices of the above affine-transformed TLEM 2.0 bone geometry and the subject-specifically morphed TLEM 2.0 bone geometry using the available facility in the AMS. To avoid the poor extrapolation properties of RBF functions, corners of a bounding box

defined around each bone were included in the mapping. Finally, a reverse rigid-body transformation was defined based on the previously used bony landmarks to bring the morphed musculoskeletal geometry back from the CT reference frame to the body model reference frame in the AMS. Geometry-based morphing was impossible for the talus due to an incomplete CT scan. Therefore, talus was morphed with an affine transformation based on selected bony landmarks only. After morphing, the post-operative geometry files, including the prosthesis, were aligned with the pre-operative geometries using a rigid-body registration (Figure 2.1c) to provide the subject-specific post-operative geometrical model.

To obtain accurate joint centers and axes, we performed analytical surface fits on the post-operative bones (Figure 2.1d): the hip joint center was determined through a spherical fit to the femoral head, the tibiofemoral and patellofemoral joint axes by fitting two different cylindrical surfaces around the femoral component, and the talocrural joint axis by fitting two spherical surfaces to talus[39].

Since the CT scan did not include all bones in the model, a different approach had to be taken for the scaling of the remaining segments. For the bones morphed above, we assumed symmetry between the left and right legs. To scale the length of the remaining upper body segments, the pelvic bone width and the foot lengths, a nonlinear least-square optimization problem was defined using a linear segment scaling law[40]. This optimization problem minimized the difference between model markers and experimentally recorded marker positions during one frame of a standing reference trial (PS_staticfor2), using the method of Andersen et al.[41], while enforcing the idealized joint constraints. Skin markers placed directly on bony landmarks and the shoe of the subject were manually placed on the musculoskeletal model at the estimated corresponding locations. After the optimization of the segment lengths, the local coordinates of all markers in clusters placed on the thigh and shank were computed in the segment reference frames and saved in files together with the optimal segment lengths for later use.

Muscle model and strength scaling

Muscle dynamics was defined by three-element Hill type models as proposed by Zajac[42]. Each muscle-tendon unit in the TLEM 2.0 dataset was assigned an isometric muscle strength, F_o, calculated by multiplying the PCSA by a factor

of 27 N/cm². The PCSA was derived from a cadaver-based muscle volume divided by the optimum fiber length. Force-length and force-velocity relations were included in the definition of muscle strength to account for the length- and velocity-dependent effect on the instantaneous muscle strength. Tendon slack lengths were calibrated using dedicated calibration routines included in the TLEM 2.0 leg model.

A length-mass scaling approach was employed to scale the muscle strength of the standard TLEM 2.0 model to the specific subject of interest, using a method originally proposed by Rasmussen et al.[40]. Specifically, the isometric muscle strength of each muscle unit was scaled using segment-specific strength scaling factors based on the length and mass of the segment relative to the generic TLEM 2.0 model.

A reduced strength of the flexor/extensor muscles has been reported for patients who undergo TKA[43], which could be quantified in a 31% reduction of the isometric flexion/extension peak torque, on average, but with reductions of up to 40% at low flexion angles. Consequently, all muscles involved in flexion/extension in the model were affected by a reduction of 35% of their nominal PCSA and, hence, their strength. Ideally, the subject-specific muscle strength should have been scaled based on direct measurement of lower extremity maximal joint torques. Unfortunately, the strength reductions applied could not be verified as strength measurements were not available for this subject.

Muscle recruitment problem

The muscle recruitment problem was solved by minimizing a polynomial cost function G (Eq. 3a), subject to the equilibrium equations (Eq. 3b) and to the constraint that muscles can only pull and cannot generate a force larger than the instantaneous strength (Eq. 3c), as previously described[44]. In the TLEM 2.0, muscles with a wide origin/insertion area were split into multiple branches. However, as shown by Holmberg and Klarbring, such a subdivision of muscles affects the muscle and joint reaction force estimates[45]. Consequently, a normalization factor based on the muscle volume[46] was introduced, that accounts for a proper subdivision of the force among split and non-split muscles:

$$G\left(\mathbf{f}^{(M)}\right) = \sum_{i=1}^{n^{(M)}} V_i \left(\frac{f_i^{(M)}}{N_i}\right)^3, \qquad\qquad (3a)$$

$$\mathbf{C}\,\mathbf{f} = \mathbf{d} \qquad\qquad (3b)$$

$$0 \le f_i^{(M)} \le N_i, \qquad i = 1, \dots, n^{(M)} \qquad\qquad (3c)$$

where G is the cost function to minimize, M indicates the muscles, $\mathbf{f}^{(M)}$ is the vector of the $n^{(M)}$ unknown muscle forces. More precisely, $n^{(M)}$ is the number of all muscle units after the geometrical splitting, $f_i^{(M)}$ denotes the individual i-th muscle force and N_i is the instantaneous muscle strength, depending on the current working conditions of the Hill-type model, namely the force-length, and force-velocity relationships. $\mathbf{C}$ is a coefficient matrix for all the unknown forces in the problem, $\mathbf{f}$, which includes joint reactions as well as muscle forces, and $\mathbf{d}$ contains all the external loads and inertia forces. Finally, V_i is the volume of each muscle unit and, for split muscles, each unit was assigned the corresponding fraction of the total muscle volume resulting from a uniform subdivision by the number of units. The muscle volume we computed as the product of PCSA and optimum fiber length, taking into account the reduction in PCSA for all knee flexors and extensors.

Marker-tracking and inverse dynamics

With the model scaled, an inverse kinematics technique[47] was employed to track the marker trajectories during one normal gait (PS_ngait_og_ss1) and one right-turn (PS_rightturn6) trial from the Grand Challenge Competition dataset (Figure 2.2), providing the time history of the following body kinematics: one neck rotation, three pelvis-thorax rotations, three pelvis translations and three rotations, three hip rotations, knee flexion angle, ankle plantar-flexion, and subtalar eversion. During the marker-tracking stage, all joints were assumed idealized and the TF and PF joints were modeled as hinges (i.e. revolute joints), allowing only one rotational DOF (flexion/extension) around a fixed joint axes. Inaccuracies in the estimation of knee joint kinematics from marker data due to soft tissue artifacts (STA) have been reported[48], and the use of knee joint constraints did not result in a reduction of STA[49]. From these observations derived the choice of using hinge joint constraints for the knee and to drive only the knee flexion angle from marker data in the FDK model as well be explained later. The PF joint was
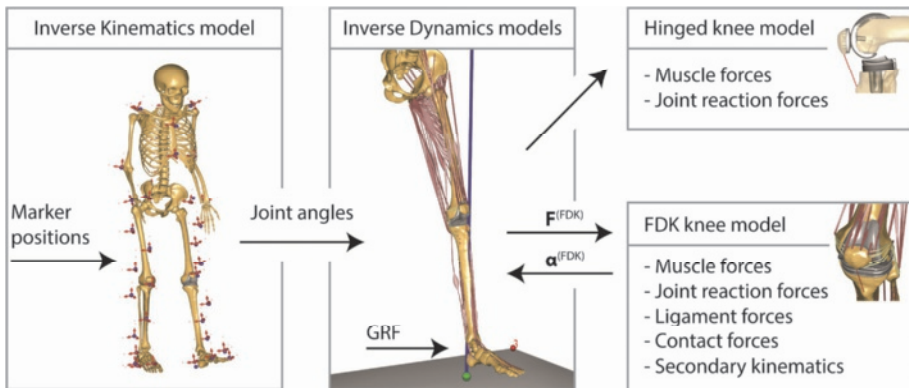
Figure 2.2 Simplified schematic of the modeling workflow. Marker trajectories are input to an inverse kinematics-based analysis that computes joint angles. Inverse dynamics-like models are developed, in which ground reaction forces (GRF) are input together with joint angles. Two types of knee models are simulated: a hinged model and an FDK model. The hinged model employed idealized constraints, whereas the FDK model finds a quasi-static kinematic configuration, α(FDK), in the FDK DOFs under the influence of the forces, F(FDK), acting in the respective DOFs. Predictions are independently produced by each model. The FDK model provides, in addition to muscle forces and joint reactions, also ligament and contact forces, and secondary knee kinematics.

further constrained by enforcing a fixed-length patellar ligament. This model did not include ligaments or contact but idealized constraints, as is typically the case when an idealized hinge joint is used to model the knee (we will refer to this as the hinged knee model).

Joint angles and ground reaction forces (GRF) were input to the inverse dynamic analyses with the hinged knee model. Only the left lower extremity, trunk and head dynamics were simulated, and six residual forces and moments were inserted at the pelvis. Muscle and joint reaction forces were the outputs of these type of simulations.

Force-dependent kinematics model

A second model containing a total of 11 knee DOFs, rigid-rigid contact and ligaments was developed (Figure 2.3) and solved using the FDK solver in the AMS (we will refer to this as the FDK knee model). All the TF and PF joint
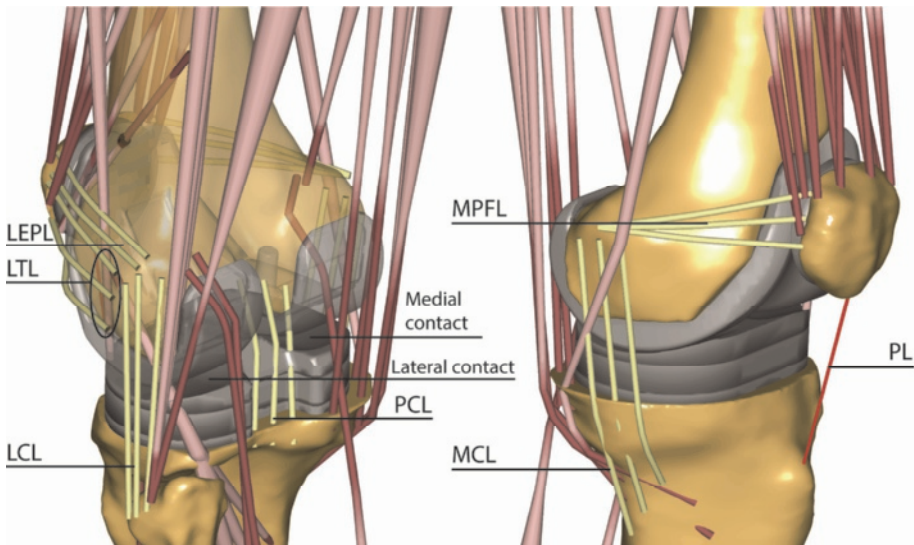
Figure 2.3 The 11-DOF knee model used in the FDK simulations. Knee flexion is driven using joint angle from an inverse kinematic-based analysis. The remaining 10 DOFs are handled by the FDK solver. Ligaments are modeled as one-dimensional string elements wrapping around geometrical shapes (abbreviations as described in the text). Medial and lateral contacts were modeled using rigid-rigid contact formulation. Patellar ligament (PL) consists of a rigid linkage between patella and tibia.

constraints were released, leaving six DOFs in the TF joint and five DOFs in the PF joint, as the patellar ligament was still considered rigid. Similarly to the hinged model, the knee flexion angle was the only knee DOF to be driven from marker data, whereas the other five TF and five PF DOFs were left free to equilibrate under the effect of external loads, muscle, ligament and contact forces, that were simultaneously computed using FDK, an enhanced inverse dynamics-based method in the AMS[50]. In summary, the FDK solver perturbed the kinematic configuration along the FDK DOFs ($\alpha^{(FDK)}$) until a quasi-static equilibrium was found, in which all the FDK residual forces ($\mathbf{F}^{(FDK)}$) in these DOFs were zero (Figure 2.2). Any dynamic effects in those 10 DOFs were neglected and quasi-static equilibrium at every simulation step was iteratively searched until force residuals fell below a specified threshold (= 0.3 N). Please notice that, although quasi-static equilibrium in the secondary knee joint kinematics was assumed, all dynamics occurring due to knee flexion/extension were taken into account and, hence, only a small fraction of the overall knee dynamics was omitted.

Ligaments were included to provide stability to the unconstrained joints in the FDK model (Figure 2.3). A total of 17 spring elements were modeled to represent the posterior cruciate ligament (PCL, 3 bundles), medial collateral ligament (MCL, 3 bundles), lateral collateral ligament (LCL, 3 bundles), medial patellofemoral ligament (MPFL, 3 bundles), lateral epicondylopatellar ligament (LEPL, 2 bundles), and lateral transverse ligament (LTL, 3 bundles). Since attachment sites could not be determined from the dataset, they were estimated according to descriptions found in the literature[51–60]. The anterior cruciate ligament (ACL) was sacrificed during the surgery and, therefore, not modeled. Force exerted by ligament bundles followed a non-linear elastic characteristic with a slack region[61]:

$$f(\varepsilon) = \begin{cases} \dfrac{k\varepsilon^2}{4\varepsilon_l}, & 0 \leq \varepsilon \leq 2\varepsilon_l \\[2ex] k(\varepsilon - \varepsilon_l), & \varepsilon > 2\varepsilon_l \\[2ex] 0, & \varepsilon < 0 \end{cases} \qquad (4)$$

where $f(\varepsilon)$ is the current force, k is the stiffness, ε is the strain, and ε_l (= 0.03) is a constant related to the transition phase towards the linear region of the force-strain curve[62]. Ligament bundle slack length, l_o, was first calibrated in an upright reference position, in which the leg was fully extended, so that:

$$l_0 = \frac{l_r}{\varepsilon_r + 1} \qquad (5)$$

where l_r is the bundle length computed at the reference position and ε_r is the reference strain estimated for that reference position. Finally, the instantaneous strain, ε, during the simulation was computed from the instantaneous bundle length, l, as follows:

$$\varepsilon = \frac{l}{l_0} - 1 \qquad (6)$$

Table 2.1 Stiffness and reference strains of the knee joint ligament bundles used in the FDK model.

Ligament bundle[a]	Stiffness (N)[b]	Reference strain[c]
aPCL	6000	−0.24
mPCL	6000	−0.10
pPCL	6000	−0.03
aMCL	2750	0.04
mMCL	2750	0.04
pMCL	2750	−0.03
aLCL	2000	−0.25
mLCL	2000	−0.05
pLCL	2000	0.08
sMPFL	2000	0.12
mMPFL	2000	0.08
iMPFL	2000	0.08
sLEPL	1000	0.06
iLEPL	1000	0.06
sLTL	1000	0.06
mLTL	1000	0.06
iLTL	1000	0.06
PL	∞	-

[a] Nomenclature: aPCL/mPCL/pPCL, anterolateral, middle and posteromedial cruciate ligament; aMCL/mMCL/pMCL, anterior, middle and posterior medial collateral ligament; aLCL/mLCL/pLCL, anterior, middle and posterior lateral collateral ligament; sMPFL/mMPFL/iMPFL, superior, middle and inferior medial patellofemoral ligament; sLEPL/iLEPL, superior and inferior epicondylopatellar ligament; sLTL/mLTL/iLTL, superior, middle and inferior lateral transverse ligament; PL, patellar ligament.
[b] Stiffness is expressed in newton per unit strain.
[c] Reference strains are referred to an upright standing reference position.

Stiffness and reference strain assigned to each ligament bundles are summarized in Table 2.1. These values were adapted from the literature[61]. No direct information was available on the stiffness and slack-length of medial (MPFL) and lateral (LEPL, LTL) patellofemoral ligaments. However, MPFL represents the major restraint to lateral patellar translation[55,63], whereas lateral structures only account for a lesser contribution. Thus, MPFL stiffness was chosen in the same range of other known ligaments (LCL, MCL), whereas lower values were assigned to LEPL and LTL bundles. Furthermore, medial retinacular structures are tight during knee extension to low flexion angles, and relax with increased flexion[60]; hence, MPFL, LPL, LTL reference strains were assigned similar positive values, providing the required stability to the PF joint. The choice of parameters was evaluated to ensure that the patellar

button always ran into the groove of the femoral component during a test flexion/extension simulation. The patellar ligament was modeled as a rigid one-bundle linkage between patella and tibia in both the hinge and FDK models and its length was estimated based on measurements from fluoroscopy images with the subject performing a leg-swing trial, as described later. Similarly to the muscle models, wrapping surfaces were employed to prevent ligaments from penetrating the bones and the implants. Specifically, one cylinder was positioned medially on the distal femur so that the MPFL bundles could wrap around the medial condyle of the femur. Another cylinder was placed on the contralateral side so that LEPL and LTL bundles would wrap around the lateral femur condyle. A third cylinder ensured that the PCL bundles did not penetrate the spine structure of the tibial insert. Lastly, one cylinder was positioned on the tibial segment to allow the MCL to wrap around the medial tibial condyle.

A rigid-rigid STL-based contact model was defined between tibial insert and femoral component and between the patellar button and the femoral component. Contact forces were computed based on linear volume approximations using the penetration depth, d_i, of a vertex of one triangle-mesh into the closest triangle of the opponent STL surface. A volume, V_i, was approximated by multiplying the vertex penetration depth by the opponent triangle area, A_i, so that for the ith vertex:

$$V_i = A_i d_i \qquad (7)$$

The contact force magnitude for an element that contributed to the total contact force was computed using a linear relationship between the penetration volume and a so-called pressure module, P:

$$F_i = P V_i \qquad (8)$$

The direction of the force was determined by the normal of the triangle. Based on previous tests, for all contact pairs, a pressure module of 9.3 GN/m³ was used. This value provided a good tradeoff between the amount of penetration obtained and the numerical issues involved in solving contact between two surfaces with high stiffness. Three contact models of the kind described above were defined, one for the medial side, one for the lateral side of the TF joint, and one for the PF joint. The forces computed from the two TF contact models where expressed in the reference frame of the tibial component, thus

permitting a direct comparison with the measured knee loads provided with the Grand Challenge dataset. Finally, linear and rotational springs with small stiffness values were included at each of the ten FDK DOFs in the FDK knee model, which served exclusively to help the FDK algorithm in searching the static equilibrium among those DOFs by ensuring that there was always stiffness in the model, even if the solver explored non-physiological configurations. The stiffness of these springs did not need to be tuned, and care was taken that the spring forces remained negligible once the solution had been found.

The time history of joint angles and ground reaction forces (GRF) were input to the FDK analyses. Only the left lower extremity, trunk and head dynamics were simulated, and six residual forces and moments were inserted at the pelvis. Muscle, ligament, contact, and joint reaction forces along with secondary knee kinematics were the outputs of the FDK simulations (Figure 2.2).

Estimation of secondary knee kinematics

An unloaded leg-swing fluoroscopy trial (PS_legswing2) from the dataset was used to obtain an estimate of knee kinematics in the sagittal plane, namely TF and PF translations, PF and patellotibial (PT) flexion angles. During the trial, the subject performed a knee flexion-extension movement with his left leg while standing on the other (right) leg. The left knee was imaged through an X-ray fluoroscope at a frame rate of 30 images per second. Twenty-seven fluoroscopic images from the trial were segmented using custom code written in MATLAB v. 8.1.0 (The Mathworks Inc., Natick, MA). The available range of motion for these images spanned from approximately 100 to 30 degrees of knee flexion. The pixel size was determined by manually registering the 3-D geometric model of the femoral component (with known dimensions) to one fluoroscopy frame. Relative angles and displacements between patella, femoral and tibial component projections were detected using edge- and line-detection routines based on the Hough transform. The trajectories of the superior tip of the femoral component (TF tip shift) and of the patella (PT shift) were expressed relatively to a reference frame placed on the extreme anterior edge of the tibial tray, as depicted in Figure 2.4. The same local frames were defined in the hinge and FDK models allowing a direct comparison between fluoroscopy-detected and model-predicted kinematics.
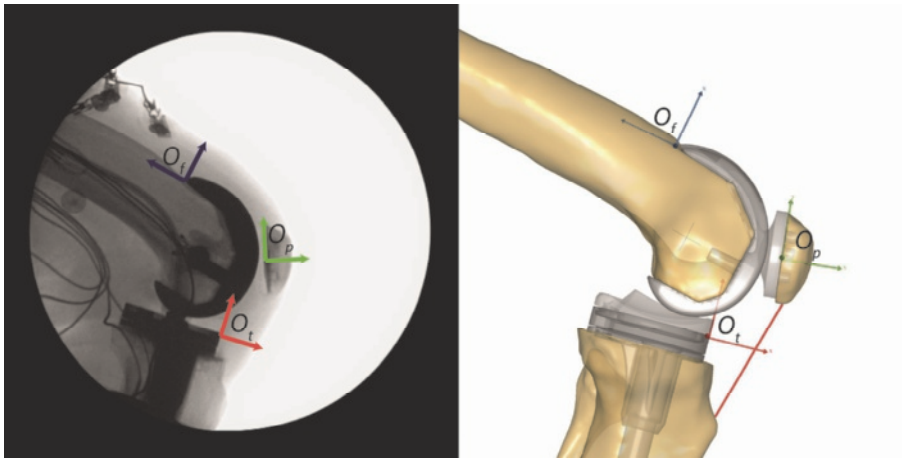
Figure 2.4 Reference frames used to express the knee planar knee kinematics during the leg-swing trial in the fluoroscopy images (left) and in the MS model (right). The PF flexion is defined as the rotation of the femoral frame (Of) relative to the patellar frame (Op); PT flexion is the rotation of the tibial frame (Ot) relative to the patellar frame; TF tip and PT shift are given by the two coordinates of displacement (posterior-anterior and distal-proximal) of femoral frame and patellar frame, respectively, relative to the tibial frame. Muscles are hidden in the model view and the hinged model version is shown.

The fluoroscopy-detected tibia-femur flexion was used to drive the knee flexion angle in the inverse dynamic and FDK simulations. Hip and ankle rotations were not directly available, and they were visually estimated from a movie recorded while the subject was performing the task. The distance between the inferior tip of the patella and the tibial tuberosity was manually measured in all fluoroscopy frames. The mean value was used as an estimate of subject-specific patellar ligament length for both hinge and FDK models.

No fluoroscopy data were available for the gait and right-turn trials and, therefore, only the unloaded leg-swing fluoroscopy trial was used for the evaluation of secondary knee kinematics.

Model evaluation

Tibiofemoral joint compressive contact forces were estimated with both the hinged model and the FDK model during a gait trial and a right-turn trial, leading to four different simulations. Predictions were expressed in units of fractions of body weight (BW) and re-sampled on a 0-100% trial duration scale

with a step interval of 1% from heel strike to the subsequent heel strike. Medial and lateral TF joint forces were obtained from the hinged model using regression equations provided in the Grand Challenge Competition dataset, whereas in the FDK model, they were independently computed from the two separate medial and lateral contact models. Ligament forces predicted by the FDK model are also reported for the gait and right-turn trials.

Knee kinematics during the leg-swing fluoroscopy trial were estimated with both the hinge and the FDK knee models, leading to two additional analyses. Model-predicted and fluoroscopy-detected results were re-sampled to a 0-100% trial duration scale with a step interval of 1%.

Differences between model predictions and experimental measurements were quantified in terms of root mean square error ($RMSE$), squared Pearson correlation coefficient (r^2), coefficient of determination (R^2) , and the Sprague and Geers metrics of magnitude (M), phase (P) and combined error (C)[64,65]. Sprague and Geers metrics can quantify magnitude and phase prediction errors independently and they are both zero when the compared curves are identical; C combines the two errors, and was computed as the root of the sum of squares of M and P.

RESULTS

Tibiofemoral joint forces

Predicted *versus* experimental TF contact forces during the gait and right turn trials are depicted in Figure 2.5. Experimental data from the instrumented knee implant revealed a double-peaked total force during the gait cycle, with a first peak of 2.2 body weights (BW) occurring at the beginning of stance and a second peak of 2.1 BW occurring towards the end of the stance phase. Both the hinge and FDK knee model captured this pattern (R^2 = 0.9, $RMSE$ < 0.3 BW) and predicted the first and second peaks equal to 2.0 and 2.4 BW, respectively. Lateral forces were in general under-predicted by both the hinged model (M = -0.3) and the FDK model (M = -0.4), and a considerable phase error was observed (P = 0.2). Medial forces were slightly over-predicted by both models (M = 0.1). Right-turn total forces were in overall good agreement with the experimental forces ($RMSE$ = 0.3 BW), as predicted by both hinge model (R^2 = 0.8) and FDK model (R^2 = 0.9) simulations; moderate
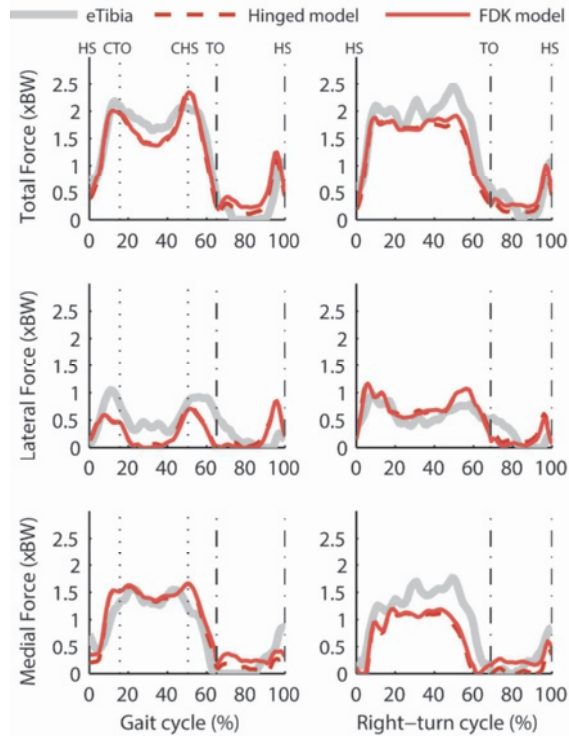
Figure 2.5 Total, lateral and medial compressive TF contact forces predicted during one gait trial (left column) and one right-turn trial (right column) using an idealized knee joint model and the FDK knee model. Experimental measurements are reported for the same trial. Overall good agreement between measured and predicted total forces is noted. Lateral (respectively medial) forces are slightly under-predicted (respectively over-predicted) in the gait trial. Lateral (respectively medial) forces are slightly over-predicted (respectively under-predicted) in the right-turn trial.

medial side force under-prediction (M = -0.3) and lateral side over-prediction (M = 0.2) were observed. Both FDK and hinged model captured the overall shape and timing of the measured TF contact forces (Table 2.2).

Ligament forces during the gait and right-turn trial predicted with the FDK model are depicted in Figure 2.6. The PCL was moderately stretched right after toe-off during the gait (resp. right-turn) trial, when knee flexion angle was approximately 60 deg, with a peak force of 68 N (resp. 62 N). The MPFL, MCL and LEPL generated the most considerable force throughout both cycles.

Table 2.2 Agreement between predicted and experimental TF joint compressive contact forces during gait and right-turn trials.

Trial	FDK knee model						Hinge knee model					
	$RMSE^a$	r^2	R^2	M	P	C	$RMSE^a$	r^2	R^2	M	P	C
Gait												
Total Force	0.26	0.90	0.89	-0.06	0.06	0.08	0.25	0.91	0.90	-0.07	0.05	0.09
Lateral Force	0.35	0.23	-0.26	-0.35	0.22	0.41	0.34	0.21	-0.19	-0.31	0.21	0.38
Medial Force	0.26	0.85	0.79	0.12	0.07	0.14	0.25	0.85	0.81	0.08	0.08	0.11
Right-turn												
Total Force	0.29	0.94	0.87	-0.14	0.04	0.15	0.34	0.93	0.83	-0.17	0.05	0.18
Lateral Force	0.21	0.65	0.33	0.17	0.10	0.20	0.21	0.64	0.32	0.21	0.10	0.23
Medial Force	0.38	0.82	0.62	-0.29	0.08	0.30	0.44	0.83	0.48	-0.33	0.10	0.35

[a] RMSE is in units of body-weights (BW)
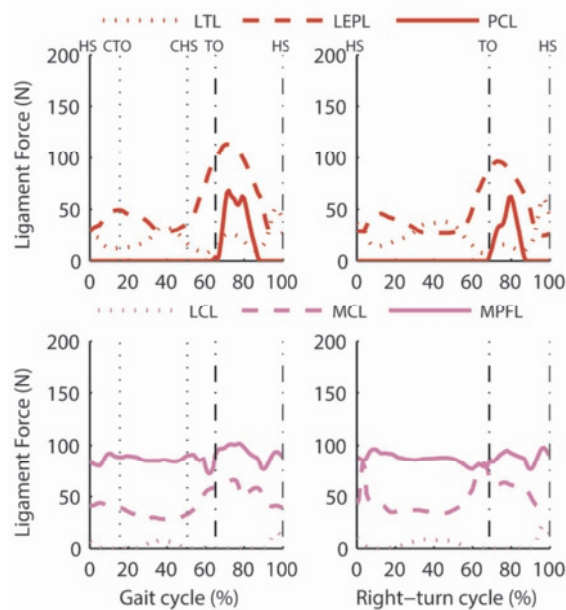
Figure 2.6 Ligament forces predicted during gait (left) and right-turn (right) trials using the FDK model. Each force shown in the graphs was computed as the root of the summed squares of each ligament individual bundle force. The PCL is being activated after toe-off in both trials, and MPFL, MCL, LEPL exert considerable amount of force throughout the trials.

Mean forces predicted were 88 N, 43 N, 55 N, respectively, in the gait trial simulation, and were 87 N, 48 N, 47 N, respectively, in the right-turn trial simulation. The predicted LCL force was less than 30 N throughout the cycle in both trials.

Secondary Knee Kinematics

The experimental PF and PT flexion curves during the unloaded leg-swing fluoroscopy trial were almost linear relative to the knee flexion angle and spanned from approximately 74-20 degrees and 25-9 degrees, respectively, from flexion to extension (Figure 2.7, left). The PF flexion was perfectly predicted by the FDK model ($R^2 = 0.99$), and the hinged model resulted in a larger prediction error ($M = 0.26$, $R^2 = 0.52$) with respect to the experimental curve. The PT flexion was also much better predicted using the FDK model ($R^2 = 0.7$) than using the hinged model ($R^2 < 0$), as explained by the larger
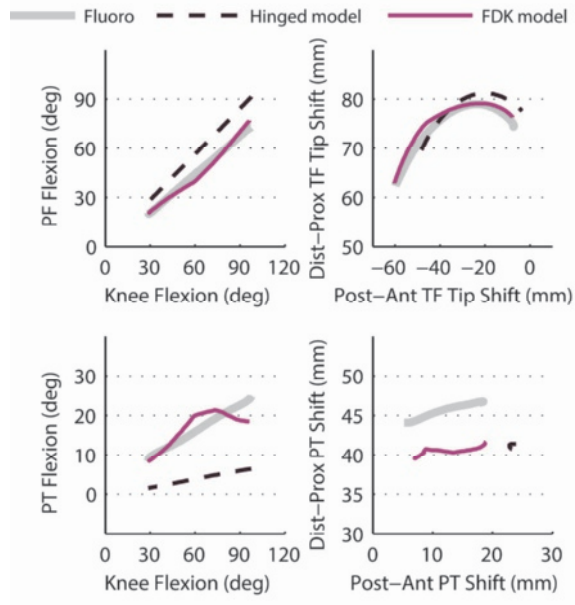
Figure 2.7 Experimental versus predicted PF flexion (top left) and PT flexion (bottom left), plotted relative to knee flexion angle; TF tip shift (top right) and PT shift (bottom right). The FDK model predictions are generally more accurate than hinged model predictions. Note the inability of the hinged model to predict PT shifts, due to the absence of femoral roll-back.

magnitude error in the hinged model prediction (M = -0.75). The posterior-anterior TF tip shift (Figure 2.7, top right) was overall well predicted by both the hinged model (R^2 = 0.88) and the FDK model (R^2 = 0.96), whereas the distal-proximal TF tip shift was much better predicted by the FDK model (R^2 = 0.96) than by the hinged model (R^2 = 0.38). The hinged model fails almost completely at tracking the PT displacements (Figure 2.7, bottom right), resulting in large combined errors. The FDK model predictions are better than the ones from the hinged model with regards to the postero-anterior PT shift (R^2 = 0.92). However, the distal-proximal PT shift is systematically under-predicted (M = -0.1). Evaluation metrics for all the measures are summarized in Table 2.3. The average combined error for all the predictions from the FDK (respectively hinged) model was equal to 0.06 (respectively 0.34).

Table 2.3 Agreement between predicted and detected secondary knee kinematics during unloaded leg-swing fluoroscopy trial.

Quantity[a]	FDK knee model						Hinge knee model					
	RMSE[b]	r^2	R^2	M	P	C	RMSE[b]	r^2	R^2	M	P	C
PF flexion	2.33	0.99	0.99	0.00	0.02	0.02	13.3	1.00	0.52	0.26	0.01	0.26
PT flexion	3.05	0.71	0.70	-0.05	0.05	0.08	13.3	1.00	-4.83	-0.75	0.03	0.75
TF tip shift												
Posterior-Anterior	3.69	0.99	0.96	0.07	0.02	0.08	6.79	1.00	0.88	-0.18	0.01	0.18
Distal-Proximal	1.09	0.97	0.96	0.01	0.00	0.01	4.21	1.00	0.38	0.05	0.01	0.05
PT shift												
Posterior-Anterior	1.32	0.93	0.92	-0.02	0.03	0.04	11.2	0.38	-4.79	0.69	0.11	0.70
Distal-Proximal	5.19	0.85	-26.3	-0.11	0.00	0.11	4.57	1.00	-20.2	-0.10	0.01	0.10

a Nomenclature: PF flexion, patellofemoral flexion; PT flexion, patellotibial flexion; TF tip shift, tibiofemoral tip shift; PT shift, patellotibial shift.
b RMSE is in units of degrees for PF and PT flexion angles, and millimeters for TF and PT shifts

DISCUSSION

The first goal of this study was to present a musculoskeletal modeling framework based on subject-specific CT images, motion capture and force plate data as input to an inverse dynamics-based method that concurrently predicts musculoskeletal dynamics and detailed *in vivo* knee joint mechanics. Several aspects presented lend novelty and uniqueness to our musculoskeletal modeling approach: the FDK method permitted the estimation of knee joint mechanics that also include contribution of soft tissues and contacts, while still employing motion-capture and force-plate data as the only information required to drive the model. A bone-morphing technique was employed to anatomically scale the generic MS architecture to the specific patient, including muscle attachment sites.

Our second aim was to evaluate the validity of the model predictions during walking activities performed by a subject with TKA using experimental data publicly available from the Grand Challenge Competition[8]. Our models predicted TF contact forces which were in good agreement with the experimental measurements (*RMSE* < 0.3 BW during the gait trial). Previous models have predicted TF forces with an *RMSE* of 0.41 BW[29], 0.45 BW[66], and 0.67 BW[27] during gait. The time history and the value of peak contact forces were also identified with a good accuracy in both the gait and right-turn simulations (Figure 2.5), with a maximum error of 0.3 BW on the second peak of stance during gait. Other authors have reported errors in peak value estimation up to 0.35[28], 0.39[27], 0.65[66], and 0.80 BW[30], on average. We included the Sprague and Geers' metrics to evaluate the goodness of our model predictions, along with *RMSE*, squared Pearson's *r* (r^2) and coefficient of determination (R^2). Pearson's r^2 is usually good when the trends are overall captured even in presence of large magnitude errors; whereas the coefficient of determination, R^2, may results in low or even negative values in presence of magnitude errors or offsets even if the trends are well predicted. The interpretation of negative R^2 values is often difficult. Therefore, we believe that Sprague and Geers' metrics provide a more immediate way to quantify the magnitude and phase errors, especially when comparing time histories of quantities predicted by musculoskeletal models and, therefore, their use should be encouraged.

The level of agreement of our results may also suggest that the criteria used for solving the muscle recruitment problem, as well as the muscle modeling and strength scaling applied, were able to approximate the particular musculoskeletal biomechanics for this specific subject to a great extent. The over- or under-predictions of medial and lateral forces did not follow a particular trend, i.e. during the gait trial, the medial force was over-predicted, whereas in the right-turn, the lateral side was over-predicted, and vice versa. In general, the TF contact distribution is affected by the line of action of the GRF; during gait, it normally passes medially relative to the knee joint center resulting in a contact force more pronounced on the medial side[67]. The main contribution to support during walking is mainly given by muscle forces[68] and these, in turn, determine the forces exchanged at the joints. Therefore, the causes of the discrepancies between measured and predicted TF contact forces should be searched in the musculoskeletal architecture of the model, including muscle strength, moment arms and joint axes. The position of the lower extremity joints was not measured directly, and the foot model geometry could not be entirely reconstructed from medical images. The inevitable inaccuracies could have, therefore, resulted in small deviations in the predicted TF forces.

Estimates of ligament forces during the gait and right-turn trials were obtained using the FDK model. In a robotic *in vitro* study, Li et al. measured the *in situ* force of PCL in CR-TKA and they observed that PCL force peaked at a knee flexion angle of 90 deg (39 ± 36 N)[69]. We predicted peak PCL forces of less than 70 N for both gait and right turn trials, occurring right after toe-off at approximately 70% of the gait cycle, when the knee is flexed of about 60 deg. However, differences between the static setup used in the experiment and the dynamic nature of our simulations make this comparison questionable. Overall, predicted PCL forces compared qualitatively well with other model predictions in the literature. Thelen et al. predicted a peak PCL force during gait of less than 200 N at about 70% of the gait cycle[27], whereas Kia et al. predicted PCL peaks of about 100 N at approximately 50% of the gait cycle[29]. Patterns of LCL and MCL forces agreed with those reported by Kia et al.[29], but differ from the ones of Thelen et al[27].

As our third aim we were interested in assessing whether a more complex representation of the knee joint substantially alter the model predictions. Tibiofemoral forces predicted using a hinged model formulation were

generally comparable to the ones predicted by the FDK model (differences of less than 5% BW in *RMSE* of total force predictions). This reveals that using a different mechanical formulation for the knee joint, i.e. including more DOFs, did not substantially alter the load predictions at the tibial implant. Possible explanations for this are that the employed TKA implant is largely circular and a hinge joint is hence a good overall approximation of the knee joint structure, and the amount of knee motion predicted during the FDK simulations did not substantially alter the load distribution at the knee joint. The comparison against the fluoroscopic data does, however, reveal that the hinged model is less accurate at tracking the detailed joint kinematics compared to the FDK model, as revealed by the larger *RMSE* found for that model (Table 2.3). Whether this accuracy is sufficient depends on the application, but for instance for wear simulations, simultaneous estimates of contact forces as well as detailed joint kinematics are required. For such wear simulations, the FDK model should be preferred.

The ability to obtain subject-specific information on the conditions of the MS system is crucial if diagnostic information is to be carried out and interventions are to be planned based on the MS model outputs[8,9]. The approach presented was able to personalize a generic MS model to a great extent based on a vast amount of subject-specific information. Primarily, bones and muscle architecture of the subject's lower extremity were scaled using an advanced non-linear morphing technique[35], from which derives that also all muscle attachments sites followed anatomical origin and insertion sites on the bony surfaces. This aspect is essential since muscle forces are directly influenced by the line of action and moment arm during motion. No other studies did, to our knowledge, include a thorough and accurate anatomical representation of the MS architecture on a subject-specific body-scale level together with detailed models of the TF and PF joints. Several studies have used generic linear scaling law based on anthropometric information on the subject, i.e. body weight, height, age or gender[27–30,66]. Other studies have modified the anatomical description of the muscle architecture by including attachment sites taken from MRI scans from a different subject[70,71]. In our model, axes and joint centers of the lower extremity joints were extracted by fitting analytical geometrical shapes to the implant and bone geometries of the subject. Extracting the joint position from

subject-specific images was recently proved to be a robust method in the frame of musculoskeletal simulations[72].

Several studies have recently indicated the sensitivity of muscle-tendon architecture in inverse dynamics-based simulations[66,73]. In this study, we have estimated the strength-related muscle-tendon parameters by using linear scaling laws[40], in which length and mass of each segment served to further compute segment-specific strength coefficients. The knee flexor and extensor muscle strengths in our model were further decreased by 35% to account for weakening observed in the flexor-extensor mechanism in subjects following TKA[43]. To this regard, Hast and Piazza[30] predicted TF forces during gait with a forward-dynamic model of an elderly subject, and they reduced uniformly by 50% all the muscle strength, to account for an age-related weakening of the MS system. Ideally, we could have included subject-specific strength in our model, if such information were made available.

Similarly to the model of Thelen et al., we introduced a weighting factor in the objective function of the muscle recruitment problem[27], that accounted for the partial volume of the muscle branches. This was a major fundamental choice, considering the muscle architecture in our model. It has been shown that the estimated muscle forces in an inverse dynamics-based simulation are influenced by how the muscles are decomposed, to an extent that depends on the type of the recruitment criterion used and, particularly for polynomial criteria, on the power of the polynomial[45]. Many muscles in our lower extremity model were split to account for a large insertion area, while others were not. In particular cases, such as for *soleus* (split, 3 units) and *gastrocnemius* (not split), if no further normalization was introduced, the muscle recruitment problem would have seen it more favorable to activate *gastrocnemius* than *soleus* muscle (e.g. to plantar-flex the ankle). This is because the only *gastrocnemius* unit had a much larger strength compared to each of the three units of *soleus*. As this behavior was unwanted, muscle volume normalization factors were introduced in the objective function that accounted for the partial muscle volume of each individual muscle unit.

Although ligament forces were shown to contribute to only a minor extent to the TF contact forces[67], we have shown that they might instead have a larger influence in determining internal knee kinematics. In the simulation of leg-swing trial with the FDK knee model, TF and PF joint secondary sagittal plane

kinematics were generally better approximated with FDK model simulations (Figure 2.7), essentially because an unconstrained joint allowed motions that a hinge joint could not. In particular, the total absence of femoral roll-back when using the hinged model was most likely the cause of erroneous prediction of the PT kinematics. The FDK model, instead, could correctly predict the posterior-anterior displacement, but under-predicted the distal-proximal displacement. Therefore, although an overall agreement was reported, further studies are needed to determine whether ligament parameters used in the model are representative of a real situation, and it is likely that calibration routines will be required to fine-tune the joint restraint during the full range of knee flexion.

Simulations with the FDK model took approximately 4½ hours, for the gait and right turn trial simulations, and 2¾ hours for the leg-swing trial, respectively, to compute on a Windows 7, 64-bit 3.2 GHz Intel Core i5 CPU, 16 GB RAM computer. The FDK residual forces were smaller than 1 N in the FDK simulations of right-turn and leg-swing trial, and were smaller than 3 N in the gait trial simulation. Hinged model simulations required on average two minutes to complete. It should be emphasized that almost 90% of the time during an FDK analysis is spent on searching for the closest points during the contact force computation. This aspect should primarily be addressed in future studies for improving the computational speed of FDK simulations, for example by utilizing surrogate modeling techniques[74].

This study includes some limitations that are worth discussing. Firstly, we modeled the patellar ligament as a rigid linkage between patella and tibia. This may have slightly affected the predicted PCL strain, PF contact force, and TF kinematics during the knee range of motion[75]. However, the use of a stiff but extensible patellar ligament model need to be investigated further. Secondly, the knee joint motions during the leg-swing fluoroscopy trial were detected for the quasi-sagittal fluoroscopy plane only. This might have introduced inaccuracies when evaluating the model-predicted sagittal plane kinematics, due to the presence of small out-of-plane motions. Furthermore, frontal and transversal plane PF and TF kinematics could not be evaluated with this method. Thirdly, ligaments were modeled as one-dimensional non-linear elastic springs, wrapping around geometrical shapes preventing bone and implant penetration. This approach allowed large model simplifications, but could not certainly grasp the complex stress-deformation characteristic of

ligament tissue in 3-D. In addition, tuning of the tibiofemoral ligament properties was not performed for this subject, and the sensitivity of the corresponding ligament parameters on the model predictions was not assessed. We anticipate that knowledge of ligament insertion sites (for example by MRI images of the subject's knee), in conjunction with laxity tests, could provide further calibration material for tuning the ligament parameters on a subject-specific basis. It is also worth mentioning that, although the effect of additional linear and rotational springs in the FDK model was negligible in the gait and right-turn trial simulations, contributions of up to 20 Nm were observed in the leg-swing trial FDK simulation at large flexion angles (approximately 70-100 deg). By removing the rotational spring at the tibial internal-external rotation FDK DOF, we understood that a large force was being recruited to restrain tibial external rotation at large flexion angles, and none of the modeled ligaments were able to support this motion, as both collateral ligaments were slack at high flexion. We concluded that the ligament configuration used in the model was not sufficient to completely stabilize the knee joint at large knee flexion angles. Further research will address a more detailed representation of the ligamentous restraint in the FDK knee model, we anticipate that the improvement of the popliteus complex representation on the posterolateral aspect of the knee might help further stabilizing the knee joint in flexion[76]. Fourthly, time histories of predicted muscle activations were not evaluated, but their validity could be indirectly estimated through the evaluation of the joint forces. Notwithstanding the common practice of using EMG to validate muscle activations, muscle force production and EMG signal are two different physical phenomena related by complex mechanisms[42], and the EMG signal magnitude is location-dependent. Therefore, comparing EMG signal magnitude with model-predicted muscle activity cannot be regarded as the gold standard in assessing the validity of dynamic MS models. Also, the extent of leg muscle co-contraction was not evaluated in this study. The simultaneous activations of antagonistic muscles can result in increased joint forces[77], and this phenomenon can be regarded as physiological, to some extent, during load-bearing activities, as it may stiffen and further stabilize the joints. Considering the use of a purely muscle activity minimizing criterion for solving the muscle recruitment problem, it is likely that muscle co-contraction was under-estimated in our models.

In conclusion, we have presented a novel multi-body dynamics framework for the study of the musculoskeletal system capable of directly integrating subject-specific clinical images, motion capture data and ground reaction forces, for simultaneously predicting internal TF forces, body-level dynamics and secondary knee kinematics *in vivo*. We compared our model predictions to publicly accessible experimental data from a TKA patient, and found distinctly good agreement. Compared to use of a hinge knee model, use of more complex FDK TF and PF models did not result in improved prediction of knee contact forces but did result in more accurate prediction of secondary knee kinematics. The proposed workflow for developing subject-specific models may have potential application as a diagnostic tool and in aiding clinical decision-making.

ACKNOWLEDGMENT

FUNDING

REFERENCES

1.   Westerhoff, P., Graichen, F., Bender, A., Rohlmann, A. & Bergmann, G. An instrumented implant for in vivo measurement of contact forces and contact moments in the shoulder joint. *Med. Eng. Phys.* **31**, 207–213 (2009).

2.   Bergmann, G. *et al.* In vivo glenohumeral contact forces-Measurements in the first patient 7 months postoperatively. *J. Biomech.* **40**, 2139–2149 (2007).

3.   D'Lima, D. D., Fregly, B. J., Patil, S., Steklov, N. & Colwell, C. W. Knee joint forces: prediction, measurement, and significance. *Proc. Inst. Mech. Eng. H.* **226**, 95–102 (2012).

4.   Bergmann, G. *et al.* Hip contact forces and gait patterns from routine activities. *J. Biomech.* **34**, 859–71 (2001).

5.   Damm, P., Graichen, F., Rohlmann, A., Bender, A. & Bergmann, G. Total hip joint prosthesis for in vivo measurement of

forces and moments. *Med. Eng. Phys.* **32**, 95–100 (2010).

6.   D'Lima, D. D., Townsend, C. P., Arms, S. W., Morris, B. A. & Colwell, C. W. An implantable telemetry device to measure intra-articular tibial forces. *J. Biomech.* **38**, 299–304 (2005).

7.   Bergmann, G. Orthoload.com. *Charité Universitaetsmedizin Berlin* (2008). Available at: http://www.orthoload.com/?page_id=7. (Accessed: 25th January 2018)

8.   Fregly, B. J. *et al.* Grand challenge competition to predict in vivo knee loads. *J. Orthop. Res.* **30**, 503–13 (2012).

9.   Erdemir, A., McLean, S., Herzog, W. & van den Bogert, A. J. Model-based estimation of muscle forces exerted during movements. *Clin. Biomech. (Bristol, Avon)* **22**, 131–54 (2007).

10.   Goislard de Monsabert, B., Vigouroux, L., Bendahan, D. & Berton, E. Quantification of finger joint loadings using musculoskeletal modelling clarifies mechanical risk factors of hand osteoarthritis. *Med. Eng. Phys.* **36**, 177–84 (2014).

11.   Mellon, S. J. *et al.* Individual motion patterns during gait and sit-to-stand contribute to edge-loading risk in metal-on-metal hip resurfacing. *Proc. Inst. Mech. Eng. H.* **227**, 799–810 (2013).

12.   Lemieux, P.-O., Nuño, N., Hagemeister, N. & Tétreault, P. Mechanical analysis of cuff tear arthropathy during multiplanar elevation with the AnyBody shoulder model. *Clin. Biomech. (Bristol, Avon)* **27**, 801–6 (2012).

13.   Lemieux, P. O., Tétreault, P., Hagemeister, N. & Nuño, N. Influence of prosthetic humeral head size and medial

offset on the mechanics of the shoulder with cuff tear arthropathy: a numerical study. *J. Biomech.* **46**, 806–12 (2013).

14.   Weber, T. *et al.* Measuring functional outcome after total hip replacement with subject-specific hip joint loading. *Proc. Inst. Mech. Eng. H.* **226**, 939–46 (2012).

15.   Weber, T., Al-Munajjed, A. a, Verkerke, G. J., Dendorfer, S. & Renkawitz, T. Influence of minimally invasive total hip replacement on hip reaction forces and their orientations. *J. Orthop. Res.* (2014). doi:10.1002/jor.22710

16.   Grujicic, M. *et al.* Musculoskeletal computational analysis of the influence of car-seat design/adjustments on long-distance driving fatigue. *Int. J. Ind. Ergon.* **40**, 345–355 (2010).

17.   Rasmussen, J., Tørholm, S. & de Zee, M. Computational analysis of the influence of seat pan inclination and friction on muscle activity and spinal joint forces. *Int. J. Ind. Ergon.* **39**, 52–57 (2009).

18.   Mirakhorlo, M., Azghani, M. R. & Kahrizi, S. Validation of a musculoskeletal model of lifting and its application for biomechanical evaluation of lifting techniques. *J. Res. Health Sci.* **14**, 23–8 (2014).

19.   Kinney, A. L. *et al.* Changes in in vivo knee contact forces through gait modification. *J. Orthop. Res.* **31**, 434–440 (2013).

20.   Zelle, J., Heesterbeek, P. J. C., De Waal Malefijt, M. & Verdonschot, N. Numerical analysis of variations in posterior cruciate ligament properties and balancing techniques on total knee arthroplasty loading. *Med. Eng. Phys.* **32**, 700–7 (2010).

21.   Mootanah, R. *et al.* Development and validation of a computational model of the

knee joint for the evaluation of surgical treatments for osteoarthritis. *Comput. Methods Biomech. Biomed. Engin.* **17**, 1502–17 (2014).

22.   Van Duren, B., Pandit, H., Murray, D. & Gill, H. Approximation of the functional kinematics of posterior stabilised total knee replacements using a two-dimensional sagittal plane patello-femoral model: comparing model approximation to in vivo measurement. *Comput. Methods Biomech. Biomed. Engin.* (2014). doi:10.1080/10255842.2014.887697

23.   Lund, M. E., de Zee, M., Andersen, M. S. & Rasmussen, J. On validation of multibody musculoskeletal models. *Proc. Inst. Mech. Eng. H.* **226**, 82–94 (2012).

24.   Roberts, T. J. & Gabaldón, A. M. Interpreting muscle function from EMG: lessons learned from direct measurements of muscle force. *Integr. Comp. Biol.* **48**, 312–20 (2008).

25.   Meyer, A. J. *et al.* Are external knee load and EMG measures accurate indicators of internal knee contact forces during gait? *J. Orthop. Res.* **31**, 921–9 (2013).

26.   Herzog, W., Longino, D. & Clark, A. The role of muscles in joint adaptation and degeneration. *Langenbecks. Arch. Surg.* **388**, 305–15 (2003).

27.   Thelen, D. G., Won Choi, K. & Schmitz, A. M. Co-simulation of neuromuscular dynamics and knee mechanics during human walking. *J. Biomech. Eng.* **136**, 021033 (2014).

28.   Guess, T. M., Stylianou, A. P. & Kia, M. Concurrent prediction of muscle and tibiofemoral contact forces during treadmill gait. *J. Biomech. Eng.* **136**, 021032 (2014).

29.   Kia, M., Stylianou, A. P. & Guess, T. M. Evaluation of a musculoskeletal model with prosthetic knee through six experimental gait trials. *Med. Eng. Phys.* **36**, 335–44 (2014).

30.   Hast, M. W. & Piazza, S. J. Dual-joint modeling for estimation of total knee replacement contact forces during locomotion. *J. Biomech. Eng.* **135**, 021013 (2013).

31.   Andersen, M. S. & Rasmussen, J. Total knee replacement musculoskeletal model using a novel simulation method for non-conforming joints. in *Proceedings of the International Society of Biomechanics Conference* (International Society of Biomechanics, ISB, 2011).

32.   Pellikaan, P., van der Krogt, M., Carbone, V., Verdonschot, N. & Koopman, B. Are muscle volumes linearly scalable in musculoskeletal models? *J. Biomech.* **45**, S498 (2012).

33.   Carbone, V., Krogt, M. Vd, Koopman, B. & Verdonschot, N. Functional scaling of subject-specific musculo-tendon parameters in the lower extremity. *J. Biomech.* **45**, S492 (2012).

34.   Redert, A., Kaptein, B., Reinders, M., van den Eelaart, I. & Hendriks, E. Extraction of semantic 3D models of human faces from stereoscopic image sequences. *Acta Stereol.* **18**, 255–264 (1999).

35.   Pellikaan, P. *et al.* Evaluation of a morphing based method to estimate muscle attachment sites of the lower extremity. *J. Biomech.* **47**, 1144–50 (2014).

36.   Kirking, B., Krevolin, J., Townsend, C., Colwell, C. W. & D'Lima, D. D. A multiaxial force-sensing implantable tibial prosthesis. *J. Biomech.* **39**, 1744–1751 (2006).

37. Damsgaard, M., Rasmussen, J., Christensen, S. T., Surma, E. & de Zee, M. Analysis of musculoskeletal systems in the AnyBody Modeling System. *Simul. Model. Pract. Theory* **14**, 1100–1111 (2006).

38. Carbone, V. *et al.* TLEM 2.0 – A comprehensive musculoskeletal geometry dataset for subject-specific modeling of lower extremity. *J. Biomech.* **48**, 734–741 (2015).

39. Parr, W. C. H., Chatterjee, H. J. & Soligo, C. Calculating the axes of rotation for the subtalar and talocrural joints using 3D bone reconstructions. *J. Biomech.* **45**, 1103–7 (2012).

40. Rasmussen, J. *et al.* A general method for scaling musculo-skeletal models. in *International Symposium on Computer Simulation in Biomechanics* (2005).

41. Andersen, M. S., Damsgaard, M., MacWilliams, B. & Rasmussen, J. A computationally efficient optimisation-based method for parameter identification of kinematically determinate and over-determinate biomechanical systems. *Comput. Methods Biomech. Biomed. Engin.* **13**, 171–83 (2010).

42. Zajac, F. E. Muscle and tendon: properties, models, scaling, and application to biomechanics and motor control. *Crit. Rev. Biomed. Eng.* **17**, 359–411 (1989).

43. Silva, M. *et al.* Knee strength after total knee arthroplasty. *J. Arthroplasty* **18**, 605–611 (2003).

44. Rasmussen, J., Damsgaard, M. & Voigt, M. Muscle recruitment by the min/max criterion — a comparative numerical study. *J. Biomech.* **34**, 409–415 (2001).

45. Holmberg, L. J. & Klarbring, A. Muscle decomposition and recruitment criteria influence muscle force estimates. *Multibody Syst. Dyn.* **28**, 283–289 (2012).

46. Happee, R. & Van Der Helm, F. C. T. The control of shoulder muscles during goal directed movements, an inverse dynamic analysis. *J. Biomech.* **28**, 1179–1191 (1995).

47. Andersen, M. S., Damsgaard, M. & Rasmussen, J. Kinematic analysis of over-determinate biomechanical systems. *Comput. Methods Biomech. Biomed. Engin.* **12**, 371–84 (2009).

48. Benoit, D. L. *et al.* Effect of skin movement artifact on knee kinematics during gait and cutting motions measured in vivo. *Gait Posture* **24**, 152–64 (2006).

49. Andersen, M. S., Benoit, D. L., Damsgaard, M., Ramsey, D. K. & Rasmussen, J. Do kinematic models reduce the effects of soft tissue artefacts in skin marker-based motion analysis? An in vivo study of knee kinematics. *J. Biomech.* **43**, 268–73 (2010).

50. Andersen, M. S., Damsgaard, M. & Rasmussen, J. Force-dependent kinematics: a new analysis method for non-conforming joints. in *XIII International Symposium on Computer Simulation in Biomechanics* (2011).

51. Bowman, K. F. & Sekiya, J. K. Anatomy and biomechanics of the posterior cruciate ligament, medial and lateral sides of the knee. *Sports Med. Arthrosc.* **18**, 222–9 (2010).

52. Chwaluk, A. & Ciszek, B. Anatomy of the posterior cruciate ligament. *Folia Morphol. (Warsz).* **68**, 8–12 (2009).

53. Starok, M., Lenchik, L., Trudell, D. & Resnick, D. Normal patellar retinaculum: MR and sonographic imaging with

cadaveric correlation. *AJR. Am. J. Roentgenol.* **168**, 1493–9 (1997).

54. Baldwin, J. L. The anatomy of the medial patellofemoral ligament. *Am. J. Sports Med.* **37**, 2355–61 (2009).

55. Desio, S. M., Burks, R. T. & Bachus, K. N. Soft tissue restraints to lateral patellar translation in the human knee. *Am. J. Sports Med.* **26**, 59–65 (1998).

56. Dopirak, R. M., Steensen, R. N. & Maurus, P. B. The medial patellofemoral ligament. *Orthopedics* **31**, 331–8 (2008).

57. Philippot, R., Boyer, B., Testa, R., Farizon, F. & Moyen, B. The role of the medial ligamentous structures on patellar tracking during knee flexion. *Knee Surg. Sports Traumatol. Arthrosc.* **20**, 331–6 (2012).

58. Heegaard, J. *et al.* Influence of soft structures on patellar three-dimensional tracking. *Clin. Orthop. Relat. Res.* 235–43 (1994).

59. Nomura, E., Horiuchi, Y. & Kihara, M. Medial patellofemoral ligament restraint in lateral patellar translation and reconstruction. *Knee* **7**, 121–127 (2000).

60. Amis, A. A., Firer, P., Mountney, J., Senavongse, W. & Thomas, N. P. Anatomy and biomechanics of the medial patellofemoral ligament. *Knee* **10**, 215–20 (2003).

61. Blankevoort, L., Kuiper, J. H., Huiskes, R. & Grootenboer, H. J. Articular contact in a three-dimensional model of the knee. *J. Biomech.* **24**, 1019–31 (1991).

62. Butler, D. L., Kay, M. D. & Stouffer, D. C. Comparison of material properties in fascicle-bone units from human patellar tendon and knee ligaments. *J. Biomech.* **19**, 425–432 (1986).

63. Conlan, T., Garth, W. P. & Lemons, J. E. Evaluation of the medial soft-tissue restraints of the extensor mechanism of the knee. *J. Bone Joint Surg. Am.* **75**, 682–693 (1993).

64. Sprague, M. A. & Geers, T. L. Spectral elements and field separation for an acoustic fluid subject to cavitation. *J. Comput. Phys.* **184**, 149–162 (2003).

65. Schwer, L. E. Validation metrics for response histories: Perspectives and case studies. *Eng. Comput.* **23**, 295–309 (2007).

66. Chen, Z. *et al.* Prediction of in vivo joint mechanics of an artificial knee implant using rigid multi-body dynamics with elastic contacts. *Proc. Inst. Mech. Eng. H.* **228**, 564–575 (2014).

67. Shelburne, K. B., Torry, M. R. & Pandy, M. G. Contributions of muscles, ligaments, and the ground-reaction force to tibiofemoral joint loading during normal gait. *J. Orthop. Res.* **24**, 1983–1990 (2006).

68. Anderson, F. C. & Pandy, M. G. Individual muscle contributions to support in normal walking. *Gait Posture* **17**, 159–169 (2003).

69. Li, G. *et al.* Cruciate-retaining and cruciate-substituting total knee arthroplasty: an in vitro comparison of the kinematics under muscle loads. *J. Arthroplasty* **16**, 150–6 (2001).

70. Lin, Y.-C., Walter, J. P., Banks, S. A., Pandy, M. G. & Fregly, B. J. Simultaneous prediction of muscle and contact forces in the knee during gait. *J. Biomech.* **43**, 945–52 (2010).

71. Kim, H. J. *et al.* Evaluation of predicted knee-joint muscle forces during gait using an instrumented knee implant. *J. Orthop. Res.* **27**, 1326–31 (2009).

72.   Martelli, S., Valente, G., Viceconti, M. & Taddei, F. Sensitivity of a subject-specific musculoskeletal model to the uncertainties on the joint axes location. *Comput. Methods Biomech. Biomed. Engin.* **18**, 1555–1563 (2015).

73.   Correa, T. A. & Pandy, M. G. A mass-length scaling law for modeling muscle strength in the lower limb. *J. Biomech.* **44**, 2782–2789 (2011).

74.   Lin, Y.-C., Haftka, R. T., Queipo, N. V & Fregly, B. J. Surrogate articular contact models for computationally efficient multibody dynamic simulations. *Med. Eng. Phys.* **32**, 584–94 (2010).

75.   Sheehan, F. T. & Drace, J. E. Human patellar tendon strain. A noninvasive, in vivo study. *Clin. Orthop. Relat. Res.* 201–7 (2000).

76.   Athwal, K. K., Hunt, N. C., Davies, A. J., Deehan, D. J. & Amis, A. a. Clinical biomechanics of instability related to total knee arthroplasty. *Clin. Biomech. (Bristol, Avon)* **29**, 119–28 (2014).

77.   Hughes, R., Bean, J. & Chaffin, D. Evaluating the effect of co-contraction in optimization models. *J. Biomech.* **2**, 875–878 (1995).

Evaluation of a surrogate contact model in force-dependent kinematic simulations of total knee replacement

Marco A. Marra, Michael S. Andersen, Michael Damsgaard, Bart F.J.M. Koopman, Dennis Janssen, and Nico Verdonschot.

ABSTRACT

Knowing the forces in the human body is of great clinical interest and musculoskeletal models are the most commonly used tool to estimate them in vivo. Unfortunately, the process of computing muscle, joint contact and ligament forces simultaneously is computationally highly demanding. The goal of this study was to develop a fast surrogate model of the tibiofemoral (TF) contact in a total knee replacement (TKR) model and apply it to force-dependent kinematic simulations of activities of daily living (ADLs). Multiple domains were populated with sample points from the reference TKR contact model, based on reference simulations and design-of-experiments. Artificial neural networks learned the relationship between TF pose and loads from the medial and lateral sides of the TKR implant. Normal and right-turn gait, rising-from-a-chair, and a squat were simulated using both surrogate and reference contact models. Compared to the reference contact model, the surrogate contact model predicted TF forces with a root-mean-square error (RMSE) lower than 10 N and TF moments lower than 0.3 Nm over all simulated activities. Secondary knee kinematics were predicted with RMSE lower than 0.2 mm and 0.2 degrees. Simulations that used the surrogate contact model ran on average three times faster than those using the reference model, allowing the simulation of a full gait cycle in 4.5 min. This modeling approach proved fast and accurate enough to perform extensive parametric analyses, such as simulating subject-specific variations and surgical-related factors in TKR.

INTRODUCTION

The calculation of forces acting on the musculoskeletal (MS) system during activities of daily living (ADLs) is of great interest as it aids in understanding how hard and soft tissues interact throughout the human body and at the joint level, and may help researchers and clinicians to understand better the mechanical pathways of MS pathologies. Body-level forces and moments are solved using multi-rigid body dynamic methods, which are normally inexpensive computationally: given a known motion and the external forces acting on the body, muscle and joint forces can be calculated by means of forward dynamics assisted data tracking and inverse dynamics with optimization-based muscle recruitment. The reader is referred to a previous extensive review of these techniques[1]. At the joint and tissue level, more advanced techniques—such as finite-element (FE) or elastic-foundation (EF) analyses—are required to represent the contact interactions between articulating surfaces and solve for ligament forces and secondary motions of the joints.

Despite its great appeal, the coupling of such techniques for solving tissue-level and body-level mechanics is overall a highly computationally demanding process, up to a point that may hinder its clinical applicability or impede parametric and/or optimization analyses on a large scale. Recently, the force-dependent kinematic (FDK) method[2] was applied to estimate leg muscle forces, knee ligament and contact forces and secondary kinematics simultaneously in a MS model of a patient having a total knee replacement (TKR)[3]. However, the computational burden in that study was considerable, as it took more than four hours to analyze a single cycle of normal gait.

Surrogate models have been proposed to reduce the computational burden of MS simulations while retaining a reasonable level of accuracy. Halloran et al. demonstrated adaptive surrogate modeling techniques to accelerate the optimization of a jump height in a combined MS-FE model of the foot[4]. Surrogate models for the analysis of native knee joint forces[5,6], cartilage stresses[7] and tibiofemoral (TF) contact interactions and wear in total knee replacement (TKR)[8–11] were also reported. These models utilized a variety of techniques, such as response surface optimization[6], Lazy Learning[4], nonlinear dynamic models[5], Kriging[8–10], and artificial neural networks (ANN)[5,7,11]. Recently, Eskinazi and Fregly proposed a surrogate modeling approach based

on ANN to accelerate an FE deformable contact model of TKR[11]. Artificial neural networks are known, among others, for their ability to learn virtually any complex relationship between a set of input and output variables[12]. For instance, for the knee joint, one would train ANNs using outcomes of repeated contact analyses of expensive reference FE or EF models, and subsequently fit the relationships between TF pose and the resultant TF contact forces and moments. Then, within a musculoskeletal analysis, the surrogate model would replace the reference contact model, providing a significant reduction in computation time. However, the performance of surrogate contact models for the simultaneous estimation of muscle forces, TF ligament and contact forces and secondary kinematics during activities of daily living (ADLs) has not been demonstrated yet.

The aim of this study is to create and test a surrogate contact model of a TKR and to demonstrate its applicability in predicting muscle, ligament and TF contact forces and secondary kinematics simultaneously during normal gait, right-turn gait, rising-from-a-chair, and squat. We addressed the following specific questions: 1) how much reduction in simulation time is obtained and 2) how well is accuracy retained when a surrogate contact model is used instead of the reference contact model?

METHODS

A previously validated patient-specific MS model of a patient with a telemetric knee prosthesis was the basis for this study[3]. The model was built using the AnyBody Modeling System (AMS, version 6, AnyBody Technology A/S, Aalborg, Denmark)[13] and included head, two arms, trunk, pelvis and two legs. Further details can be found elsewhere[3]. The analysis workflow consisted of two stages: a motion optimization (MO) and force-dependent kinematics (FDK), which applies inverse dynamic analysis as part of the solution process. In the first stage (MO), the full-body model was driven using marker trajectories from motion-capture data, and joint kinematics were optimized using an inverse kinematic analysis[14]. The AMS applies a full Cartesian formulation in which each body is described by the translation of the segment origin and the segment orientation specified with Euler parameters. The relative movement between the segments is restricted by constraint equations, which, in this case, allowed three translation and three rotations of

the pelvis segment relative to the global reference frame, three pelvis-trunk rotations, neck extension and for each leg, three hip rotations, knee flexion, ankle plantarflexion and subtalar eversion. In the second stage (FDK), the optimized joint kinematics from MO stage and the experimental ground reaction forces and moments (GRF&Ms) were input to an FDK model, which solved for the 166 Hill-type muscle element forces spanning the lower extremity, TF ligament and contact forces, and secondary TF joint kinematics under an assumption of quasi-static equilibrium within the joint[2]. To save computation time, the right (unaffected) leg and both arms were excluded from the FDK analyses and artificial reaction forces and moments were added to the pelvis segment to compensate for kinematic-kinetic inconsistencies.

Description of the reference contact model

The reference TKR contact model of a left knee used in this study was extracted from the aforementioned MS model. It consisted of two contact pairs defined by the femoral component and the medial and lateral side of the tibial insert, respectively. Implant geometries were obtained from the 5th "Grand Challenge Competition to Predict In Vivo Knee Loads" dataset[15]. TF contact forces and moments were calculated using a linear pressure-overclosure relationship between the articulating surfaces, in which the contact forces were a linear function of the penetration volume, with a factor (pressure modulus) of 9.3 GN/m³, as in a previous model[3].

To generate a surrogate contact model of TKR, it was necessary to find the relationship between contact forces and moments resulting from the relative pose between the tibial and femoral component. For this, we used a design-of-experiment approach to define a model sampling scheme to obtain the desired input-output relations. Subsequently, we fitted the samples obtained from repeated evaluation of the reference contact model using ANN until convergence criteria were reached. Details of this procedure are herein provided.

The tibial component, consisting of medial and lateral contact surfaces, was fixed to the global reference frame. The femoral component was free to move in space having 6 DOFs relative to the global frame. Thus, the relative TF pose could be defined by three translations and three rotations between tibial (fixed) and femoral (moving) frames of reference (Figure 3.1). Tibiofemoral
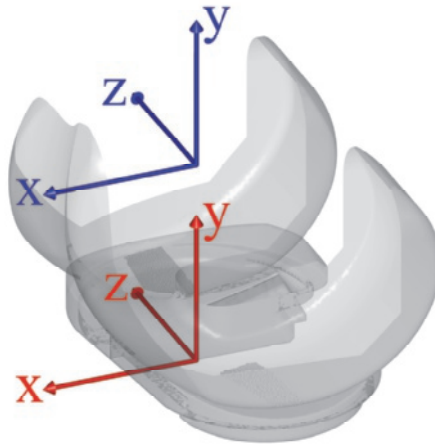
Figure 3.1 Contact model of TKR. The TF pose is defined by the relative translation and rotation between the femoral component frame (blue) and the tibial component frame (red). Tibiofemoral translations are expressed in the tibial component frame of reference, and represent anterior femur translation (x), joint distraction (y), and medial femur translation (z). Tibiofemoral rotations are expressed in the femoral component frame of reference with Cardan angles using the *z-y-x* sequence of rotations, where the first rotation represent knee extension, the second, tibial external rotation, and the third, knee abduction. Rigid surface contact based on pressure-overclosure is defined between medial and lateral side of tibial component and femoral component. To obtain samples for the surrogate model, this contact model is evaluated using repeated static analyses.

translations were defined as the translations of the femoral component frame measured with respect to the tibial frame of reference, and corresponded to anterior femur translation (*x*), joint distraction (*y*), and medial femur translation (*z*), respectively. Tibiofemoral rotations were defined using Tait-Bryan angles with the 'z-y-x' sequence of intrinsic rotations from the femoral component body frame to the tibial component body frame. This rotation sequence allowed the description of knee abduction (θ_x) around a well-defined axis fixed in the tibial body. As will become clearer in the next section, knee abduction was a sensitive rotation, therefore, it was allowed to vary according to the abduction torque applied. Letting knee abduction be the last rotation in the sequence, a change in the rotation did not affect the remaining two non-sensitive rotations (θ_z and θ_y). Please note that the used sequence ('z-y-x' rotations from femur to tibia) is equivalent to a 'x-y-z' rotation sequence from tibia to femur, as defined in a previous paper[11], with an opposite sign

convention. Furthermore, the assumptions of conservative (friction-less) and linear elastic contact were made. Under these conditions, it was possible to simplify the contact formulation and assume the contact forces and moments to depend purely on TF pose. Tibio-femoral forces and moments resulting from medial and lateral contact analyses were measured with respect to the origin of the femoral coordinate system and expressed in the tibial reference frame. They will be referred to as F_x^{Med}, F_y^{Med}, F_z^{Med}, M_x^{Med}, M_y^{Med}, M_z^{Med}, for the medial side, and F_x^{Lat}, F_y^{Lat}, F_z^{Lat}, M_x^{Lat}, M_y^{Lat}, M_z^{Lat}, for the lateral side, in which the subscripts indicate the direction of application of the load. The resultant forces and moments from the medial and lateral sides combined could be conveniently expressed as the total TF loads: F_x^{Tot}, F_y^{Tot}, F_z^{Tot}, M_x^{Tot}, M_y^{Tot}, M_z^{Tot}.

Sampling of the reference contact model

An efficient sampling plan was necessary to ensure coverage of the design space. Ideally, the surrogate model should have a perfect fit in all areas of the design space, which are likely to occur in a simulation, and also adequate in less probable areas, in order to prevent the contact algorithm from producing unacceptably large prediction errors. Due to the particular geometry of the articulating surfaces in TKR, there are specific directions in which minimal variations of the TF pose induce very large variations in the corresponding TF loads. These are referred to as *sensitive directions*[8]. To identify possible sensitive directions in our contact model, we configured a reference TF pose in which all rotations and the anterior and medial femur translation were null and the femoral component "just touched" the tibial component. Subsequently, we perturbed the TF pose and analyzed the TF load response. We identified two sensitive directions, being the joint distraction (y) and the knee abduction (θ_x), respectively. The presence of sensitive directions suggested a definition of sample points as combinations of pose parameters in non-sensitive directions and loads in sensitive directions: {x, F_y^{Tot}, z, M_x^{Tot}, θ_y, θ_z}, as in a previous paper[8]. This definition was adopted to sample two-sided contact and contact boundary cases. To ensure a wider coverage of the design space, one ought to include also out-of-contact and single-sided contact cases[11]. In such cases, we adopted different definitions of the sample point, namely {x, y, z, θ_x, θ_y, θ_z} for out-of-contact cases, for which the femoral component could be freely moved far away from the tibial insert, and {x, F_y^{Tot},

z, θ_x, θ_y, θ_z} for single-sided contact cases, for which the knee abduction angle could be explicitly prescribed so as to produce lift-off on either sides, as in a previous paper[11].

To define reasonable boundaries for the design space, we estimated and extracted TF load-pose data from five reference FDK analyses of ADLs obtained using our MS model with the reference contact model. These activities included one walking cycle of normal gait, one of right-turn gait, an unloaded leg-swing, two repetitions of a rising-from-a-chair task, and four repetitions of a squatting motion, for which motion-capture data were available as part of the Grand Challenge dataset[15]. Differently than in the study of Eskinazi and Fregly, in which reference curves were extracted from 14 gait cycles[11], we included reference curves from several types of ADLs, with the aim of generalizing the capabilities of the surrogate contact model for future use, as we plan to apply the surrogate model in MS analyses involving different loading conditions and ranges of motion.

To take into account different contact cases, we adopted a multi-domain approach, as in the study of Eskinazi and Fregly[11], and we chose the Hammersley quasi-random (HQ) sequence[16] to evenly distribute points in each domain (Table 3.1). However, some different choices were made for distributing samples points across domains, as detailed below. By using multiple domains, we attempted to maximize the coverage of areas of the design space that are as likely to occur as normal two-sided contact during the analysis of ADLs, for instance including lift-off of one or both of the two sides of the implant, or situations where the implant surfaces are barely in contact. Domain 1 consisted of data points spanning the boundaries of ± 1 standard deviation (SD) from the time-varying envelopes of each of the aforementioned reference analyses. This domain compared to domains D1 and D2 in the study of Eskinazi and Fregly[11], with the differences being the expansion factor of 1 SD (our method) as opposed to 20 % and 100 % (their method), and the fewer points sampled. For each time-frame, 20 data points were sampled, resulting in 18060 points. Our Domain 2 was comparable to domain D3 in a previous paper[11], though the sampling process was different. We first performed a principal component analysis (PCA) of the reference data, then we enlarged the envelopes of the principal components (PCs) by 50 % and we sampled data points in the new PC space. Finally, we transformed the PC samples back to the original variables space. By pre-transforming the domain space using

Table 3.1 Sampling domains, number of samples and approximate sampling time for each domain.

Domain	Description	Number of training samples	Number of testing samples	Approximate sampling time[a] core time (effective time)
1	Time-varying local envelopes of reference simulations expanded by 1 SD	18 060	-	102 (25) hours
2	Global envelopes of reference simulations expanded by 50 %	27 253	3 416	226 (57) hours
3	Single-sided contact (lift-off cases)	10 000	1 765	47 (12) hours
4	Contact boundary (swing phase)	9 990	1 755	70 (17) hours
5	Out-of-contact, proximity cases (y up to 2 mm, in four steps)	67 760	11 958	11 (3) hours
6	Out-of-contact, far away cases (y up to 10 cm, coarse)	2 000	353	15 (4) min
	Total	134 973	19 247	456 (114) hours

PCA, the resulting samples points were more densely distributed around the data points of the reference curves. This domain enlarged substantially the coverage with respect to the Domain 1, while still retaining the gross inter-variability between the sampling variables, owing to PCA pre-transformation. Domain 3 represented single-sided contact, similarly to domain D4 in a previous paper[11], which simulated lift-off of one of the two sides of the implant. The sampling point was defined as $\{x, F_y^{Tot}, z, \theta_x, \theta_y, \theta_z\}$. Differently than in a previous paper[11], the PCA approach was used for the TF pose parameters and an upper boundary equal to 100 N was set on F_y^{Tot} (lower boundary was 0 N), which covered situations with low contact forces on either sides. Domain 4 consisted of contact boundary points, similar to domains D6 and D7 in a previous paper[11], in which one or both sides were barely touching. This domain accounted, for instance, for situations in which the leg would enter the swing phase of gait, and the TF loads would progressively decrease. The sample point definition for this domain was $\{x, F_y^{Tot}, z, M_x^{Tot}, \theta_y, \theta_z\}$, thus we set an upper boundary of 100 N on F_y^{Tot}, and a lower and upper boundary

of $\pm$ 5 Nm on $M_x{}^{Tot}$. This choice differed from that of Eskinazi and Fregly for domain D6 and D7, in which the medial and lateral vertical contact forces were kept fixed at 5 N, simultaneously or alternately, while sampling the TF pose parameters. Domains 5 and Domain 6 were populated with samples representing both sides out-of-contact cases, in which the femoral component was in the proximity (Domain 5) and far away (Domain 6) from the tibial insert, respectively. The sample point definition was $\{x, y, z, \theta_x, \theta_y, \theta_z\}$. Our Domain 5 was comparable to domain D5 in ref.[11], but we sampled a much larger number of points. In this domain, the contact boundary samples were re-used, and the distraction was raised up to 2 mm in four increments (as opposed to three in a previous paper[11]). Furthermore, we extended the out-of-contact coverage with Domain 6, to ensure that the response of the surrogate model did not diverge dramatically when the femoral component separated substantially from the tibial component, providing additional robustness to the surrogate model. In Domain 6, boundaries on the y translation were set between the maximum y translation of contact boundary cases and 10 cm.

All sample points were evaluated by repeated static analyses using the reference contact model (Figure 3.1), to obtain the combinations of TF pose and corresponding TF loads. As for Domains 5 and 6—in which samples consisted purely of pose parameters—the analysis was displacement-driven and TF loads solved for using ordinary inverse dynamics. Sampling domains that included sensitive directions for certain loads (Domains 1-to-4) were analyzed using a combination of displacement-driven and force-driven analyses, where TF pose parameters in non-sensitive directions and loads in sensitive directions were prescribed, whereas TF pose parameters in sensitive directions and loads in non-sensitive directions were simultaneously solved for using FDK analyses. In these cases, the FDK algorithm solved for the unknown TF pose parameters in sensitive directions that put the system in static equilibrium, under the application of TF loads in sensitive directions and the prescribed pose in non-sensitive directions. Errors of up to 0.1% of the applied loads were tolerated, whereas samples that led to larger errors were discarded. Additionally, samples that led to TF component overclosure larger than 2 mm were also filtered out. Approximately 85% of all the successful sample points were allocated for surrogate model training. The remaining 15% were assigned to a separate testing dataset. No samples were allocated for
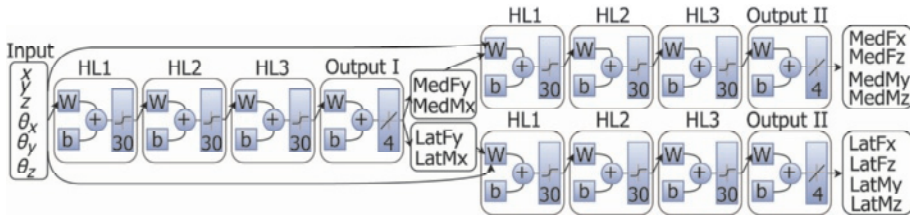
Figure 3.2 Diagram of the 2-stage feedforward artificial neural network (ANN). The stage I network (left) learned the relations between TF loads in sensitive directions (F_y^{Med}, T_x^{Med}, F_y^{Lat}, T_x^{Lat}) and the TF pose parameters; in stage II (right) the remaining TF loads of medial (lateral) side are obtained as functions of the TF pose and the medial (lateral) TF loads from stage I. HL: hidden layers, W: network weights, b: network biases.

testing in Domain 1, as the accuracy in this sort of domain would be better evaluated by FDK analysis of ADLs.

Training of the surrogate contact model

Multiple-input multiple-output feedforward ANNs were configured in MATLAB (version 8.6.0, The MathWorks Inc., Natick, MA) using the Neural Network Toolbox (Figure 3.2). As opposed to the study of Eskinazi and Fregly, who interconnected multiple ANNs, each with multiple inputs and a single output[11], we opted for ANNs with multiple inputs and multiple outputs in an attempt to exploit the correlation likely to exist between different output variables. Similarly to a previous paper[11], the training phase consisted of two stages: in the first stage, one ANN learned the relationship between medial and lateral TF loads in sensitive directions, $\{F_y^{Lat}, M_x^{Lat}, F_y^{Med}, M_x^{Med}\}$, and the TF pose, $\{x, y, z, \theta_x, \theta_y, \theta_z\}$; in the second stage, two additional ANNs learned the relations between the remaining medial and lateral TF loads separately, and a combination of TF pose parameters and sensitive loads of either side. This allowed proper learning of the out-of-contact cases, in which zero loads may correspond to many different combinations of pose parameters and to have fully independent medial and lateral surrogate contact models.

Given the impossibility to establish *a priori* the correct number of layers and neurons, a heuristic method was used to decide both number of network layers and neurons per layer. We started with two hidden layers and ten neurons per layer. We started the network training and recorded the value of the performance function after one hour. If the performance value fell below

0.001, then we would accept the current network configuration, else we would primarily add ten neurons to each layer (up to forty neurons in total per layer) and, secondly, add one more hidden layer. After each network modification we would repeat the one-hour training test. This process led us to a final network configuration consisting of three hidden layers with thirty neurons per layer, having hyperbolic tangent sigmoid transfer function. The network was then completed with one output layer of purely linear neurons.

Each network was trained using the MATLAB training function *trainbr*, which uses Bayesian regularization within the Levenberg-Marquardt backpropagation algorithm. According to this training scheme, the performance function to be minimized was a linear combination of squared errors and weights, in which the coefficients were continuously updated to prevent data over-fitting and lead to networks with good generalization qualities. Each network trained for at least 18 hours and the training was stopped only after the performance function visibly converged.

After training succeeded, the weights and biases of each network were exported as standalone functions using built-in MATLAB capabilities. Custom-written MATLAB routines translated those standalone functions into C++ code. The Eigen template library[17] was used to represent and operate on numerical data in the C++ surrogate model functions. The latter were then built together as a dynamic-link library (DLL) to maximize efficiency. A post hoc condition was defined in the surrogate model functions: if the medial or lateral TF force in the *y* direction was negative or equal to zero, then all remaining loads on the respective side were immediately assigned zero as well, without calculating the output of the second stage.

Testing of the surrogate contact model and performance of simulated ADLs

We used the surrogate contact model functions to evaluate the sample points from the testing dataset, and reported the testing performances using the coefficient of determination (R^2, defined by 1 - sum of squares of residuals divided by total sum of squares) and the root-mean-square error (RMSE) of output medial and lateral TF loads relative to targets.

We then replaced the reference contact model of the MS model with the newly built surrogate contact model. This was achieved using C++ hook

capabilities of the AMS, which can load external DLL functions and make them available to the model during run time. In this way, the medial and lateral TF contact loads were obtained by executing function calls to the respective medial and lateral surrogate model DLL functions, using the current TF pose as input argument. Differently from our previous MS model[3], in which the computation of muscles and ligament lines of action—or wrapping algorithm—was carried out using numerical methods, in this study, we opted for an analytical solution[*], to prevent possible hindrances to the true performances of the surrogate model. Moreover, since we were interested in testing a surrogate model of a TKR TF joint, we replaced the patellofemoral (PF) joint with an ideal revolute joint and let the only DOF of patella be controlled by an elastic patellar ligament (stiffness 1187 N/mm). During an analysis, the FDK algorithm explored the TF pose space until a quasi-static equilibrium was reached, and to do so it iteratively executed function calls to the surrogate model, rather than executing function calls to the reference contact model. To evaluate the performance of the surrogate contact model for the analysis of dynamic motor tasks, we simulated four ADLs using both the reference and the surrogate contact model. We simulated one walking cycle of normal gait, one of right-turn gait, two repetitions of a rising-from-a-chair task, and four repetitions of a squatting motion for which motion capture data were available as part of the Grand Challenge dataset[15]. For each activity and for each contact model, we estimated TF forces, moments and six-DOF knee kinematics and we evaluated the accuracy of the surrogate model predictions compared to the predictions obtained with the reference model. We calculated R^2, RMSE, and maximum prediction errors for all TF forces, moments, and kinematics. Knee kinematics were defined according to a knee joint coordinate system consistent with the description of Grood and Suntay[18]. Tibiofemoral rotations were defined using Tait-Bryan angles with the 'z-x-y' sequence of intrinsic rotations from the femoral component body frame to the tibial component body frame. Note that this convention differed from that used during the sampling process; however, this choice was justified to provide a physically meaningful description of knee kinematics; namely,

---

[*] The algorithm for the analytical solution is not part of the AMS release and it was provided separately to us by AnyBody Technology A/S in a prototype version that solved a single cylindrical wrapping case.

Table 3.2 RMS (maximum) prediction errors of medial (Med) and lateral (Lat) TF loads for the testing dataset in each sampling domain.

Domain	Side	F_x (N)	F_y (N)	F_z (N)	M_x (Nm)	M_y (Nm)	M_z (Nm)
2	Med	3.8 (58)	18 (462)	3.2 (32)	0.44 (9.7)	0.09 (1.4)	0.21 (6.5)
	Lat	12 (379)	69 (1863)	9.3 (315)	1.8 (50)	0.32 (11)	1.1 (41)
3	Med	3.9 (32)	20 (113)	6.8 (81)	0.46 (2.9)	0.14 (1.5)	0.21 (1.7)
	Lat	5.2 (48)	29 (191)	8.0 (126)	0.71 (5.3)	0.19 (2.3)	0.40 (6.7)
4	Med	2.1 (23)	9.9 (108)	3.9 (41)	0.26 (2.3)	0.07 (0.58)	0.12 (2.3)
	Lat	2.3 (14)	13 (77)	3.3 (49)	0.35 (2.3)	0.07 (0.51)	0.14 (1.1)
5	Med	0.13 (3.2)	1.0 (16)	0.44 (8.0)	0.03 (0.57)	0.01 (0.11)	0.01 (0.16)
	Lat	0.15 (5.3)	1.4 (25)	0.20 (5.4)	0.04 (0.42)	0.00 (0.21)	0.01 (0.15)
6	Med	8.4 (140)	17 (273)	3.2 (41)	0.72 (12)	0.13 (2.0)	0.02 (0.3)
	Lat	44 (602)	76 (1192)	51 (727)	1.9 (28)	1.8 (21)	0.77 (11)

anterior tibial translation, joint distraction, lateral tibial translation, knee flexion, knee adduction, and tibial external rotation. Additionally, we compared the computation times required to complete the FDK analyses with either contact model.

RESULTS

On the testing dataset, the surrogate model predicted medial and lateral TF loads with an R^2 value greater than 0.99 and 0.96, respectively, for all components of force and moment. The largest medial and lateral RMS force errors (Table 3.2) were observed in F_y^{Lat} (76 N, Domain 6) and F_y^{Med} (20 N, Domain 3), respectively. The largest medial and lateral RMS moment errors were observed in M_x^{Med} (0.72 Nm, Domain 6) and M_x^{Lat} (1.9 Nm, Domain 6). Maximum errors were in most cases one to two orders of magnitude larger than RMS errors, indicating the presence of extreme outliers. The largest maximum errors were 1863 N in F_y^{Lat} and 50 Nm in M_x^{Lat}, both found on Domain 2.

On the simulations of normal gait, right-turn gait, rising-from-a-chair, and squat, medial and lateral TF loads were predicted with an R^2 value greater than 0.99 and 0.98 in all cases (Figure 3.3). The knee kinematics obtained with the surrogate model agreed to those obtained with the reference model with an R^2 value greater than 0.96 in all cases (Figure 3.4), except for lateral tibial translation in the normal gait ($R^2 = 0.93$). The largest RMS errors among all
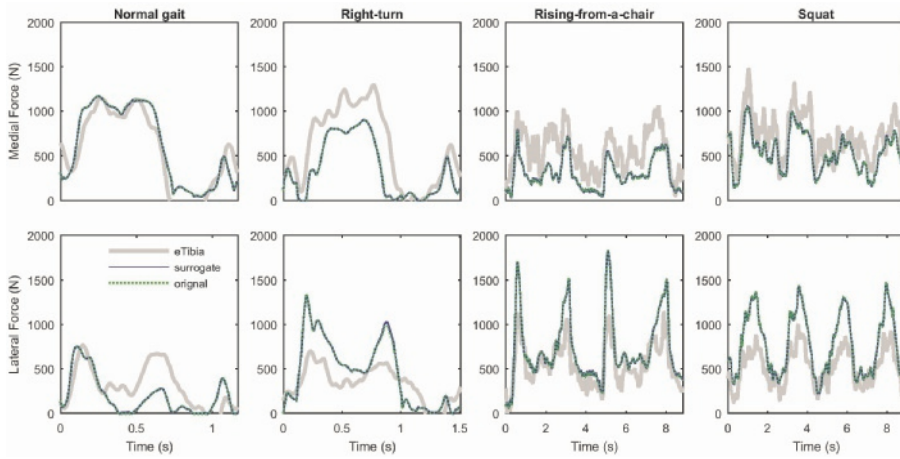
Figure 3.3 Medial (top) and lateral (bottom) TF compressive forces during normal gait, right-turn, rising-from-a-chair, squat simulation. Reference measured force (eTibia, shaded), predictions using surrogate (solid) and reference (dotted) contact model.

Table 3.3 RMS (maximum) prediction errors of medial (Med) and lateral (Lat) TF loads for normal gait, right-turn, rising-from-a-chair, and squat.

Trial	Side	F_x (N)	F_y (N)	F_z (N)	M_x (Nm)	M_y (Nm)	M_z (Nm)
Normal gait	Med	0.50 (2.2)	4.2 (14)	1.1 (11)	0.17 (1.4)	0.02 (0.09)	0.04 (0.17)
	Lat	0.50 (2.0)	4.4 (17)	0.43 (2.7)	0.12 (0.54)	0.02 (0.08)	0.01 (0.05)
Right-turn	Med	0.49 (3.0)	4.3 (24)	2.2 (11)	0.14 (0.65)	0.04 (0.18)	0.04 (0.16)
	Lat	0.95 (4.8)	9.9 (47)	2.2 (21)	0.26 (1.2)	0.03 (0.17)	0.10 (0.6)
Rising-from-a-chair	Med	0.85 (2.7)	5.6 (13)	0.51 (1.5)	0.11 (0.28)	0.01 (0.04)	0.06 (0.14)
	Lat	0.57 (2.0)	5.7 (13)	0.66 (2.1)	0.11 (0.30)	0.02 (0.07)	0.06 (0.16)
Squat	Med	0.34 (1.1)	4.2 (10)	0.51 (2.0)	0.10 (0.23)	0.01 (0.02)	0.06 (0.15)
	Lat	0.29 (0.96)	3.7 (11)	0.55 (2.2)	0.10 (0.23)	0.01 (0.04)	0.04 (0.13)

trials (Table 3.3) were 5.6 N in F_y^{Med} and 9.9 N in F_y^{Lat}, and 0.17 Nm in M_x^{Med} and 0.26 Nm in M_x^{Lat}. The largest maximum errors on TF loads were 47 N for F_y^{Lat} in the right-turn and 1.4 Nm for M_x^{Med} in the normal gait. The largest RMS errors in knee kinematics (Table 3.4) were found in lateral tibial translation (0.13 mm) and tibial external rotation (0.17 degrees) in the right-turn. Maximum errors reached up to 0.90 mm for anterior tibial translation and up to 1.27 degrees for tibial external rotation, both in the right-turn.
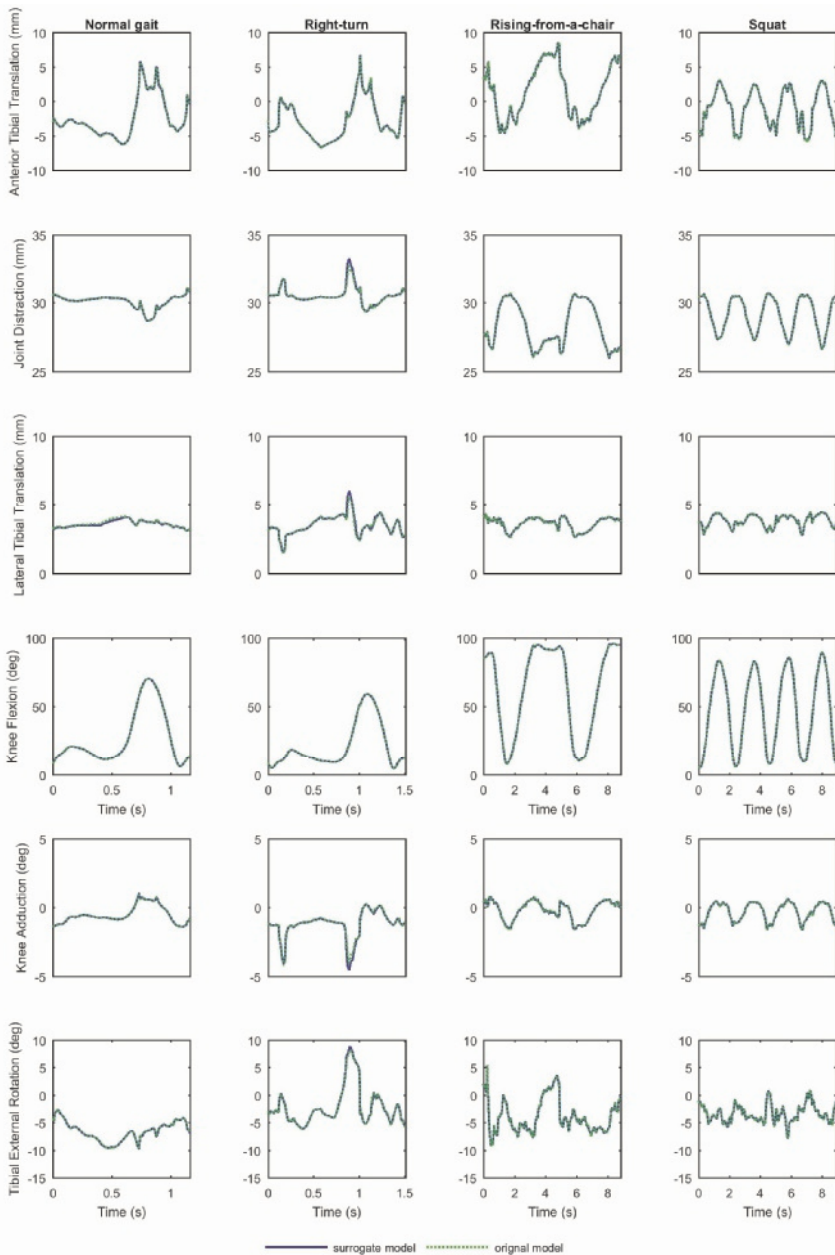
Figure 3.4 Anterior tibial translation, joint distraction, lateral tibial translation, knee flexion, knee adduction and tibial external rotation predicted using the reference contact model (solid line) and the surrogate contact model (dotted line) during normal gait, right-turn, rising-from-a-chair, and squat simulation.

Table 3.4 RMS (maximum) prediction errors of knee kinematic parameters for normal gait, right-turn, rising-from-a-chair, and squat.

Trial	Anterior Tibial Translation (mm)	Joint Distraction (mm)	Lateral Tibial Translation (mm)	Knee Flexion (deg)	Knee Adduction (deg)	Tibial External Rotation (deg)
Normal gait	0.06 (0.34)	0.01 (0.06)	0.07 (0.15)	0.00 (0.00)	0.01 (0.06)	0.04 (0.30)
Right-turn	0.12 (0.90)	0.10 (0.62)	0.13 (0.84)	0.09 (0.43)	0.14 (0.72)	0.17 (1.27)
Rising-from-a-chair	0.03 (0.16)	0.01 (0.03)	0.01 (0.08)	0.01 (0.02)	0.01 (0.06)	0.03 (0.14)
Squat	0.02 (0.10)	0.00 (0.01)	0.00 (0.03)	0.00 (0.02)	0.01 (0.02)	0.03 (0.10)

Table 3.5 Simulation times and speed improvement for surrogate vs. reference contact model for normal gait, right-turn, rising-from-a-chair, and squat.

Trial	Number of time-frames	Trial duration (s)	FDK simulation time		Speed improvement
			Reference model (min)	Surrogate model (min)	
Normal gait	146	1.2	13.6	4.5	3.0×
Right-turn	187	1.5	22.7	7.3	3.1×
Rising-from-a-chair	1066	8.8	70.3	27.2	2.6×
Squat	1074	8.9	96.4	38.5	2.5×

Simulation times (Table 3.5) were 4.5 and 13.6 min for the normal gait, 7.3 and 22.7 min for the right-turn trial, 27.2 and 70.3 min for the rising-from-a-chair trial, and 38.5 and 96.4 min for the squat trial, when using the surrogate and reference contact model, respectively. The speed improvement introduced by the surrogate model was greater than 2.5 times for the squat and rising-from-a-chair trials, and greater than 3 times for the normal gait and right-turn trials, thus it was greatest in trials with a short duration and a fewer number of time frames analyzed (less than 2 s/200 frames), as opposed to trials with a longer duration (more than 8 s/1000 frames).

DISCUSSION

In this study, we successfully incorporated a surrogate contact model of a TKR based on ANNs into a MS model that solved for lower extremity muscle, TF ligament and contact forces and secondary TF kinematics simultaneously. Tibiofemoral contact forces and moments and secondary kinematics were predicted almost as accurately as with the reference contact model in all ADLs, but within a third of the time. The ability to reduce the computation time of MS analyses is an important step forward towards the application of MS models in extensive parametric studies and/or the planning of orthopedic interventions through optimization.

The prediction errors remained low across the different ADLs analyzed and among different components of the loads. For instance, RMS errors on TF compressive forces were on average less than 1% of peak forces reported for gait[19]. The RMS and maximum errors were lower than 10 N/0.26 Nm and 47 N/1.4 Nm for all load components, respectively. The sampling scheme based on multiple domains proved thus effective in providing a good coverage for the contact conditions arising during the ADLs simulated.

The RMS errors for the prediction of TF contact forces and moments during gait simulations (1.9 N/0.063 Nm) were on the same order of magnitude but slightly lower than the errors reported by Eskinazi and Fregly (2.6 N/0.078 Nm)[11]. Sub-millimeter and sub-degree accuracy was also achieved in predictions of secondary knee kinematics in all ADLs investigated, indicating that the iterative process that computed the quasi-static equilibrium in the secondary knee DOFs converged to very similar results. Moreover, when the goal is to capture the overall kinematics for various ADLs, as was in the current study, small errors in the TF loads predicted by the surrogate model do not critically affect the kinematic results of the simulations. None of the previous studies reported on the accuracy of secondary knee kinematics predicted concurrently with muscle, ligament and contact forces using a surrogate TF contact model.

The time to complete an FDK analysis of the ADLs investigated in this study was reduced by about three times when the surrogate contact model replaced the reference contact model. The speed improvement appeared quite modest and warranted further exploration. To exclude possible hidden overhead

within the surrogate model functions, we investigated the execution time of isolated surrogate contact model function calls: this was on the order of 77 μs per evaluation, as opposed to 78 ms for the reference contact model. Thus, at the level of isolated function calls, the surrogate model was about 1000x faster than the reference contact model, as expected, however such a speed improvement did not extend to FDK analyses of ADLs. This can be explained by other time-consuming processes taking place within such analysis; namely, the kinematic analysis, and the optimization that solved the muscle recruitment problem. Both processes were solved numerically using iterative algorithms which themselves added overhead. Replacing the reference contact model with a faster surrogate contact model removed a part of this overhead.

A full gait cycle could be analyzed in just 4.5 min, using a surrogate contact model, which is of practical advantage in many cases. Extensive parametric studies often require repeating similar analyses hundreds or thousands of times to assess the influence of individual parameters. For instance, it could be interesting to study the performances of a certain implant design under varying subject-specific factors, such as height, weight, muscle strength, soft tissue characteristics, and limb alignment and/or implant related factors, such as implant alignment. In all these cases, very low computation times would be highly beneficial, as it would eliminate an important bottleneck in the implementation of such analyses.

The simulation time to analyze one walking cycle of normal gait (4.5 min) was almost one order of magnitude smaller than the time reported by a previous study that used surrogate contact models of both TF and PF joints (42 min)[9]. Our model did not include a PF joint contact model; however, it included 166 Hill-type muscles elements spanning the entire lower extremity, in addition to TF ligaments and contact forces, as opposed to the other study, which included only eleven muscles spanning the knee joint and omitted all knee ligaments except the patellar ligament[9]. Other studies which did not employ surrogate models reported simulation times to complete a forward and inverse dynamic analysis of one walking cycle which were comparable to ours (a few to ten minutes)[20–22]. However, these models did not include muscles and some motions were input to the simulations; namely, knee anterior-posterior translation and internal-external rotation. The analysis approach of the present study solved for the muscle forces of the entire lower extremity and did not prescribe any of the secondary knee kinematics. We believe that

estimating muscle, ligament and joint contact forces and secondary knee kinematics simultaneously—rather than prescribing or neglecting any of them—is essential if the aim is to investigate the effect of implant-related factors on the overall joint function, as any of the aforementioned outcomes may affect and/or be affected by the different implant conditions. Thus, when the higher computational complexity of our modeling approach is taken into account, the time performances appear more than justified.

When evaluating the surrogate model over a testing dataset, RMS prediction errors were all lower than 76 N (F_y^{Lat} on Domain 6) and 1.9 Nm (M_x^{Lat} on Domain 6). The presence of extreme outliers was also noted, as testified by maximum errors in certain domains that were orders of magnitude higher than the RMS errors in those domains: 1863 N for F_y^{Lat} and 50 Nm for M_x^{Lat}, both on Domain 2. This signifies the presence of tiny areas of the design space that the surrogate model could not learn accurately enough and for which it produced large errors. This could have happened if, for instance, too few sample points were available in those areas during training of the surrogate model, resulting in large testing errors, or if an insufficient number of hidden layers was used in the ANN. A careful inspection of the 'problematic' points revealed that the corresponding pose parameters referred to non-physiological situations, with the femoral component almost below the tibial insert and/or rotated to a very large extent. Such cases are very unlikely encountered in realistic contact situations, and, therefore, they should not constitute a serious problem. If we exclude from the comparison our Domain 6, which does not have an analogous in a previous study[11], then the largest errors were found on analogous domains in both studies; namely, our Domain 2 and their domain 'D3', which represented an expansion of the global reference curves. In these analogous domains, the largest RMS (maximum) errors in our study were 69 N/1.8 Nm (1863 N/50 Nm) as opposed to 14 N/0.4 Nm (249 N/4.7 Nm) in a previous paper[11]. Thus, our RMS (maximum) errors were up to five (ten) times larger, which could be due to the different sampling choices (we used an expansion factor that was twice as large) and/or different surrogate model architectures.

A surrogate contact modeling toolbox (SCMT) for the creation of surrogate contact models was recently presented and made freely available by Eskinazi and Fregly[23]. This toolbox was tested for the replacement of an EF contact model of both TF and PF joints in a TKR model. In this study, we developed

our own surrogate model creation process, as the reference contact model of TKR was already available, as part of a previously published MS model validated against knee forces and kinematics[3]. Furthermore, the previously published toolbox could not easily connect to our modeling environment, which let us pursue the development of a dedicated surrogate model creation process.

Our surrogate modeling approach introduced some novel aspects, as compared to previous studies, which are worth discussing. First, an advantage of the used FDK approach is that it eliminates the sensitivity of predicted muscle, ligament, and joint contact forces to errors in the location of a fixed knee flexion-extension axis when such is assumed in the applied knee model. When a fixed knee flexion-extension axis is used, typically only muscle forces are assumed to contribute to the net joint moment about the fixed axis, whereas the contribution from contact and ligament forces are neglected. Using FDK, the joint DOFs are left free to equilibrate under the compound action of muscle, ligaments and contact forces (in a quasi-static fashion) and no assumptions are required about the DOFs to which contact (and ligament) forces do not, and do, contribute. This methodology relieves very much the efforts when modeling complex non-conforming joints, such as the knee[2]. Second, pre-transforming the sampling variables using PCA in Domain 2 and Domain 3 likely made our sampling scheme more efficient, as the resulting sample points could be more densely distributed close to the data points from the reference curves. This is due to the PCA being able to decouple the original variables, thus allowing sampling along the principal directions of the reference data points. Third, although an explicit comparison was not performed in this study, choosing multiple-output instead of single-output ANNs may have benefitted the final accuracy, as the covariance existing between the output loads was taken into account during the fitting process, whereas single-output ANNs would fit each of the output variables independently from the others. However, this should be investigated in a future study. Fourth, using Bayesian regularization as part of the ANN training algorithm helped preventing data over-fitting and producing ANNs with good generalization qualities. Using a training algorithm that does not intrinsically over-fit the data has also the practical advantage of not requiring a constant monitoring of the training state and/or an additional dataset on which to perform validation.

We should note that our surrogate model creation process is not limited uniquely to the contact model presented in this study, but can be easily extended to virtually any other FE or EF contact models, provided that the assumptions of elastic and friction-less contact are met. In that respect, the surrogate model could provide a fast and valid alternative to contact models which cannot directly interface to the modeling system of use. Furthermore, the surrogate model resulting from our creation process can be exploited in virtually any simulation software capable of integrating an external DLL module. This represents a very viable way to describe complex structural models, without actually simulating them.

The time required to generate the sample points amounted to almost 5 days of continuous computation on all four cores of an Intel® Core™ i5-4570 quad-core CPU equipped with 16 gigabytes of RAM. About 60 additional hours were necessary to train the ANNs. The total surrogate model generation time was considerable, however, both the sampling process and the training of the neural networks could be massively parallelized and executed on multiple processing units, or machines with many cores. This approach would easily bring the generation time to more manageable levels. It should also be noted that the generation time for a given implant design is paid only once upfront, but the resulting surrogate model can be reused for the evaluations of many conditions and multiple patients. Another way to reduce the generation time would be to reduce the number of training points, but this aspect requires further investigation.

The sample generation process relied heavily on reference curves and/or variables bounds extracted from existing reference simulations performed with the reference model. This approach may work well when such data are already available—or if they can easily be obtained from experimental measurements—however, this is seldom the case. Perhaps the most challenging case is that of a patient-specific knee model, generated *ex novo* from medical images of the patient. In such a case, although some joint kinematics may be extracted using *in vivo* imaging techniques, no reference load curves are available and a different sampling strategy should be devised. The definition of bounds for the sample points could also be based on the geometrical conformity between the articulating surfaces, and bounds on joint loads in sensitive directions could be obtained from the literature. However, these approaches require further investigation.

The activities simulated in this study were also incidentally used during the sampling stage to provide reference curves. If activities were to be simulated which involved joint loads and/or kinematics very different from the ones in the training dataset, it is almost impossible to know whether the surrogate model predictions would still be sufficiently accurate. One possible solution could be to build accuracy maps over various regions of the design space and, subsequently, to relate the distance of new query points from the dataset of training points prior to the surrogate model evaluation to estimate the expected accuracy for the new points. However, mapping the accuracy over a multi-dimensional domain is not trivial.

We introduced a discontinuity in the surrogate model, which prevented negative forces in the TF distraction (y) direction, and avoided the estimation of TF loads in non-sensitive directions when the compressive force was lower than or equal to zero. To find the configuration of static equilibrium in the TF joint, the FDK method solves a set of nonlinear equations using gradient information. Therefore, our choice made the gradient of the system of equations potentially discontinuous, whereas a smooth transition to zero would be a better choice. However, the reference contact model contained the same discontinuity and the surrogate contact model did not exacerbate this problem.

Friction between the articular implant surfaces was neglected and the contact was assumed to be linear elastic based on penetration volume. The friction-less assumption may not allow proper study of polyethylene wear of the tibial insert under dynamic conditions. However, for all other cases of interest (e.g., parametric variation, knee kinematic studies and ligament force predictions), this assumption does not represent a major limitation. With regards to the linear elastic assumption, previous studies have failed to demonstrate the superiority of non-linear contact models over linear models to describe the load response of the polyethylene component[24]. However, the surrogate contact model creation process should work just as well for non-linear elastic contact models, as long as the contact forces and moments can be represented as functions of only model pose.

In conclusion, we successfully applied surrogate modeling techniques based on ANNs to reduce the computation time of knee joint loads and kinematics in MS models. We evaluated its accuracy and demonstrated its performance

in the simulation of four ADLs. Accuracy was comparable to that of the reference model, while simulations were performed three times as fast, with a full gait cycle analyzed in only 4.5 min. We believe that these performances will promote the applicability of MS models in extensive parametric studies and/or planning of orthopedic interventions through optimization.

FUNDING

REFERENCES

1.   Erdemir, A., McLean, S., Herzog, W. & van den Bogert, A. J. Model-based estimation of muscle forces exerted during movements. *Clin. Biomech. (Bristol, Avon)* **22**, 131–54 (2007).

2.   Andersen, M. S., Damsgaard, M. & Rasmussen, J. Force-dependent kinematics: a new analysis method for non-conforming joints. in *XIII International Symposium on Computer Simulation in Biomechanics* (2011).

3.   Marra, M. A. *et al.* A subject-specific musculoskeletal modeling framework to predict in vivo mechanics of total knee arthroplasty. *J. Biomech. Eng.* **137**, 020904 (2015).

4.   Halloran, J. P., Erdemir, A. & van den Bogert, A. J. Adaptive surrogate modeling for efficient coupling of musculoskeletal control and tissue deformation models. *J. Biomech. Eng.* **131**, 011014 (2009).

5.   Mishra, M., Derakhshani, R., Paiva, G. C. & Guess, T. M. Nonlinear surrogate modeling of tibio-femoral joint interactions. *Biomed. Signal Process. Control* **6**, 164–174 (2011).

6.   Lin, Y.-C., Farr, J., Carter, K. & Fregly, B. J. Response surface optimization for joint contact model evaluation. *J. Appl. Biomech.* **22**, 120–30 (2006).

7.   Lu, Y., Pulasani, P. R., Derakhshani, R. & Guess, T. M. Application of neural networks for the prediction of cartilage stress in a musculoskeletal system. *Biomed. Signal Process. Control* **8**, 475–482 (2013).

8.   Lin, Y.-C., Haftka, R. T., Queipo, N. V & Fregly, B. J. Surrogate articular contact models for computationally efficient

multibody dynamic simulations. *Med. Eng. Phys.* **32**, 584–94 (2010).

9. Lin, Y.-C., Walter, J. P., Banks, S. A., Pandy, M. G. & Fregly, B. J. Simultaneous prediction of muscle and contact forces in the knee during gait. *J. Biomech.* **43**, 945–52 (2010).

10. Lin, Y.-C., Haftka, R. T., Queipo, N. V & Fregly, B. J. Two-dimensional surrogate contact modeling for computationally efficient dynamic simulation of total knee replacements. *J. Biomech. Eng.* **131**, 041010 (2009).

11. Eskinazi, I. & Fregly, B. J. Surrogate modeling of deformable joint contact using artificial neural networks. *Med. Eng. Phys.* **37**, 885–91 (2015).

12. Hornik, K., Stinchcombe, M. & White, H. Multilayer feedforward networks are universal approximators. *Neural Networks* **2**, 359–366 (1989).

13. Damsgaard, M., Rasmussen, J., Christensen, S. T., Surma, E. & de Zee, M. Analysis of musculoskeletal systems in the AnyBody Modeling System. *Simul. Model. Pract. Theory* **14**, 1100–1111 (2006).

14. Andersen, M. S., Damsgaard, M. & Rasmussen, J. Kinematic analysis of over-determinate biomechanical systems. *Comput. Methods Biomech. Biomed. Engin.* **12**, 371–84 (2009).

15. Fregly, B. J. *et al.* Grand challenge competition to predict in vivo knee loads. *J. Orthop. Res.* **30**, 503–13 (2012).

16. Hammersley, J. M. Monte carlo methods for solving multivariable problems. *Ann. N. Y. Acad. Sci.* **86**, 844–874 (2006).

17. Guennebaud, G., Jacob, B. & others. Eigen v3. (2010). Available at: http://eigen.tuxfamily.org.

18. Grood, E. S. & Suntay, W. J. A joint coordinate system for the clinical description of three-dimensional motions: application to the knee. *J. Biomech. Eng.* **105**, 136–44 (1983).

19. D'Lima, D. D., Fregly, B. J., Patil, S., Steklov, N. & Colwell, C. W. Knee joint forces: prediction, measurement, and significance. *Proc. Inst. Mech. Eng. H.* **226**, 95–102 (2012).

20. Bei, Y. & Fregly, B. J. Multibody dynamic simulation of knee contact mechanics. *Med. Eng. Phys.* **26**, 777–89 (2004).

21. Fregly, B. J., Sawyer, W. G., Harman, M. K. & Banks, S. A. Computational wear prediction of a total knee replacement from in vivo kinematics. *J. Biomech.* **38**, 305–14 (2005).

22. Fregly, B. J., Banks, S. A., D'Lima, D. D. & Colwell, C. W. Sensitivity of knee replacement contact calculations to kinematic measurement errors. *J. Orthop. Res.* **26**, 1173–9 (2008).

23. Eskinazi, I. & Fregly, B. J. An Open-Source Toolbox for Surrogate Modeling of Joint Contact Mechanics. *IEEE Trans. Biomed. Eng.* **63**, 269–77 (2016).

24. Fregly, B. J., Bei, Y. & Sylvester, M. E. Experimental evaluation of an elastic foundation model to predict contact pressures in knee replacements. *J. Biomech.* **36**, 1659–68 (2003).

Chapter 4

Anterior referencing of tibial slope in total knee arthroplasty considerably influences knee kinematics

A musculoskeletal simulation study

Marco A. Marra, Marta Strzelczak, Petra J.C. Heesterbeek, Sebastiaan A.W. van de Groes, Dennis Janssen, Bart F.J.M. Koopman, Ate B. Wymenga, and Nico Verdonschot.

ABSTRACT

Purpose. In total knee arthroplasty (TKA) the posterior tibial slope is not always reconstructed correctly, and the knee ligaments may become too tight in flexion. To release a tight flexion gap, surgeons can increase the posterior tibial slope using two surgical resection techniques: the anterior tibial cortex- (ACR) or the centre of tibial plateau- (CPR) referencing. It is not known how this choice affects the knee laxity and function during activities of daily living. The aim of this study was to investigate the effect of tibial slope on knee laxity, kinematics and forces during a squatting activity using computer simulation techniques. We hypothesised that the effects depend on the referencing technique utilised.

Methods. A validated musculoskeletal model of TKA was used. Knee laxity tests were simulated in flexion and extension. Then, a squat motion was simulated to calculate: movement of the tibio-femoral joint (TFJ) contact points and patello-femoral joint (PFJ) contact force. All analyses were repeated with more anterior (-3°), neutral (0°), and more posterior tibial slope (+3°, +6°, +9°), and with two referencing techniques (ACR, CPR).

Results. Knee laxities increased dramatically with more posterior slope with the ACR technique (up to 400 %), both in flexion and in extension. The CPR technique, instead, had much smaller effects (up to 42 % variations). During squatting, more slope with the ACR technique resulted in larger movements of the TFJ contact point. The PFJ contact force decreased considerably with more slope with the CPR technique (12 % body-weight reduction every 3° more posterior slope), thanks to the preservation of the patellar height and quadriceps-femur load sharing.

Conclusion. ACR technique alters considerably the knee laxity, both in flexion and extensions and surgeons should be cautious about its use. More slope with CPR technique induces more favourable TFJ kinematics and loading of the knee extensor apparatus, and does not substantially alter knee laxity. Preferably, the tibial slope resection should be pre-planned thoroughly and performed using CPR technique as accurately as possible. Surgeons can directly translate the results of this study into the clinical practice.

INTRODUCTION

A successful total knee arthroplasty (TKA) should reduce knee pain and restore function to normal levels. For this purpose, the reconstructed tibio-femoral joint (TFJ) should be stable throughout the whole range of knee flexion. The posterior tibial slope was shown to affect substantially the knee laxity, hence the stability, in a cadaveric study[1].

In conventional TKA, the posterior tibial slope cannot always be reconstructed correctly, due to uncertainty of the surgical instruments and a large inter-patient variability (95% CI [1.0°, 15.8°])[2]. Often, an arbitrary angle of posterior slope is aimed for (3° or 7° are common choices) according to the recommendation of the prosthesis manufacturer. In cruciate-retaining (CR) TKA, particularly, an insufficient posterior tibial slope may result in flexion gap tightness and reduced post-operative flexion[1,3,4]. To increase the flexion gap, surgeons tend to increase the posterior tibial slope intra-operatively, using the anterior tibial cortex as a reference (anterior tibial cortex-referencing, ACR)[4]. This technique lowers the TFJ line and affects the tension of the soft tissues. Based on clinical observations of the authors, a little increase of posterior tibial slope could increase the flexion gap considerably, and cause laxity in flexion with subsequent aberrant kinematics. These factors may put the implant at increased risk of wear[5] and lead to (mid-)flexion instability. A different surgical approach is to plan the desired tibial slope pre-operatively, based on the knee system, and to reference the tibial bone cut from the midpoint of the tibial plateau (centre of tibial plateau-referencing, CPR). In the latter case, the choice of the posterior tibial slope does not substantially alter the TFJ line at the centre of the cut surface of the proximal tibia[6]. Only a limited number of studies were found in literature on the effect of posterior tibial slope in TKA, which show contradictory results[1,7–9]. Also little attention was paid to the surgical referencing technique used, and the effect of tibial slope on the forces in the TFJ, PFJ and knee ligaments during activities of daily living (ADLs).

The purpose of this study was, therefore, to investigate the effect of alterations of the tibial slope on TFJ laxity and kinematics, quadriceps, patello-femoral and ligament forces during a demanding activity, and to elucidate possible differences arising from the surgical referencing technique. The hypothesis was that the tibial slope influences the knee laxity, kinematics and loads both
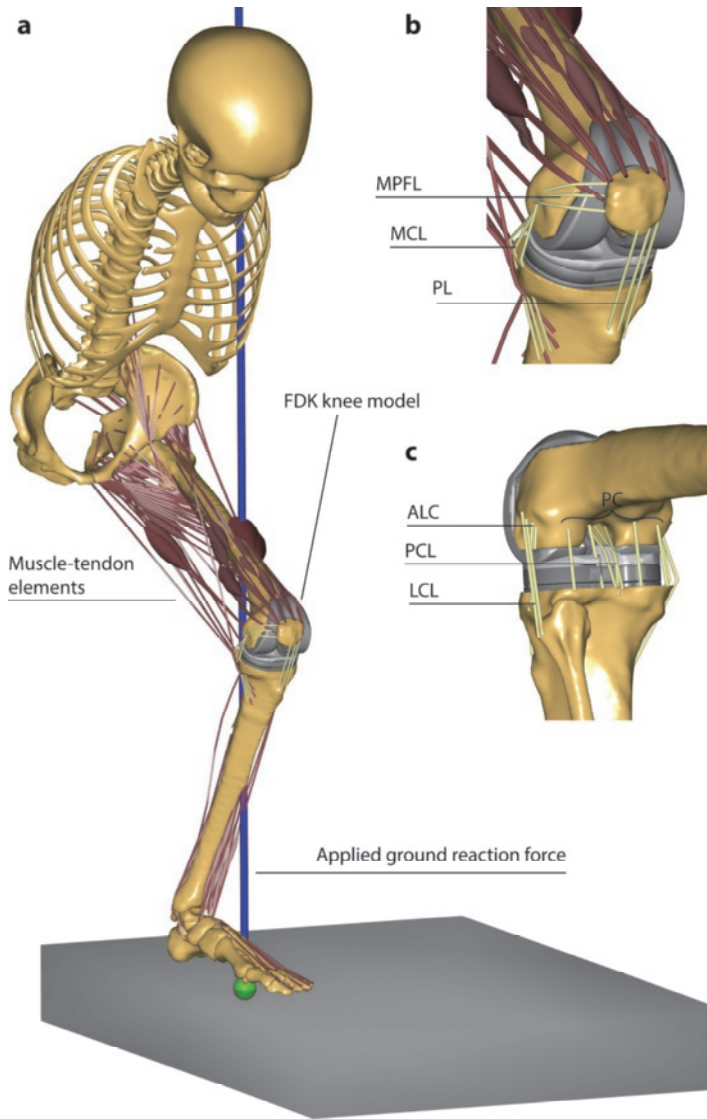
Figure 4.1 A snapshot of the musculoskeletal model used in this study. a) The model includes head, trunk, and the leg side with the implanted knee. The lower extremity is actuated by 166 muscle-tendon elements. Ground reaction forces and squatting kinematics are applied as input. The tibio- and patello-femoral joints are modelled using force-dependent kinematics (FDK) and include spring ligaments and articular surface contact: b) antero-medial view of the knee with medial patellofemoral ligament (MPFL), medial collateral ligament (MCL) and patellar ligament (PL); c) postero-lateral view of the knee with antero-lateral complex (ALC), posterior capsule (PC), lateral collateral ligament (LCL).

in flexion and extension, and that the effect depends on the referencing technique. This study presents novel findings on the effects of tibial slope and surgical techniques on the biomechanics of the reconstructed knee, which may be translated directly into the clinical practice.

MATERIALS AND METHODS

An existing patient-specific musculoskeletal model of CR-TKA was used for this study (Figure 4.1)[10]. The model was previously validated against experimental measurements of TFJ contact forces during normal and right-turn gait in a patient with a telemetric knee prosthesis, and sagittal plane kinematics during unloaded leg-swing trial under fluoroscopic examination[11]. Details of the model are provided in a separate Appendix. The tibial insert (Congruent NK-II CR, Zimmer Biomet, Warsaw, IN, USA) of the knee prosthesis had a conforming shape, with upwardly sloping lipped bearings at both the anterior and posterior rims of the insert. The post-operative posterior tibial slope was quantified as the angle of built-in slope of the tibial insert plus the angle of the post-operative tibial resection, measured relative to the tibial mechanical axis. The tibial mechanical axis was defined as the axis connecting the tibial intercondylar eminence, proximally, to the centre of the inferior tibial articular surface (tibial plafond), distally. The post-operative tibial slope was equal to 0° (neutral slope) and represented the baseline case for successive comparisons.

To assess the effect of surgical referencing technique, two series of analyses were designed. In the first series, the tibial slope was altered by rotating the tibial component on the sagittal plane around a pivot-point located at the anterior aspect of the proximal tibia (ACR technique, Figure 4.2a). With such technique, a more posterior tibial slope would shift distally all the points of the tibial plateau, and a more anterior slope, would shift them proximally. In the second series, the pivot-point was defined as the midpoint between the centres of the medial and lateral tibial plateaus (CPR technique, Figure 4.2b). In this situation, a more posterior tibial slope would shift distally all the points located posteriorly to the pivot-point, and proximally all the points located anteriorly, and *vice versa* for a more anterior slope. In addition to the neutral slope case (0°), four more cases were analysed, three with more
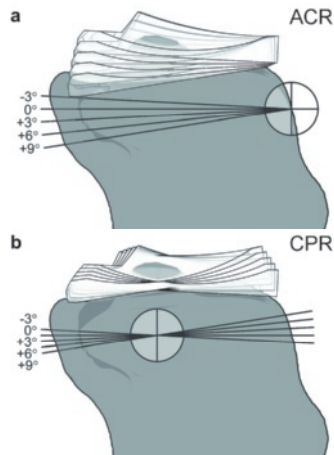
Figure 4.2 Schematic representation of a) anterior tibial cortex-referencing (ACR) and b) centre of tibial plateau-referencing (CPR) techniques used in this study to alter the tibial slope. The crossed circles represent the pivot point for the virtual resection. The outline of the tibial insert from -3° to +9° of tibial slope is superimposed. With ACR technique a more posterior tibial slope shifts all points on the tibial plateau distally, and a more anterior slope, proximally (a). With CPR technique, changing the degree of tibial slope does not alter the joint line in correspondence of the pivot point (b).

posterior slope (+3°, +6°, +9°) and one with more anterior slope (-3°), with both ACR and CPR technique, leading to five slope cases in each technique.

Anterior-posterior (AP) and *varus-valgus* (VV) laxity tests were simulated. An unloaded case was first analysed, in which the knee joint sought its own equilibrium position throughout a 0–90° knee flexion range. The anterior tibial translation and *varus* angle were calculated according to Grood and Suntay's joint coordinate system definition[12]. Subsequently, anterior and posterior forces of 70 N in magnitude[13] were applied to the proximal tibia, and the correspondent AP translations recorded. Similarly, *varus* and *valgus* loads of 15 Nm in magnitude[14] were applied to the tibia by means of 50 N-forces, applied 30 cm below the TFJ line and directed medially and laterally, respectively. The correspondent *varus* and *valgus* rotations were recorded. Measurements of laxity were obtained at 0°, 30°, 60°, 90° of knee flexion. The anterior and posterior laxities were calculated as the tibial translation during the anterior and posterior laxity tests, respectively, minus the tibial translation in the unloaded case. The *varus* and *valgus* laxities were calculated

as the knee angle during the *varus* and *valgus* laxity tests, respectively, minus the knee angle in the unloaded case.

To investigate the knee kinematics and forces under loading, a two-legged squatting motor task (PS_2legsquat1) from the fifth *Grand Challenge Competition To Predict In Vivo Knee Loads* dataset[11] was analysed, which started from a standing position, followed by a descending phase and an ascending phase. The range of knee flexion was approximately 0–90°. Throughout the squatting task the following outcomes were calculated: the displacement of the TFJ contact point, calculated as the centre of pressure of the medial and lateral TFJ contact forces, the forces in the MCL, LCL and PCL, the quadriceps muscle forces, the force exchanged between the quadriceps tendon and the femur condyles through wrapping (quadriceps-femur force), and the PFJ contact force.

RESULTS

Laxity with ACR technique

The anterior laxity increased with more posterior slope with the ACR technique, in all knee flexion angles (Figure 4.3, blue series). The posterior laxity increased with more posterior slope, in extension, whereas it did not show a clear trend for the other flexion angles. Both *valgus* and *varus* laxities increased with more posterior slope in all knee flexion angles. Both anterior, posterior, *valgus* and *varus* laxities decreased with more anterior slope (-3°), in all knee flexion angles.
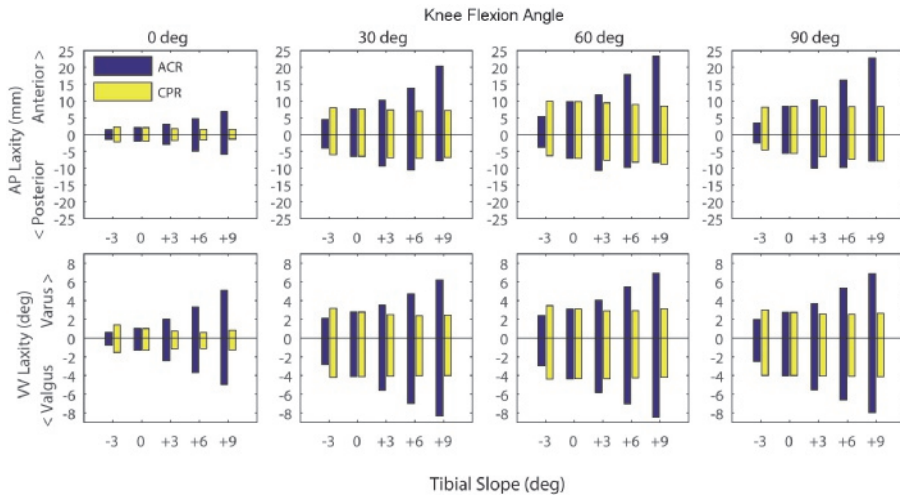
Figure 4.3 Anterior-posterior (top) and varus-valgus (bottom) laxities at 0°, 30°, 60°, and 90° of knee flexion for different degrees of tibial slope and for anterior tibial cortex-referencing (ACR) and centre of tibial plateau-referencing (CPR) techniques. Note the large effect of tibial slope on laxity with ACR technique, and the minor effects of CPR technique.

Laxity with CPR technique

Knee laxity was less affected by changes in tibial slope with CPR technique (Figure 4.3, yellow series), than with ACR technique. The anterior laxity decreased with more posterior tibial slope with the CPR technique, in all knee flexion angles. *Valgus* and *varus* laxities slightly decreased with more posterior slope, in extension. In all other knee flexion angles, only marginal changes (less than 0.4°) in *valgus* and *varus* laxity occurred with more posterior slope. A more anterior slope caused changes in laxity, which were less than 20 % of the neutral case values, with the exception of the *varus* laxity in extension, which increased by 0.4° (+39 %).

Kinematics and loads during squatting

The distance travelled by the TFJ contact point increased on both medial and lateral side with more posterior tibial slope with ACR technique, and it was not altered substantially with the CPR technique (Figure 4.4).
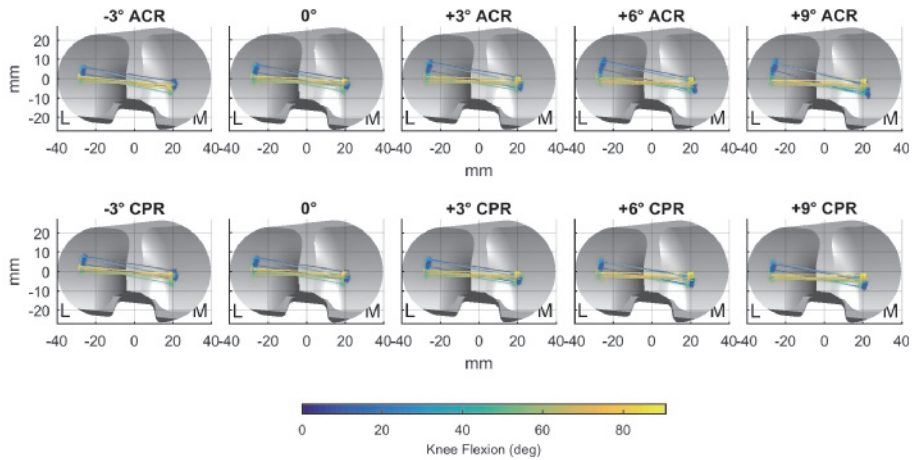
Figure 4.4 Displacement of the tibio-femoral contact point during squatting at baseline (0°), with an anterior slope (-3°) and posterior slope (+3°, +6°, +9°) and for anterior tibial cortex-referencing (ACR, top) and centre of tibial plateau-referencing (CPR, bottom) techniques. Contact points on the lateral (L) and medial (M) side of the tibial plateau are connected together and colour-coded according to the knee flexion angle.

The peak PCL force during squatting decreased with more posterior slope with both referencing techniques (Figure 4.5, left). Both medial and lateral collateral ligament peak forces decreased with more posterior slope (Figure 4.5, centre and right). However, with the CPR technique neither ligament became slack, and the force reduction was more moderate, when compared to the ACR technique.

The peak quadriceps force during squatting decreased by 5.2 % body-weight (BW), on average, for every 3° more posterior slope with the ACR technique (Figure 4.6, left). Similarly, the quadriceps-femur force decreased by 11 % BW (Figure 4.6, centre), and the peak PFJ contact force decreased by 5 % BW, on average (Figure 4.6, right). With the CPR technique, the peak quadriceps force during squatting decreased by 3.5 % BW, on average, for every 3° more posterior slope; the peak quadriceps-femur force slightly increased, and the peak PFJ contact force decreased by 12 % BW, on average.
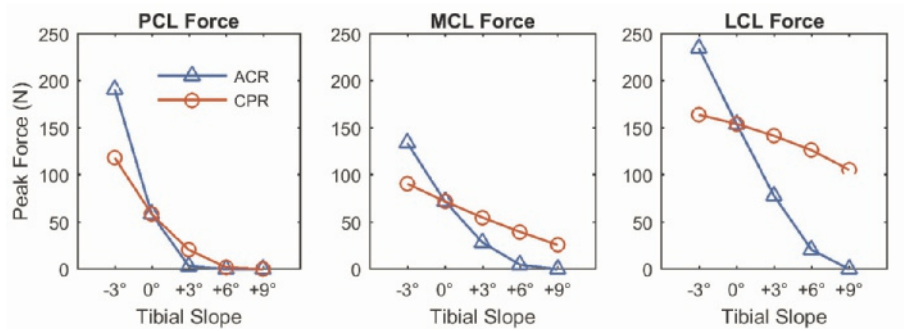
Figure 4.5 Peak posterior cruciate ligament (PCL, left), medial collateral ligament (MCL, middle) and lateral collateral ligament (LCL, right) force during squatting at varying degrees of tibial slope and referencing techniques. Note how the effect of tibial slope on knee ligaments is more moderate with CPR than with ACR technique.
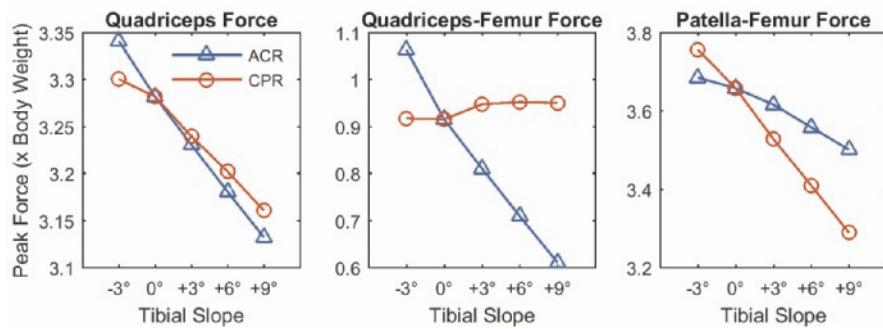
Figure 4.6 Effect of tibial slope on peak quadriceps (left), quadriceps-femur (middle) and patella-femur (right) forces during squatting. Note the different patterns of quadriceps-femur and patella-femur force between ACR and CPR techniques.

DISCUSSION

The main finding of this study was that the knee laxity increased substantially, both in flexion and, unexpectedly, also in extension with more posterior tibial slope in case the ACR technique was simulated. In contrast, varying the tibial slope with the CPR technique had little effects on knee laxity. The tension of the TFJ ligaments during simulated squat decreased with more posterior tibial slope for both referencing techniques, indicating a progressive loosening of the TFJ gap with more posterior slope, although the changes were more

distinct with the ACR technique. Also a previous study found decreased PCL strain with more posterior tibial slope[4]. No aberrant TFJ contact point movements were observed during simulated squat, even with large degrees of posterior tibial slope, when the CPR technique was simulated. This is in agreement with a previous fluoroscopic study on knee kinematics during stair ascent, getting up from and sitting down on a chair and single-leg climbing up a step[15], in which the original slope was restored and the post-operative slope ranged from -2° to 10°. Therefore, the concern for increased risk of wear, due to extreme roll-back with more posterior tibial slope[5], does not appear much justified, based on results of this study, as long as the TFJ gap is successfully balanced in both flexion and extension. In contrast, more slope with the ACR technique resulted in larger excursions of the TFJ contact point in extension on both medial and lateral side, owing to a loosened TFJ gap, which in turn may lead to increased wear of the polyethylene insert. A more posterior location of the TFJ contact point can, in principle, increase the quadriceps moment arm and reduce the quadriceps force[16,17]. Previous studies found more posterior TFJ contact point (*in vivo*)[18] and reduced quadriceps forces (*ex vivo*)[19] with more posterior tibial slope. In the present study, the peak quadriceps forces were reduced during squatting with more posterior tibial slope with both referencing techniques. The patella shifted superiorly relative to the femur condyles with more posterior tibial slope with the ACR technique, due to lowering of the TFJ line. This reduced the force exchanged between quadriceps tendon and femoral condyles by wrapping (Figure 4.7). With the CPR technique, the patellar height remained unchanged, and the quadriceps-femur load sharing was preserved. Also the PFJ contact force was more effectively reduced with more posterior tibial slope with the CPR technique (-12 % BW every 3°) relative to the ACR technique (-5 % BW every 3°). Although the difference was relatively small, decreased PFJ contact forces may contribute to reduce anterior knee pain and implant wear[20] after following CR-TKA.

In the present study, a validated patient-specific musculoskeletal model was used to simulate laxity tests and a squatting activity, under different tibial slope conditions. Furthermore, a highly controlled and parameterised study design was adopted, in which the degree of tibial slope and the referencing technique were the sole variables. A major strength of this approach lies in the possibility to isolate the effect of tibial slope from the effect of all the other
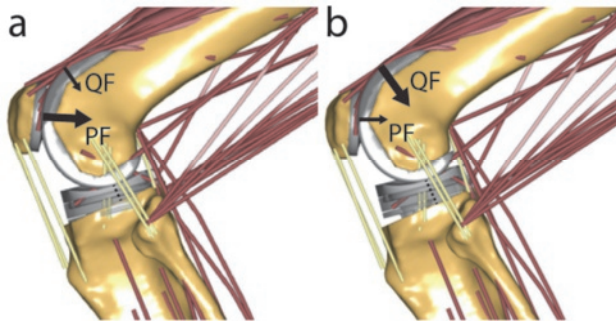
Figure 4.7 Conceptual representation of the quadriceps-femur (QF) and patella-femur (PFJ) load sharing with +9° of tibial slope with a) anterior tibial cortex-referencing (ACR) and b) centre of tibial plateau-referencing (CPR) techniques. The quadriceps muscle force decreases with more posterior slope both with ACR and CPR techniques. However, with ACR the position of the patella relative to the femur condyles is higher than with CPR, and a much lower quadriceps force can be transmitted via the quadriceps tendon directly through the femur, thus the patella-femur force is reduced only by a little amount; with CPR technique the amount of quadriceps force transmitted through the femur is higher, thus the patella-femur force is reduced more importantly.

variables that may possibly affect the outcomes of TKA, and which in previous literature may have acted as confounders. Distinct biomechanical pathways could be identified from altering the tibial slope with different referencing techniques. Also previous studies found important effects of tibial slope on knee laxity, especially those which used a referencing technique similar to the ACR of this study[1,4]. Conversely, more posterior tibial slope obtained with the CPR technique did not cause such big effects on TFJ laxity, in the present study. Also Whiteside and Amador found no major differences in the mean knee laxity parameters after increasing the posterior tibial slope[9], using posteriorly-sloped tibial inserts. Their method did not alter the level of the TFJ line in correspondence of the centre of the tibial plateaus and is analogous to the CPR technique simulated in this study.

Posterior tibial slope has been proposed as a viable alternative to PCL release to address flexion gap tightness in CR-TKA[1,7]. In the present study it was shown that a more posterior slope with CPR technique loosens the TFJ in flexion. This finding is supported by the study of Okazaki et al. (2014), which shows an increase in the flexion gap of 2 mm for every 5° increase in the posterior tibial slope, using the CPR technique[6]. In any case, the increase of tibial slope should never be at the expenses of the tibial insertions of PCL[21]. In

CR-TKA the PCL has a major role in governing the stability of the TFJ[22]. Therefore, caution should be used when performing the proximal tibial resection with an increased slope, and the appropriate surgical tools should be used to prevent damage of the PCL tibial insertion.

Interestingly a more posterior tibial slope, obtained with the ACR technique – which is meant to address a flexion tightness problem – produces, in fact, remarkable effects also in extension. This can be explained by noting that the ACR technique shifts all points of the tibial plateau distally, which, in turn, loosens the TFJ throughout the whole knee flexion-extension range. In clinical practice, if the extension gap has been already successfully balanced, any further increase of the posterior tibial slope (using the ACR technique) will alter the level of the TFJ line, which reduces the tension of the soft tissues (MCL, LCL and PCL), and increases the laxity of the knee both in flexion and in extension. Surgeons should, therefore, pay much attention when altering the tibial slope using the ACR technique, as it may have serious consequences for the overall stability of the knee.

The results of this study suggest that a thorough pre-planning of the desired tibial slope should be made, which considers both the type of implant available and the surgical technique utilised, and that the execution of the tibial resections should be as accurate as possible. One factor in the decision is the knee system used. Some systems have tibial inserts available with a built-in slope of 3-4°. With these systems, the surgeon should be careful to aim for too much slope with the primary cut, and rather aim for 0-3°. With other systems, that do not have slope in the insert, the surgeon could aim for more slope, e.g. 3-6° in the tibial cut, but referenced from the centre of the tibial plateau. Another factor is the native tibial slope of the patient. When a patient has a large native tibial slope, e.g. 10°, the surgeon can anticipate a tight knee in flexion when using a limited sloped cut. A pre-operatively planned slope, referenced from the centre of the tibial plateau, may help creating a correct balance and prevent the disadvantages of the anterior referenced slope for such a patient. The native tibial slope of the present case study was about 7°, as measured on the available pre-operative CT images. Interestingly, the simulated cases with +6° and +9° of slope with CPR technique – being the nearest to the native slope – both provided the best biomechanical results. The native tibial slope may be an important parameter to take into account in

the pre-operative planning, which is also very easy to measure on pre-operative radiographs.

Obviously, this study had several limitations. The musculoskeletal computer model represented a CR-TKA, and the results should not be generalised to other implant designs such as the PS-TKA. Although the principles behind knee surgery are similar, the mechanisms by which stability is achieved in flexion are radically different, as the CR-TKA relies on the preservation of the PCL, whereas the PS-TKA relies on a post-cam mechanism embedded in the prosthesis.

Nearly complete slackening of the PCL was observed in the present study, already with +3° slope. This effect may be due to the strain parameters assigned to the bundles of the PCL. It should be noted that the sagittal plane knee kinematics were validated against experimental measurements of a free leg-swing fluoroscopy trial, which showed some signs of PCL laxity. It is plausible that the parameters of the PCL of the present model reflected those of a relatively lax PCL, and that knees with a perfectly functional PCL after CR-TKA will likely exhibit less slackening of the PCL in flexion.

The effects of tibial slope on the knee biomechanics were analysed during a single squatting motor task, by simulating multiple cases of tibial slope. In principle, it would be possible to analyse also other motor tasks, e.g. corresponding to several ADLs, but this would require additional computer analyses, which would add to the computation time. A squatting motion was chosen for the simulations, since it included both a wide range of flexion-extension and a significant muscular endeavour around the knee joint. Care should also be taken not to extrapolate the results of the present study to deep flexion, as this range was not investigated.

When analysing squatting, it was assumed that the overall body kinematics and loading conditions would hold among different configurations of the tibial slope. Some neuro-motor adaptations may occur as a result of alterations of the prosthesis alignment, but the study of those fell out of the scope of the present study. Nevertheless, the computational analysis technique employed allowed to predict changes in knee kinematics and forces, resulting from changes in the tibial slope, as intended.

CONCLUSION

Changes in posterior tibial slope have considerable effects on knee laxity, kinematics and forces. More posterior tibial slope with the ACR technique increases the knee laxity in flexion, but also, unexpectedly, in extension. More posterior slope with CPR technique leaves the knee laxity almost uninfluenced, is beneficial for the knee extensor apparatus, and relieves the pressure on the PFJ. The tibial resection should be pre-planned and executed as accurately as possible using CPR technique.

AUTHORS' CONTRIBUTIONS

MAM implemented the analyses through musculoskeletal modelling, analysed the data and drafted the manuscript. MS helped to draft the manuscript and carry out the analyses. DWJ, BFJMK, SAWvdG helped in the analysis and interpretation of the data and critically revised the manuscript for intellectual content. PJCH participated in the design and coordination of the study and helped to draft the manuscript. ABW and NV conceived of the study and contributed to the interpretation of the data. All authors read and approved the final manuscript.

FUNDING

APPENDIX A

Detailed description of the musculoskeletal model

The model of CR-TKA used in this study was built upon the Twente Lower Extremity Model 2.0 (TLEM 2.0) template for subject-specific models[23], which included head, trunk, two arms and two legs, connected by idealised joints (Figure 4.1). The lower extremities were scaled to the patient's morphology, using patient-specific medical images. Three-dimensional models of the CR-TKA implant were incorporated into the patient's left knee. Reflective skin

marker trajectories from the available motion capture data were used as input to derive the kinematics of the idealised joint degrees-of-freedom (DOFs), using a motion optimization algorithm[24]. Subsequently, the TFJ and PFJ constraints were removed, and ligaments and articular surface contacts introduced to provide stiffness and support to the unconstrained joints. Recorded ground reaction forces and moments (GRF&M) were input to an inverse-dynamic model, actuated by 166 Hill-type muscle-tendon elements. Muscle forces, ligament forces and articular contact forces were solved simultaneously using inverse-dynamic coupled with force-dependent kinematic (FDK) analyses[10]. Some variations were introduced with respect to a previously published model[10]: the patellar ligament (PL) was modelled as three non-linear elastic springs with large stiffness, in place of a rigid rod; the lateral PFJ ligament bundles were removed from the analysis to save computation time, since they were found to remain slack throughout a series of trial model analyses; the path of the muscle *vastus medialis* was further optimised by means of an ellipsoidal wrapping object, to account for the obliquity of the fascicles at its patellar insertion[25,26].

REFERENCES

1.   Jojima, H., Whiteside, L. A. & Ogata, K. Effect of tibial slope or posterior cruciate ligament release on knee kinematics. Clin. Orthop. Relat. Res. 426, 194–8 (2004).

2.   de Boer, J. J., Blankevoort, L., Kingma, I. & Vorster, W. In vitro study of inter-individual variation in posterior slope in the knee joint. Clin. Biomech. (Bristol, Avon) 24, 488–92 (2009).

3.   In, Y. et al. Factors affecting flexion gap tightness in cruciate-retaining total knee arthroplasty. J. Arthroplasty 24, 317–21 (2009).

4.   Singerman, R., Dean, J. C., Pagan, H. D. & Goldberg, V. M. Decreased posterior tibial slope increases strain in the posterior cruciate ligament following total knee arthroplasty. J. Arthroplasty 11, 99–103 (1996).

5.   Wasielewski, R. C., Galante, J. O., Leighty, R. M., Natarajan, R. N. & Rosenberg, A. G. Wear patterns on retrieved polyethylene tibial inserts and their relationship to technical considerations during total knee arthroplasty. Clin. Orthop. Relat. Res. 299, 31–43 (1994).

6.   Okazaki, K. et al. Influence of the posterior tibial slope on the flexion gap in total knee arthroplasty. Knee 21, 806–9 (2014).

7.   Zelle, J., Heesterbeek, P. J. C., De Waal Malefijt, M. & Verdonschot, N. Numerical analysis of variations in posterior cruciate ligament properties and balancing techniques on total knee arthroplasty loading. Med. Eng. Phys. 32, 700–7 (2010).

8.   Oka, S. et al. The influence of the tibial slope on intra-operative soft tissue balance in cruciate-retaining and posterior-stabilized total knee arthroplasty. Knee Surg. Sports Traumatol. Arthrosc. 22, 1812–8 (2014).

9.   Whiteside, L. A. & Amador, D. D. The effect of posterior tibial slope on knee stability after Ortholoc total knee arthroplasty. J. Arthroplasty 3 Suppl, S51-7 (1988).

10.   Marra, M. A. et al. A subject-specific musculoskeletal modeling framework to predict in vivo mechanics of total knee arthroplasty. J. Biomech. Eng. 137, 020904 (2015).

11.   Fregly, B. J. et al. Grand challenge competition to predict in vivo knee loads. J. Orthop. Res. 30, 503–13 (2012).

12.   Grood, E. S. & Suntay, W. J. A joint coordinate system for the clinical description of three-dimensional motions: application to the knee. J. Biomech. Eng. 105, 136–44 (1983).

13.   Bull, A. M. J., Kessler, O., Alam, M. & Amis, A. A. Changes in knee kinematics reflect the articular geometry after arthroplasty. Clin. Orthop. Relat. Res. 466, 2491–2499 (2008).

14.   Heesterbeek, P. J. C., Verdonschot, N. & Wymenga, A. B. In vivo knee laxity in flexion and extension: a radiographic study in 30 older healthy subjects. Knee 15, 45–9 (2008).

15.   Catani, F. et al. Influence of tibial component posterior slope on in vivo knee kinematics in fixed-bearing total knee arthroplasty. J. Orthop. Res. 24, 581–7 (2006).

16.   Churchill, D. L., Incavo, S. J., Johnson, C. C. & Beynnon, B. D. The influence of femoral rollback on patellofemoral contact loads in total knee arthroplasty. J. Arthroplasty 16, 909–18 (2001).

17.   Fantozzi, S., Catani, F., Ensini, A., Leardini, A. & Giannini, S. Femoral rollback of cruciate-retaining and posterior-stabilized total knee replacements: in vivo fluoroscopic analysis during activities of daily living. J. Orthop. Res. 24, 2222–9 (2006).

18.   Fujimoto, E. et al. Significant effect of the posterior tibial slope on the weight-bearing, midflexion in vivo kinematics after cruciate-retaining total knee arthroplasty. J. Arthroplasty 29, 2324–30 (2014).

19.   Ostermeier, S., Hurschler, C., Windhagen, H. & Stukenborg-Colsman, C. In vitro investigation of the influence of tibial slope on quadriceps extension force after total knee arthroplasty. Knee Surg. Sports Traumatol. Arthrosc. 14, 934–9 (2006).

20.   Browne, C., Hermida, J. C., Bergula, A., Colwell, C. W. & D'Lima, D. D. Patellofemoral forces after total knee arthroplasty: effect of extensor moment arm. Knee 12, 81–8 (2005).

21.   Matziolis, G. et al. How much of the PCL is really preserved during the tibial cut? Knee Surg. Sports Traumatol. Arthrosc. 20, 1083–6 (2012).

22.   Van Opstal, N., Feyen, H., Luyckx, J. P. & Bellemans, J. Mean tensile strength of the PCL in TKA depends on the preservation of the tibial insertion site. Knee Surg. Sports Traumatol. Arthrosc. 24, 273–8 (2016).

23.   Carbone, V. et al. TLEM 2.0 – A comprehensive musculoskeletal geometry dataset for subject-specific modeling of lower extremity. J. Biomech. 48, 734–741 (2015).

24. Andersen, M. S., Damsgaard, M. & Rasmussen, J. Kinematic analysis of over-determinate biomechanical systems. Comput. Methods Biomech. Biomed. Engin. 12, 371–84 (2009).

25. Engelina, S., Antonios, T., Robertson, C. J., Killingback, A. & Adds, P. J. Ultrasound investigation of vastus medialis oblique muscle architecture: An in vivo study. Clin. Anat. 27, 1076–1084 (2014).

26. Bennett, W. F., Doherty, N., Hallisey, M. J. & Fulkerson, J. P. Insertion orientation of terminal vastus lateralis obliquus and vastus medialis obliquus muscle fibers in human knees. Clin. Anat. 6, 129–134 (1993).

Flexing and downsizing the femoral component is not detrimental to patellofemoral biomechanics in posterior-referencing cruciate-retaining total knee arthroplasty

Marco A. Marra, Marta Strzelczak, Petra J.C. Heesterbeek, Sebastiaan A.W. van de Groes, Dennis Janssen, Bart F.J.M. Koopman, Nico Verdonschot, and Ate B. Wymenga.

ABSTRACT

Purpose. When downsizing the femoral component to prevent mediolateral overhang, notching of the anterior femoral cortex may occur, which could be solved by flexing the femoral component. In this study, we investigated the effect of flexion of the femoral component on patellar tendon moment arm, patellofemoral forces and kinematics in posterior-referencing CR-TKA. Our hypothesis was that flexion of the femoral component increases the patellar tendon moment arm, reduces the patellofemoral forces and provides stable kinematics.

Methods. A validated musculoskeletal model of CR-TKA was used. The flexion of the femoral component was increased in four steps (0°, 3°, 6°, 9°) using posterior referencing, and different alignments were analysed in combination with three implant sizes (3, 4, 5). A chair-rising trial was analysed using the model, while simultaneously estimating quadriceps muscle force, patellofemoral contact force, tibiofemoral and patellofemoral kinematics.

Results. Compared to the reference case (size 4 and 0° flexion), for every 3° of increase in flexion of the femoral component the patellar tendon moment arm increased by 1 % at knee extension. The peak quadriceps muscle force and patellofemoral contact force decreased by 2 %, the patella shifted 0.8 mm more anteriorly and the remaining kinematics remained stable, with knee flexion. With the smaller size the patellar tendon moment arm decreased by 6 %, the quadriceps muscle force and patellofemoral contact force increased by 8 % and 12 %, the patellar shifted 5 mm more posteriorly. Opposite trends were found with the bigger size.

Conclusion. Flexing the femoral component with posterior referencing reduced the patellofemoral contact forces during a simulated chair-rising trial with a patient-specific musculoskeletal model of CR-TKA. There seems to be little risk when flexing and downsizing the femoral component, compared to when using a bigger size and neutral alignment. These findings provide relevant information to surgeons who wish to prevent anterior notching when downsizing the femoral component.

INTRODUCTION

Implant alignment in total knee arthroplasty (TKA) is a key factor to restore natural knee kinematics and physiological loads in the tibiofemoral (TF) and patellofemoral (PF) joints, yet sagittal plane alignment of the femoral component has received relatively little attention with respect to function and outcome[1]. Previous studies recommended that the flexion of the femoral component (FFC) should be within 0–3°, to reduce the risk of implant failure[2] and to limit the incidence of flexion contracture[3]. However, these studies addressed posterior stabilized (PS) TKA only.

Sagittal alignment is also related to the size of the femoral component, as implants aligned in flexion have typically smaller sizes[4]. This interplay often resides in the attempt to prevent mediolateral overhang. Sometimes, the femoral component is too wide in the mediolateral dimension, which irritates the surrounding soft tissues[5]. In this situation, the surgeon typically resorts to a smaller size. However, a smaller size, in turn, increases the chance of notching of the anterior femoral cortex in non-gender specific implants. Therefore, additional flexion of the femoral component is necessary to prevent notching, when using a smaller size.

In adjusting the flexion of the femoral component, the outcome may be different depending on implant design and the surgical technique utilised. With anterior referencing, the anterior femoral cortex serves as a reference for the anterior distal femur resection, thus notching is avoided. However, this technique has the disadvantage of producing variable resection of the posterior femoral condyles with subsequent difficult balancing of the flexion space[6], and the outcome may be influenced by the type of implant chosen (single- or multi-radius design). Furthermore, because the posterior condylar offset (PCO) is not controlled for, subtle increments in FFC can tighten the flexion gap substantially, as a result of over-stretching of the posterior cruciate ligament (PCL)[7]. Therefore, controlling the PCO appears essential to achieve a good TF stability. This can be achieved using posterior referencing technique, in which the posterior femoral condyles serve as reference for the posterior resection. However, the anterior resection becomes more variable and subject to notching[6].

Flexing and downsizing the femoral component could be a solution to prevent anterior notching, in alternative to a larger size. However, the effect of FFC on PF joint forces and kinematics remains largely unclear. Previous cadaver and clinical studies could not separate the effect of FFC from that of other possible confounding variables (e.g. PCO), and have shown contrasting results[8–11].

The present study examines the effect of FFC and implant size on quadriceps moment arm, PF contact forces and kinematics in posterior-referenced CR-TKA, using a highly controlled study design, in which all variables are controlled for, thus overcoming the limitations of previous cadaver studies and clinical trials. The hypothesis was that flexing and downsizing the femoral component would result in similar PF contact forces and equally stable kinematics as with neutrally aligned upper-size implant. If this hypothesis were confirmed, then FFC could represent a viable surgical option to reconstruct the knee extensor mechanism.

MATERIALS AND METHODS

For this study, a validated patient-specific musculoskeletal model was used. The creation and validation processes are described elsewhere[12]. Briefly, the model was developed using the AnyBody Modeling System (AMS, version 6, AnyBody Technology A/S, Aalborg, Denmark), it was constructed based on medical images of a patient with a telemetric CR-TKA implant, and it was validated against experimental measurements of TF contact forces and sagittal plane kinematics. In the present study, specific changes to the original model were made, which are detailed in Appendix A. Geometries of pre- and post-operative bones, and of the TKA implant, were obtained from an open-access dataset[13]. The femoral component was the size 4 of the Natural Knee CR-TKA system (Zimmer Biomet, Warsaw, IN, U.S.). The femoral component had a J-curved multi-radius design. The patella was resurfaced. Based on the post-operative model reconstruction in the AMS, the FFC angle was measured as the angle between the vertical axis of the femoral component and the mechanical axis of the femur. The vertical axis of the femoral component was the line perpendicular to the distal flat inner facet of the implant, and the mechanical axis of the femur was the line passing through the centre of the hip joint and the midpoint between the medial and lateral femoral
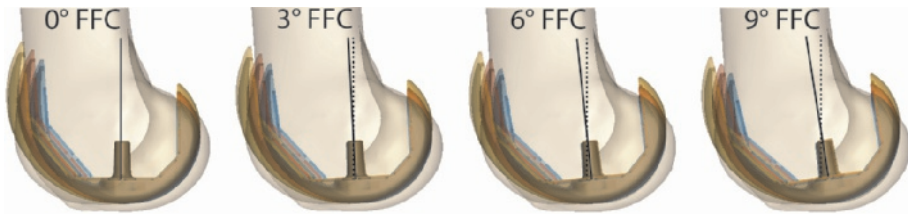
Figure 5.1 Illustration of the twelve custom post-operative cases simulated in this study. From left to right four degrees of flexion of the femoral component are shown: 0°, 3°, 6°, 9°. Three sizes of the femoral component (blue: size 3, red: size 4, yellow: size 5) plus the pre-operative bone are shown in overlay for each flexion of the femoral component (FFC) angle. Note that in every case the most distal and most posterior ends of the outlines of the femoral component are made to match tangentially, to simulate a posterior referencing and to preserve the posterior condylar offset.

epicondyles. The post-operative FFC angle was equal to 0° (neutral alignment) and represented our reference case.

One smaller size (size 3) and one bigger size (size 5) and three more FFC cases (+3°, +6°, +9°) were created, based on the reference model. These will be referred to as the *custom* post-operative cases. Geometrical models for size 3 and 5 of the femoral component were made available to us by courtesy of Zimmer Biomet (Warsaw, Indiana, U.S.) All custom cases were obtained keeping the joint space in flexion and in extension equal to that of the reference case (posterior referencing). To that aim, the femoral component geometry was translated and rotated in the sagittal plane, with the aid of the 3-D manipulation software Meshlab[14], such that its outline would always match tangentially the outline of the reference case at the most posterior and most distal ends of the implant (Figure 5.1). This allowed for preservation of the post-operative PCO and did not alter the joint line in extension. Geometrical wrapping surfaces guided the path of muscles and ligament around the knee joint, and were adapted for each combination of implant size and FFC. The same size of the tibial component as of the reference case was used in all custom cases.

In addition, an intact knee case was implemented, based on pre-operative CT images of the same patient. Given the scarce visibility of menisci and cartilaginous tissues on CT images, the articular surfaces of the tibial, patellar and femoral cartilage were estimated using an offset of the bony surfaces of

Table 5.1 Changes in knee extensor parameters due to flexion and size of the femoral component.

	+3° FFC	Size +	Size -
PTMA^{flex}	0 %	0 %	0 %
PTMA^{ext}	+1 %	+6 %	-7 %
PTF	-2 %	-5 %	+7 %
QMF	-2 %	-7 %	+8 %
QTFF	+2 %	+11 %	-15 %
PFCF	-2 %	-10 %	+12 %

Changes of patellar tendon moment arm at knee flexion (PTMA^{flex}), at knee extension (PTMA^{ext}), peak patellar tendon force (PTF), quadriceps muscle force (QMF), quadriceps tendon-to-femur force (QTFF), and patellofemoral contact force (PFCF) during rising-from-a-chair simulations due to varying size and flexion of the femoral component (FFC). Variations are expressed as average percentage increase (+) or decrease (-) relative to the reference case (size 4, 0° FFC) for every 3° increase of FFC (+3° FFC) and for a bigger size (Size +) and a smaller size (Size -).

tibia, patella and femur, respectively. The amount of offset was made equal to the average cartilage thickness found in the literature for each respective compartment[15]. Menisci were not modelled. The anterior cruciate ligament was modelled as a spring with mechanical properties adapted from the literature[16].

The model was configured to simulate a rising-from-a-chair activity, which was recorded using standard motion capture techniques and available as part of an open-access dataset (PS_chairrise1)[13]. The trial consisted of a rising phase followed by a sitting phase for a total duration of 4.375 s. The range of knee flexion, as measured, was approximately 10-96° and the chair-rise task was performed without the aid of the arms. The following parameters were continuously recorded as output of the simulations: patellar tendon moment arm (PTMA), patellar tendon force (PTF), quadriceps muscle force (QMF), quadriceps tendon-to-femur force (QTFF), PF contact force (PFCF), PF antero-posterior translation, the force in the PCL and medial patellofemoral ligament (MPFL) and the kinematics of the TF contact point. The PF antero-posterior translation was defined using a well-established knee joint coordinate system[17], adapted to describe PF kinematics. The femoral reference frame was built from the mechanical and transepicondylar axes of the femur, and the patellar reference frame was built based on anatomical landmarks
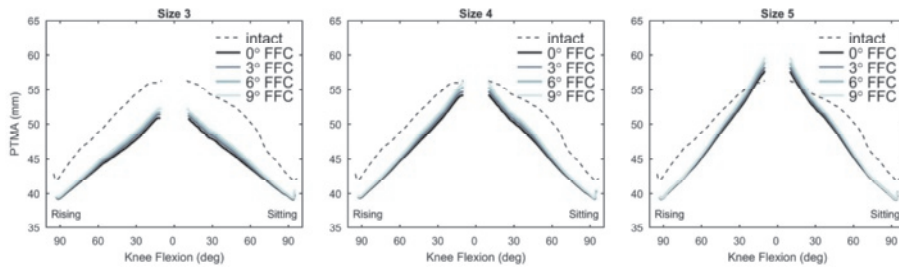
Figure 5.2 Patellar tendon moment arm (PTMA) at varying knee flexion angle during a rising-from-a-chair simulation. From left to right the results in mm for size 3, 4 and 5 are shown. Each line series correspond to a flexion of the femoral component (FFC) angle. The flexion angle in the abscissa indicates the phases of the rising and sitting motion.

identifying the most proximal and most distal, and the most medial and most lateral points of the patella.

A total of thirteen (three sizes and four FFC angles, plus one intact case) simulations were executed. The results of the custom post-operative cases were compared to those of the reference case (neutrally aligned, size 4). The PTMA and the PF antero-posterior translation from all post-operative cases were also compared to those obtained with the intact knee simulation. Joint forces were expressed as fractions of body weight (BW) and the ligament forces were expressed in units of newton (N).

RESULTS

Patellar tendon moment arm

Compared to the reference case, at knee extension, the PTMA increased with FFC and with a bigger size, and decreased with a smaller size (Table 5.1 and Figure 5.2). At knee flexion, both size and FFC had negligible effects on the PTMA. In all post-operative cases, the PTMA was about 6 % smaller than in the intact case. Detailed values of PTMA for all simulated cases are provided in Appendix B.
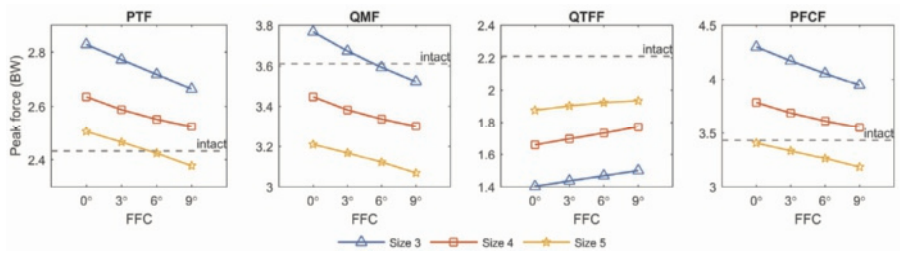
Figure 5.3 Peak forces on the knee extensor mechanism during a rising-from-a-chair simulation. From left to right: patellar tendon force (PTF), quadriceps muscle force (QMF), quadriceps tendon-to-femur force (QTFF), and patellofemoral contact force (PFCF). Results are reported in body weights (BW).

Forces on the knee extensor mechanism

The forces in the knee extensors mechanism exhibited peaked during the ascending phase, at a knee flexion angle of about 90 degrees. Peak values of PTF, QMF, QTFF, and PFCF for all simulated cases are depicted in Figure 5.3, and their variations relative to the reference case are summarized in Table 5.1. Detailed peak values for all simulated cases are provided in Appendix B.

Patellofemoral kinematics

Changes in FFC and size affected the patellar antero-posterior translation (Figure 5.4), and the effect was smaller with increased knee flexion. At knee extension (approximately 10° knee flexion), the patella shifted by 0.6, 0.8, and 1.1 mm more anteriorly for every 3° increase of FFC, with size 3, 4, and 5, respectively and it shifted about 5 mm more anteriorly with a bigger size of the femoral component. Compared to the intact case, the patella was located 10.2, 5.6, and 0.3 mm more posteriorly, at knee extension, with size 3, 4, and 5, respectively.

Ligament forces

The ligament forces were rather sensitive to changes in size and FFC. The MPFL force peaked with knee extension and the PCL force peaked at approximately 90° of knee flexion (Figure 5.5), in the reference case. On average, the peak force in the MPFL increased by 80 % for every 3° increase of FFC, especially with knee extension and mid-flexion, and increased by 314 %
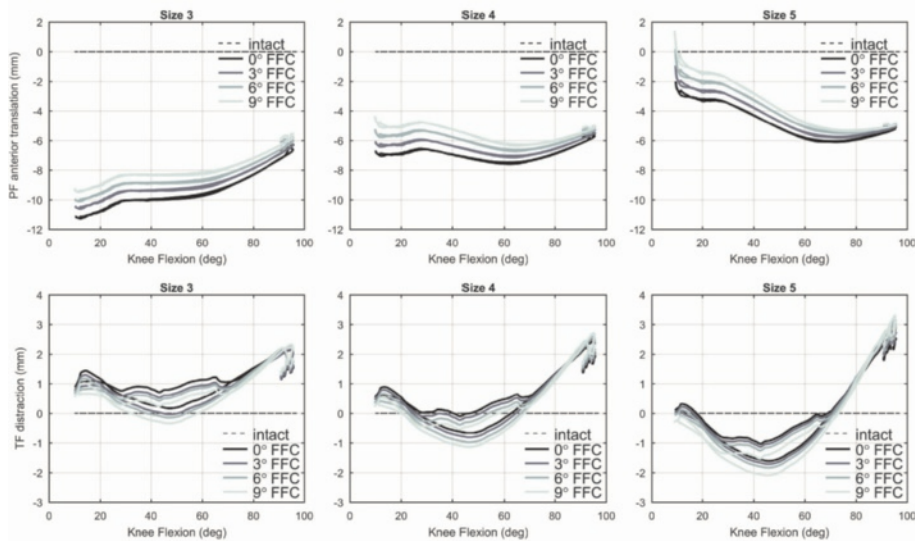
Figure 5.4 Kinematics of (a) patellofemoral antero-posterior translation and (b) tibiofemoral distraction, at varying knee flexion angle during a rising-from-a-chair simulation. From left to right the results in mm for size 3, 4, and 5 are shown. Each line series correspond to a flexion of the femoral component (FFC) angle. Kinematics from the custom cases are plotted relatively to the intact case. The rising and sitting phases for each curve are overlapped.

with a bigger size. The MPFL remained slack with size 3 regardless of the FFC angle. The peak force in the PCL increased by 18 %, for every 3° increase of FFC, increased by 96 % with a bigger size and decreased by 56 % with a smaller size.

Kinematics of the tibiofemoral contact point

The effect of FFC on the kinematics of the TF contact point was very small. The size of the femoral component had a slightly larger effect on the kinematics (Supplementary figure 5.1). A comparison of the kinematics of the TF contact point with the intact case is also provided (Supplementary figure 5.2).
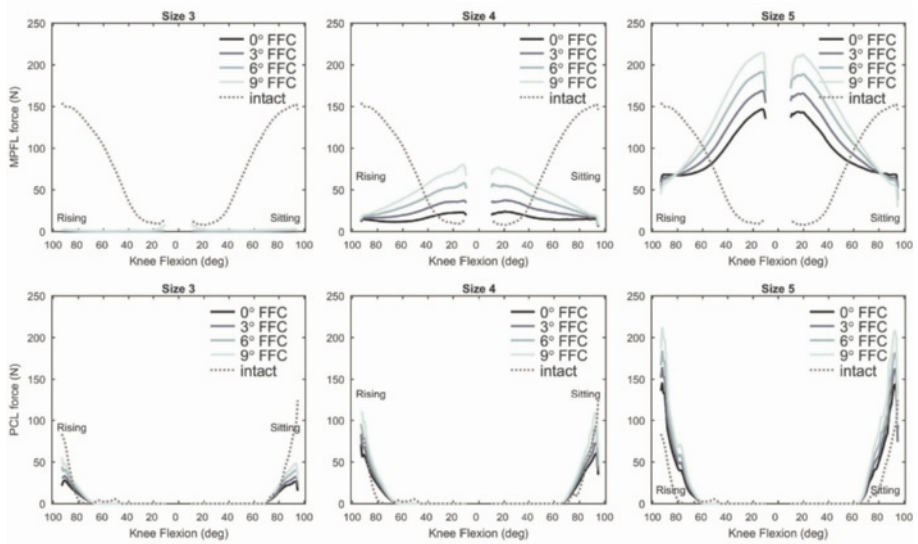
Figure 5.5 Ligament force of the (a) medial patellofemoral ligament (MPFL) and (b) posterior cruciate ligament (PCL), at varying knee flexion angle during a rising-from-a-chair simulation. From left to right the results in N for size 3, 4, and 5 are shown. Each line series correspond to a flexion of the femoral component (FFC) angle. The flexion angle in the abscissa indicates the phases of the rising and sitting motion.
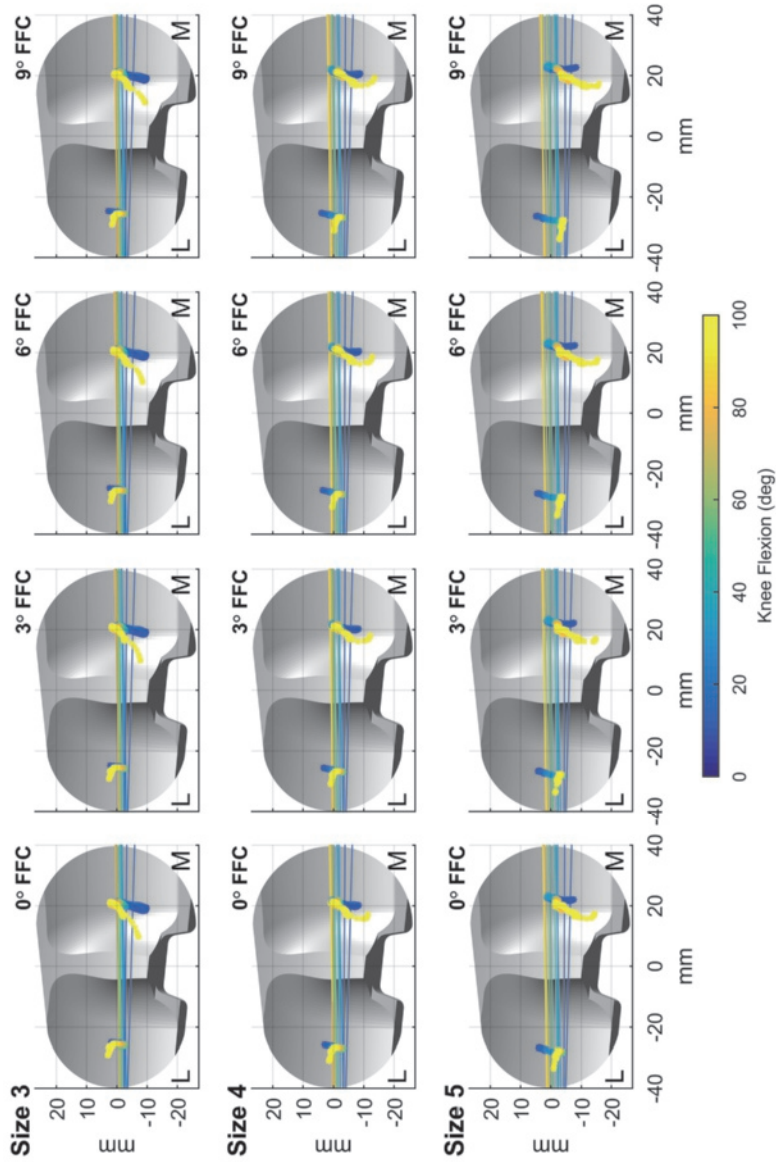
Supplementary figure 5.1 Kinematics of the tibiofemoral (TF) contact point during a rising-from-a-chair simulation with the custom post-operative models. From left to right: 0°, 3°, 6°, and 9° of flexion of the femoral component (FFC). From top to bottom: size 3, 4, and 5. The knee flexion angle is colour-coded to indicate the phases of the rising and sitting motion. Lines represent the instantaneous axis of rotation of the TF joint. Dots represent the centres of pressure of the medial and lateral TF contact forces.
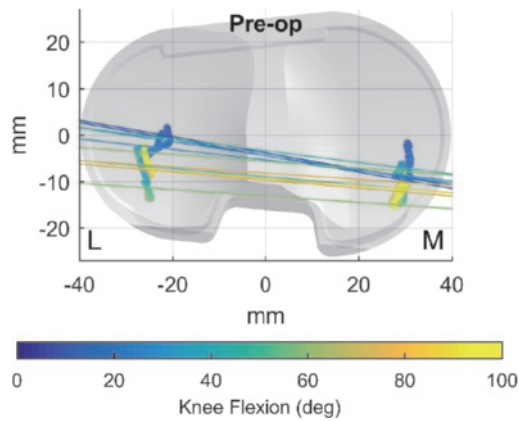
Supplementary figure 5.2 Kinematics of the tibiofemoral (TF) contact point during a rising-from-a-chair simulation with the pre-operative intact knee model. For an easier comparison with the post-operative TF kinematics, an overlay is created with the tibial insert placed in its virtual post-operative position. The knee flexion angle is colour-coded to indicate the phases of the rising and sitting motion. Lines represent the instantaneous axis of rotation of the TF joint. Dots represent the centres of pressure of the medial and lateral TF contact forces.

DISCUSSION

The two most important findings of this study are that flexing the femoral component, 1) while keeping the size, increases the knee extensor moment arm in extension, reduces the quadriceps and patellofemoral contact forces in flexion, and provided stable kinematics throughout the range of knee flexion and extension; 2) in combination with a smaller size, results in similar forces and kinematics as with a bigger size which is neutrally aligned. These results confirm our hypothesis and suggest that the femoral component can be downsized and flexed, to prevent both mediolateral overhang and anterior notching of the femur, and that this would result in an equally stable reconstruction of the knee extensors mechanism as with a neutrally aligned upsized implant.

The computational approach used in this study presented some key novel aspects. It enabled the study of size and sagittal alignment of the femoral component in a single subject case, while all the other variables were unchanged, such as the PCO, the size and alignment of the tibial and patellar

components, and the level of the joint line in extension. This aspect overcomes one big limitation of clinical studies, in which confounding variables are present inevitably. For instance, Antony *et al.* found a correlation between higher FFC and larger maximal post-operative flexion angle in CR-TKA[18], whereas Murphy *et al.* observed a larger maximal knee flexion angle at surgery, which did not translate in a functional benefit at 1 year post-operatively[19]. In both studies, the PCO was not controlled for, which may have acted thus as a confounding parameter.

Flexing the femoral component provided some positive effects. On the one hand, a more flexed implant increased the patellar tendon moment arm at knee extension and, to a lesser extent, in mid-flexion, which may be relevant for those activities involving large quadriceps action in the first arc of the knee range of motion. This first mechanism can be explained by the trochlear groove positioned more anteriorly and distally with more FFC. In other words, the patellofemoral joint becomes overstuffed. On the other hand, more FFC increased the QTFF in (mid-) flexion. This second mechanism redistributes some of the patellofemoral joint to the quadriceps tendon-femur compartment. A higher QTFF may result in larger stresses at the implant-bone (or implant-cement) interface, which may have an effect on implant fixation. However, these aspects were not investigated in the present study and warrant further attention. Summed together, the abovementioned effects of FFC provided a means for reducing the quadriceps and patellofemoral contact forces during dynamic and weight-bearing exercise.

A larger size of the femoral component, leaving the PCO unchanged and increasing the offset of the trochlea (posterior referencing), relative to the reference case, resulted in an even larger reduction in the quadriceps and PF forces with knee flexion from 0-100°, in the present study. This seems to contrasts with the finding of Kawahara *et al.*, who found higher PF contact forces at flexion angles of 90° and more with larger femoral components[20]. These authors, however, adopted an opposite approach: they increased the antero-posterior dimension of the femoral component by increasing the PCO and leaving the position of the anterior flange unchanged (anterior referencing). Moreover, they only evaluated PF contact forces in deeper flexion under static and non-weight bearing conditions, and they used PS-TKA. In contrast, we estimated PF contact forces in a CR-TKA model during a

dynamic and weight-bearing knee exercise, involving quadriceps muscle activity. Their findings, in essence, do not conflict with our results.

Ligament tensions here presented were in line with previous studies on ligament length changes in TKA[21–23]. With a bigger size, the both PCL and MPFL forces increased substantially, and much more than observed after variations in FFC alone. Higher tension in the MPFL resulted from an oversized femoral component (mediolateral overhang), and this may be detrimental to the results of TKA[5]. For this reason, over-sizing the femoral component is generally discouraged. Larger PCL forces with a bigger size of the femoral component were in agreement with findings of previous studies[24], and could be explained both by a larger TF distraction and a larger posterior tibial translation with knee flexion. In contrast, a smaller femoral component slackened the MPFL nearly entirely, due to a posterior patellar translation (understaffing) and a smaller mediolateral size of the femoral component, and the PCL force was halved, compared to the reference size. This scenario is also discouraged, as slackening of the MPFL may increase the risk of patellar instability (although no aberrant PF kinematics were observed in this study)[25] and slackening of the PCL may destabilize the knee in flexion. Flexing the femoral component could partially restore the tension in these ligaments.

The post-operative PTMA in (mid-) flexion was consistently smaller than in the intact case, which may indicate a failed reconstruction of the PTMA for other reasons. At knee extension, similar PTMA were obtained in the intact case, with size 5, and with size 4 with additional FFC. Therefore increasing the FFC may also increase the PTMA in extension. Implant size had the largest influence on patellar antero-posterior translation. Post-operatively, the patella was consistently less anterior than in the intact case, throughout the range of flexion-extension. In extension and mid-flexion, additional FFC could partially restore the antero-posterior translation.

From a purely anatomical point of view, and if we consider only the femoral antero-posterior dimension, the size 5 of the femoral implant would likely provide the best fit (Figure 5.6). However, such a choice could be less favourable concerning mediolateral overhang, as it could consequently cause an irritation of the soft tissues. Virtually, an equally good antero-posterior fit as with size 5 could be achieved using a smaller femoral component (size 4) which is flexed by about 6°. Despite the downsizing, flexing the femoral
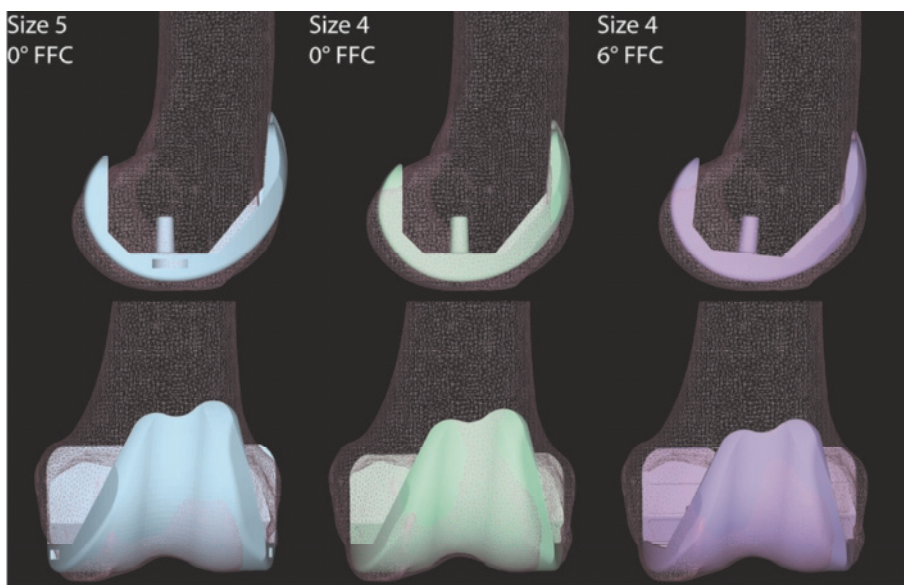
Figure 5.6 Illustrative case for the alignment in flexion of a downsized femoral component with preservation of the posterior condylar offset (PCO). Size 5 with 0° FFC fits the antero-posterior dimension of the femur, however mediolateral overhang is observed, which is detrimental. Downsizing the femoral component (Size 4, 0° FFC) reduces the mediolateral overhang, but creates anterior notching of the femoral cortex, if the PCO is preserved. Flexing the smaller component by a few degrees in the sagittal plane (Size 4, 6° FFC) may concomitantly preserve the PCO, while limiting mediolateral overhang and preventing anterior notching.

component while preserving the PCO would also ensure a proper reconstruction of the flexion space, without concerns of anterior notching of the femoral cortex.

In light of these findings, flexing and downsizing the femoral component seems to provide similar biomechanical results as using a bigger size with neutral alignment, but without the problem of mediolateral overhang and anterior notching. Moreover, flexing the femoral component does not appear detrimental to TF and PF kinematics. Therefore, surgeons may consider flexing the femoral component as an option to limit anterior femoral notching in downsized implant. Surgeons should also be aware that downsizing the femoral component might decrease the tension in the PCL and MPFL, and

flexing the femoral component may partially restore this tension, as shown in this study.

The present study elucidates biomechanical aspects related to sagittal alignment and size of the femoral component in CR-TKA with posterior referencing. Caution should be used when generalising the present findings to other implant types (e.g. PS-TKA), designs (e.g. single-radius) and surgical techniques (e.g. anterior referencing), and cases of large anatomical deformity, as these were not investigated. Furthermore, given our choice to preserve the PCO with posterior referencing, some of the simulated cases (e.g. size 3 with 0° and 3° FFC and size 5 with 6° and 9° FFC) are not plausible in practice. These hypothetical cases were included as well, to provide a more comprehensive overview of the parameters investigated. The use of a computer model to simulate the effect of size and alignment involved many assumptions and simplifications. The musculoskeletal model was based on only one patient and implant design, which minimized possible confounding variables. Future research should assess the influence of anatomical variability and validate these findings in a clinical setting; this study provides clues as to which parameters could be included.

CONCLUSION

Flexing the femoral component increases the knee extensors moment arm and reduces the quadriceps and patellofemoral contact forces in posterior-referencing CR-TKA. There seems to be little risk associated with flexing the femoral component in a downsized implant, which could have advantages in terms of preventing mediolateral overhang and anterior notching, and would result in similar patellofemoral forces and kinematics as in a neutrally positioned upsized component.

Acknowledgments

providing the computer files for the additional sizes of the femoral component used in this study.

Authors' contributions

MAM implemented the analyses through musculoskeletal modelling, analysed the data and drafted the manuscript. MS helped to draft the manuscript and carry out the analyses. DWJ, BFJMK, SAWvdG helped in the analysis and interpretation of the data and critically revised the manuscript for intellectual content. PJCH participated in the design and coordination of the study and helped to draft the manuscript. ABW and NV conceived of the study and contributed to the interpretation of the data. All authors read and approved the final manuscript.

Funding

APPENDIX A

Detailed description of the musculoskeletal model

The model used in this study was built upon a previously validated model of cruciate-retaining total knee arthroplasty model[12]. This model was based on the Twente Lower Extremity Model 2.0[26], and included: head, trunk, two arms and two legs, connected by idealised joints. The bones of the lower extremities were non-linearly scaled to match those of the patient, using morphing techniques. Three-dimensional models of the CR-TKA implant were incorporated into the patient's left knee. Time histories of reflective skin marker trajectories were used as input to derive the kinematics of the idealised joint degrees of freedom, using a motion optimization algorithm[27]. Subsequently, the tibiofemoral and patellofemoral joint constraints were removed, and ligaments and articular surface contacts were introduced to provide elastic stiffness to the unconstrained joints. Experimental ground reaction forces and optimized joint kinematics were input to a model equipped with 166 Hill-type muscle-tendon elements. Muscle and ligament forces, articular contact forces and secondary knee kinematics were solved simultaneously using force-dependent kinematics[28]. Some variations were introduced with respect to our previously published model: the patellar ligament (PL) was modelled as three non-linear elastic springs with large stiffness, in place of a rigid rod; the lateral patellofemoral ligament bundles were removed to save computation time, since they remained slack throughout a series of trial simulations; the path of the muscle *vastus medialis* was further wrapped around an ellipsoidal wrapping object, to account for the obliquity of the fascicles at its patellar insertion[29,30].

APPENDIX B

Patellar tendon moment arm in flexion (PTMA^{flex}) during chair-rising

		Size		
		3	4	5
FFC	0°	39.1	39.2	39.1
	+3°	39.2	39.3	39.1
	+6°	39.3	39.3	39.2
	+9°	39.3	39.4	39.1

Patellar tendon moment arm at knee flexion (PTMA^{flex}) during rising-from-a-chair simulations with three different sizes and four different femoral component flexion angles (FFC). Values are in mm.

Patellar tendon moment arm in extension (PTMA^{ext}) during chair-rising

		Size		
		3	4	5
FFC	0°	50.9	54.3	57.7
	+3°	51.4	54.8	58.3
	+6°	51.8	55.5	59.0
	+9°	52.3	56.2	59.6

Patellar tendon moment arm at knee flexion (PTMA^{ext}) during rising-from-a-chair simulations with three different sizes and four different femoral component flexion angles (FFC). Values are in mm.

Patellar tendon force (PTF) during chair-rising

		Size		
		3	4	5
FFC	0°	2.83	2.63	2.50
	+3°	2.77	2.59	2.47
	+6°	2.72	2.55	2.42
	+9°	2.66	2.52	2.38

Peak patellar tendon force (PTF) during rising-from-a-chair simulations with three different sizes and four different femoral component flexion angles (FFC). Values are expressed as fractions of body weight (BW).

Quadriceps muscle force (QMF) during chair-rising

		Size		
		3	4	5
FFC	0°	3.77	3.45	3.21
	+3°	3.67	3.38	3.17
	+6°	3.59	3.34	3.12
	+9°	3.52	3.30	3.07

Peak quadriceps muscle force (QMF) during rising-from-a-chair simulations with three different sizes and four different femoral component flexion angles (FFC). Values are expressed as fractions of body weight (BW).

Quadriceps tendon-to-femur force (QTFF) during chair-rising

		Size		
		3	4	5
FFC	0°	1.40	1.66	1.88
	+3°	1.44	1.70	1.90
	+6°	1.47	1.73	1.92
	+9°	1.50	1.77	1.93

Peak quadriceps tendon-to-femur force (QTFF) during rising-from-a-chair simulations with three different sizes and four different femoral component flexion angles (FFC). Values are expressed as fractions of body weight (BW).

Patellofemoral contact force (PFCF) during chair-rising

		Size		
		3	4	5
FFC	0°	4.30	3.78	3.41
	+3°	4.17	3.69	3.33
	+6°	4.06	3.61	3.26
	+9°	3.95	3.55	3.18

Peak patellofemoral contact force (PFCF) during rising-from-a-chair simulations with three different sizes and four different femoral component flexion angles (FFC). Values are expressed as fractions of body weight (BW).

REFERENCES

1.   Gromov, K., Korchi, M., Thomsen, M. G., Husted, H. & Troelsen, A. What is the optimal alignment of the tibial and femoral components in knee arthroplasty? *Acta Orthop.* **85**, 480–487 (2014).

2.   Kim, Y.-H., Park, J.-W., Kim, J.-S. & Park, S.-D. The relationship between the survival of total knee arthroplasty and postoperative coronal, sagittal and rotational alignment of knee prosthesis. *Int. Orthop.* **38**, 379–85 (2014).

3.   Lustig, S. *et al.* Sagittal placement of the femoral component in total knee arthroplasty predicts knee flexion contracture at one-year follow-up. *Int. Orthop.* **36**, 1835–9 (2012).

4.   Chen, S. *et al.* Morphological evaluation of the sagittal plane femoral load-bearing surface in computer-simulated virtual total knee arthroplasty implantation at different flexion angles. *Knee Surg. Sports Traumatol. Arthrosc.* **25**, 2880–2886 (2017).

5.   Bonnin, M. P., Schmidt, A., Basiglini, L., Bossard, N. & Dantony, E. Mediolateral oversizing influences pain, function, and flexion after TKA. *Knee Surg. Sports Traumatol. Arthrosc.* **21**, 2314–24 (2013).

6.   Fokin, A. & Heekin, R. Anterior Referencing versus Posterior Referencing in Total Knee Arthroplasty. *J. Knee Surg.* **27**, 303–308 (2013).

7.   Matziolis, G., Hube, R., Perka, C. & Matziolis, D. Increased flexion position of the femoral component reduces the flexion gap in total knee arthroplasty. *Knee Surg. Sports Traumatol. Arthrosc.* **20**, 1092–6 (2012).

8.   Brar, A. S., Howell, S. M., Hull, M. L. & Mahfouz, M. R. Does Kinematic Alignment and Flexion of a Femoral Component Designed for Mechanical Alignment Reduce the Proximal and Lateral Reach of the Trochlea? *J. Arthroplasty* **31**, 1808–13 (2016).

9.   Chen, S.-C. *et al.* Effect of Femoral Component Flexion Implantation on the Mediolateral Bone-prosthetic Fit in Total Knee Arthroplasty. *Orthop. Surg.* **9**, 91–96 (2017).

10.   Roßkopf, J., Singh, P. K., Wolf, P., Strauch, M. & Graichen, H. Influence of intentional femoral component flexion in navigated TKA on gap balance and sagittal anatomy. *Knee Surg. Sports Traumatol. Arthrosc.* **22**, 687–93 (2014).

11.   Nedopil, A. J., Howell, S. M. & Hull, M. L. What clinical characteristics and radiographic parameters are associated with patellofemoral instability after kinematically aligned total knee arthroplasty? *Int. Orthop.* **41**, 283–291 (2017).

12.   Marra, M. A. *et al.* A subject-specific musculoskeletal modeling framework to predict in vivo mechanics of total knee arthroplasty. *J. Biomech. Eng.* **137**, 020904 (2015).

13.   Fregly, B. J. *et al.* Grand challenge competition to predict in vivo knee loads. *J. Orthop. Res.* **30**, 503–13 (2012).

14.   Cignoni, P. *et al.* MeshLab: an Open-Source Mesh Processing Tool. in *Eurographics Italian Chapter Conference* (eds. Vittorio, S., Rosario, D. C. & Ugo, E.) 129–136 (Eurographics Association, 2008).

doi:10.2312/LocalChapterEvents/ItalChap/It alianChapConf2008/129-136

15. Cohen, Z. A. *et al.* Knee cartilage topography, thickness, and contact areas from MRI: in-vitro calibration and in-vivo measurements. *Osteoarthr. Cartil.* **7**, 95–109 (1999).

16. Blankevoort, L., Kuiper, J. H., Huiskes, R. & Grootenboer, H. J. Articular contact in a three-dimensional model of the knee. *J. Biomech.* **24**, 1019–31 (1991).

17. Grood, E. S. & Suntay, W. J. A joint coordinate system for the clinical description of three-dimensional motions: application to the knee. *J. Biomech. Eng.* **105**, 136–44 (1983).

18. Antony, J., Tetsworth, K. & Hohmann, E. Influence of sagittal plane component alignment on kinematics after total knee arthroplasty. *Knee Surg. Sports Traumatol. Arthrosc.* **25**, 1686–1691 (2017).

19. Murphy, M., Journeaux, S., Hides, J. & Russell, T. Does flexion of the femoral implant in total knee arthroplasty increase knee flexion: a randomised controlled trial. *Knee* **21**, 257–63 (2014).

20. Kawahara, S. *et al.* Upsizing the femoral component increases patellofemoral contact force in total knee replacement. *J. Bone Joint Surg. Br.* **94**, 56–61 (2012).

21. Halewood, C., Risebury, M., Thomas, N. P. & Amis, A. A. Kinematic behaviour and soft tissue management in guided motion total knee replacement. *Knee Surg. Sports Traumatol. Arthrosc.* **22**, 3074–82 (2014).

22. Amis, A. A., Firer, P., Mountney, J., Senavongse, W. & Thomas, N. P. Anatomy and biomechanics of the medial

patellofemoral ligament. *Knee* **10**, 215–20 (2003).

23. Li, G. *et al.* Cruciate-retaining and cruciate-substituting total knee arthroplasty: an in vitro comparison of the kinematics under muscle loads. *J. Arthroplasty* **16**, 150–6 (2001).

24. Donadio, J., Pelissier, A., Boyer, P. & Massin, P. Control of paradoxical kinematics in posterior cruciate-retaining total knee arthroplasty by increasing posterior femoral offset. *Knee Surg. Sports Traumatol. Arthrosc.* **23**, 1631–7 (2015).

25. Panagiotopoulos, E., Strzelczyk, P., Herrmann, M. & Scuderi, G. Cadaveric study on static medial patellar stabilizers: the dynamizing role of the vastus medialis obliquus on medial patellofemoral ligament. *Knee Surg. Sports Traumatol. Arthrosc.* **14**, 7–12 (2006).

26. Carbone, V. *et al.* TLEM 2.0 – A comprehensive musculoskeletal geometry dataset for subject-specific modeling of lower extremity. *J. Biomech.* **48**, 734–741 (2015).

27. Andersen, M. S., Damsgaard, M. & Rasmussen, J. Kinematic analysis of over-determinate biomechanical systems. *Comput. Methods Biomech. Biomed. Engin.* **12**, 371–84 (2009).

28. Skipper Andersen, M., de Zee, M., Damsgaard, M., Nolte, D. & Rasmussen, J. Introduction to Force-Dependent Kinematics: Theory and Application to Mandible Modeling. *J. Biomech. Eng.* **139**, 091001 (2017).

29. Engelina, S., Antonios, T., Robertson, C. J., Killingback, A. & Adds, P. J. Ultrasound investigation of vastus medialis oblique muscle architecture: An in vivo study. *Clin. Anat.* **27**, 1076–1084 (2014).

30.   Bennett, W. F., Doherty, N., Hallisey, M. J. & Fulkerson, J. P. Insertion orientation of terminal vastus lateralis obliquus and vastus medialis obliquus muscle fibers in human knees. *Clin. Anat.* **6**, 129–134 (1993).

Specific muscle strength is reduced in facioscapulohumeral dystrophy

An MRI based musculoskeletal analysis

Marco A. Marra[*], Linda Heskamp[*], Karlien Mul, Saskia Lassche, Baziel G.M. van Engelen, Arend Heerschap, and Nico Verdonschot.

---

[*] Authors contributed equally to this work

ABSTRACT

The aim was to test whether strength per unit of muscle area (*specific muscle strength*) is affected in facioscapulohumeral dystrophy (FSHD) patients, as compared to healthy controls. Ten patients and ten healthy volunteers underwent an MRI examination and maximum voluntary isometric contraction measurements (MVICs) of the quadriceps muscles. Contractile muscle volume, as obtained from the MR images, was combined with the MVICs to calculate the physiological cross-sectional area (PCSA) and muscle strength using a musculoskeletal model. Subsequently, specific strength was calculated for each subject as muscle strength divided by total PCSA. FSHD patients had a reduced quadriceps muscle strength (median [1st quartile-3rd quartile]: 2011 [905.4-2775] N *vs.* 5510 [4727-8321] N, $p<0.001$) and total PCSA (83.6 [62.3-124.8] cm^2 *vs.* 140.1 [97.1-189.9] cm^2, $p=0.015$) compared to healthy controls. Furthermore, the specific strength of the quadriceps was significantly lower in patients compared to healthy controls (20.9 [14.7-24.0] N/cm^2 *vs.* 41.9 [38.3-49.0] N/cm^2, $p<0.001$). Thus, even when correcting for atrophy and fatty infiltration, patients with FSHD generated less force per unit area of residual muscle tissue than healthy controls. Possible explanations include impaired force propagation due to fatty infiltration, reduced intrinsic force-generating capacity of the muscle fibers, or mitochondrial abnormalities leading to impaired energy metabolism.

INTRODUCTION

Facioscapulohumeral muscular dystrophy (FSHD) is a hereditary disease characterized by progressive loss of muscle strength, starting in the face, shoulder and upper arm region[1]. In addition, the trunk and lower extremity muscles are frequently involved[1]. Histopathological changes can be very diverse, ranging from mild myopathic features to overt dystrophic changes with fatty infiltration and fibrosis[2]. Magnetic Resonance Imaging (MRI) of the lower extremity muscles reveals that muscles are affected by fatty infiltration in a specific pattern[3–5]. For example, in the thigh there is early involvement of the hamstrings, adductors and *rectus femoris*, whereas the *vasti* muscles usually become involved later in the disease course.

To aid the development of new treatments for FSHD it is important to understand why muscles of FSHD patients are weak. Muscle strength depends on the physiological cross-sectional area (PCSA)[6], i.e. the cross-sectional area perpendicular to the direction of the muscle fibers. In FSHD, fatty infiltration, fibrosis and muscle fiber atrophy affect the muscle tissue and are assumed to result in a reduced PCSA and contractile muscle volume, i.e. the portion of the muscle able to generate force. Therefore, fatty infiltration, atrophy and fibrosis may all contribute to muscle weakness. Janssen et al. indeed showed that the amount of contractile muscle tissue in the quadriceps muscles of FSHD patients is related to muscle strength[3]. Furthermore, it has been suggested that reduced specific muscle strength, defined as strength per unit area of contractile muscle tissue, is an additional cause of muscle weakness in FSHD[7,8]. However, Bachasson et al. did not include imaging of the quadriceps muscles[7] and some of us investigated specific muscle strength only on a single muscle fiber level[8].

In this study, we investigate whether the specific strength of the quadriceps muscles is affected in FSHD patients as compared to healthy controls. For this aim we evaluated contractile volume, PCSA and strength of quadriceps muscles by combining quantitative MRI, quantitative muscle assessment and musculoskeletal modeling.

MATERIAL AND METHODS

Participants

FSHD patients and healthy control subjects were retrospectively recruited from two cohorts. The FSHD patients were selected from a larger database of 140 FSHD patients who are participating in a prospective cohort study (FSHD-FOCUS study, Nijmegen, The Netherlands). The control cohort consisted of a group of ten healthy volunteers who participated in the TLEM*safe* project dataset (FP7-ICT-2009-4). All subjects performed a maximum voluntary isometric contraction (MVIC) of the knee extensor muscles and underwent an MRI examination of the quadriceps muscles. On the day of MVIC examinations, all patients performed also manual muscle testing, 6-minute walking test, motor function measure, and spirometry, as part of the FSHD-FOCUS study protocol. No other tests were performed by the healthy controls on the examination days. Gender, age, height, and weight have been recorded for both groups. FSHD disease severity were assessed with a 10-point clinical severity score (Ricci score[9]). For the present study, FSHD patients and health volunteers were included if the MVIC measurement was performed correctly, and the MR images of the lower extremity covered the entire span of the quadriceps muscles and contained no artifacts, like movement or failed reconstruction of the fat and water images obtained via a 2pt-Dixon sequence.

This study was conducted according to the principles of the Declaration of Helsinki (version October 2013) and in accordance with the Medical Research Involving Human Subjects Act (WMO). In both groups, informed consent was obtained from each participant.

Experimental measurements

MR imaging

All subjects were examined on a 3T MR system (TIM Trio, Siemens, Erlangen, Germany) using a ^{1}H spine coil combined with phased array coils placed around the leg.

In the FSHD patients MR data of the thigh were recorded with a 2pt-Dixon sequence to quantify the amount of fatty infiltration (repetition time, TR:

10 ms, echo time, TE in-phase: 2.45 ms, TE out-phase: 3.675 ms, flip angle, FA: 3°, voxel size: 1.36×1.36×5.00 mm³, 1 or 2 stacks with number of slices: 72). A fat fraction map, ranging from zero to one, was calculated for each slice from the reconstructed water and fat images by dividing the signal intensities of every voxel in the fat image by the signal intensities of the same voxel in the fat and water images summed together ($F/(F+W)$).

The dataset of healthy volunteers contained T1-weighted MR images of the lower extremity from hip to ankle (TR/TE: 545/9 ms, voxel size: 1.04×1.04×3.00 mm³, number of slices: 400). These T1-weighted data did not allow for quantitative fat measurements. Visual inspection of fatty infiltration on T1-weighted images did not show any pathological fatty infiltration of the quadriceps muscles in any of the healthy subjects. Therefore, for the healthy group, fat fraction values were assumed equal to 8.4 %, 7.1 %, 6.7 % and 7.5 % in the *rectus femoris*, *vastus intermedius*, *vastus lateralis*, and *vastus medialis* respectively, based on our previous measurements in a separate group of ten healthy volunteers (unpublished data, mean [1st quartile-3rd quartile]; age: 41.5 [38-56] years old; BMI: 24.0 [21.6-24.9] kg/m²).

Strength assessment in the FSHD group

Maximum voluntary isometric contraction of the knee extensor muscles was assessed in the dominant leg of FSHD patients. Each participant was seated with both hips and knees flexed at 90° on a fixed quadriceps dynamometer. The ankle of the dominant leg was secured to the dynamometer using *Velcro* straps and located at a distance of 24.5 cm from the knee joint center. In this position, the participants were instructed to extend their leg, pushing maximally against the dynamometer. Isometric force was recorded and was fed back visually to the subject on a computer monitor. The test consisted of three consecutive knee extensor MVICs of 4 seconds each, with a resting period of 20 seconds between the tests. Hand support was not allowed throughout the test. Strong verbal and visual encouragement were employed to motivate the participants to deliver their maximal muscle effort. The maximum out of three measured forces was chosen as the final MVIC force. The MVIC force was then multiplied by the knee-to-sensor distance, resulting in the MVIC torque (τ).

Strength assessment in the control group

The MVIC in healthy controls was assessed using a Biodex Dynamometer setup (Biodex Medical Systems, Inc., Shirley, NY, USA). In brief, participants were seated on the chair of the device with both hips and knees flexed by 90°. Belts were placed around the thorax and the thigh and the ankle of the measured leg were tightened. Only the dominant leg was measured, similarly to the FSHD group. Three consecutive MVICs of 6 seconds each were performed, with a resting period of 20 seconds between the tests. Visual feedback and verbal motivation were employed. The highest of the three measured torques was taken as the final outcome.

A post hoc experiment was carried out in a separate group of 9 healthy volunteers to identify possible systematic differences in the MVIC measures between FSHD and control group, owing to different measurement devices. Bland-Altman analysis revealed a measurement bias and an intraclass correlation coefficient of 1.0 Nm and 0.94, respectively. Hence, we did not find any systematic difference in MVIC assessment when using two different measurement devices.

Data analysis

MRI and segmentation and volume/fat fraction

MR images were analyzed using the Medical Image Processing, Analysis, and Visualization software package (MIPAV, Center for Information Technology, National Institutes of Health, obtainable at http://mipav.cit.nih.gov) and MATLAB (version R2014B, The Mathworks, Inc. Natick, Massachusetts, United States). Muscle contours of the four quadriceps muscles were manually delineated every 2.5 cm in the axial direction from the most distal MRI slice to the most proximal MR slice (Figure 6.1). Caution was taken to avoid the inclusion of subcutaneous fat, fascia, and large blood vessels. Anatomical muscle volume (V_a) was determined as the number of voxels within the muscle mask across all slices multiplied by the voxel area and by the distance between slices of 2.5 cm[10]. In FSHD patients, an average fat fraction (f_{fat}) was calculated for each of the quadriceps muscles over the voxels in the muscle mask across all slices at which the quadriceps muscles were delineated.
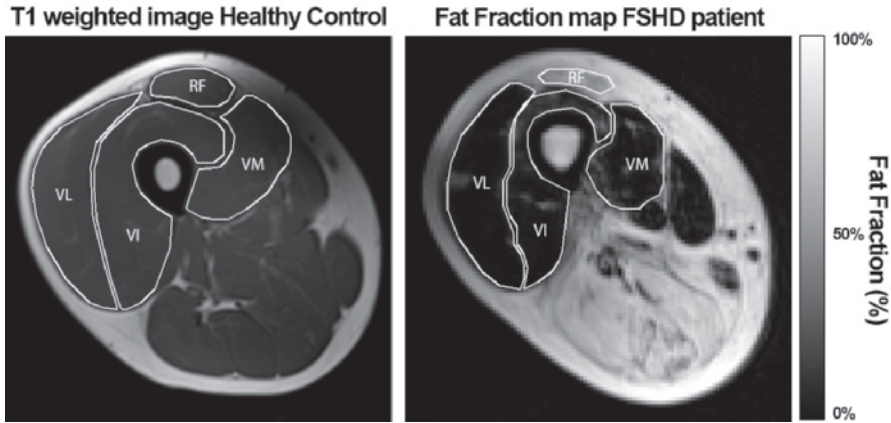
Figure 6.1 Left: T1-weighted MR image of the thigh muscles of a healthy volunteer. Right: fat fraction map of the thigh muscles of an FSHD patient acquired by a 2 pt Dixon method. Regions of interest are drawn around the *m. rectus femoris* (RF), *m. vastus lateralis* (VL), *m. vastus intermedius* (VI) and *m. vastus medialis* (VM).

It was assumed that the fatty infiltrate cannot generate force. Thus, for each muscle, the contractile muscle volume (V_c) was determined as

$$V_c = V_a \cdot (1 - f_{\text{fat}}) \tag{1}$$

where V_a is the anatomical muscle volume.

Calculation of specific muscle strength

Maximal force-generating capacity in a skeletal muscle, or muscle strength (S, in newton, N), is proportional to the muscle physiological cross-sectional area (PCSA, in cm²). S and PCSA are related by the specific muscle strength (σ, in N/cm²):

$$S = \sigma \cdot \text{PCSA} \tag{2}$$

S is also related to the experimentally measured torque (τ, in Nm) by the relation:

$$\tau = r_{\text{knee}} \cdot S \tag{3}$$

To derive r_{knee} and PCSA of the quadriceps muscles in all participants we used a musculoskeletal model. Briefly, a standard model was obtained from the AnyBody Managed Model Repository (AMMR 1.6.4) in the AnyBody Modeling
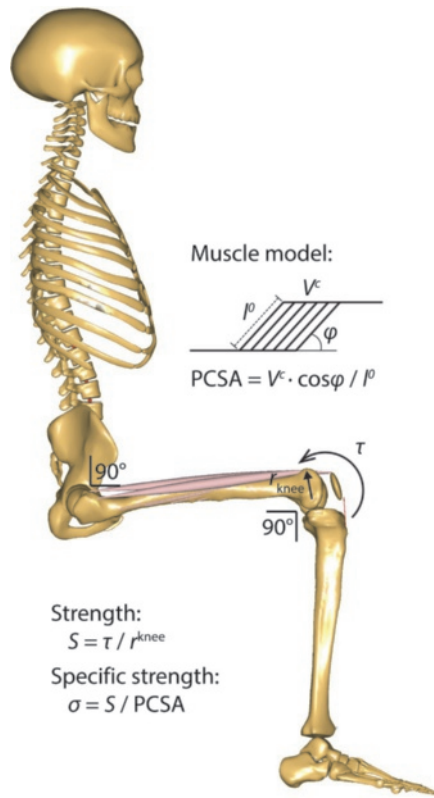
Figure 6.2 A view of the musculoskeletal model used to calculate the specific strength (σ). The model was adapted from the 'Standing Model' as available in the AnyBody Managed Model Repository (AMMR 1.6.4) in the AnyBody Modeling System (AMS, version 6.0.5, AnyBody Technology A/S, Aalborg, Denmark). The model was scaled based on the height of each subject and measurements of muscle volume. Contractile quadriceps muscle volumes (V_c) were measured by anatomical MRI and corrected using fat fraction maps. Pennation angle (φ) and optimal fiber length (l^0) values were extracted from the literature[14]. The average moment arm of quadriceps muscles (r_{knee}) was calculated at 90 degrees of knee flexion using the tendon excursion method.

System (AMS, version 6.0.5, AnyBody Technology A/S, Aalborg, Denmark)[11]. Body height was used to scale the body segments dimensions uniformly. Since the moment arm of a muscle about a joint depends on the angle of that joint, the model was configured in a sitting position similar to the one used in the experiments, with both hips and knees flexed by 90° (Figure 6.2). Existing algorithms available in the AMMR were used to calculate r_{knee} for each subject, using the tendon excursion method[12].

Table 6.1 Characteristics of patients with facioscapulohumeral dystrophy (FSHD) and healthy controls.

	FSHD (n = 10)	Controls (n = 10)
Female (%)	50.0	50.0
Age (years)	56.0 [47.8-66.5]	35.5 [24.5-57.5]
Height (cm)	174.0 [168.8-177.3]	176.0 [163.8-183.5]
Weight (kg)	72.0 [54.8-87.5]	76.8 [62.9-84.9]
BMI (kg/m²)	23.3 [19.9-27.2]	24.5 [21.7-26.4]
Ricci score	7.5 [2.8-8.0]	-

Data are shown as median [1st quartile-3rd quartile].

The PCSA of each of the quadriceps muscles was calculated from the contractile volume (V_c) divided by the optimal fiber length (l^0) and corrected for the pennation angle (φ) using the relationship[13]

$$\text{PCSA} = \frac{V_c \cos \varphi}{l^0} \tag{4}$$

in which l^0 and φ were derived from a dataset of architectural properties of cadaveric lower extremity muscles[14]. The total PCSA of the quadriceps (PCSA_{tot}) was calculated as the sum of the individual quadriceps muscles PCSAs. Finally, a specific muscle strength for each participant was calculated from Eq. 2, dividing S by PCSA_{tot}.

Statistical analysis

Statistical analysis was performed using Graphpad Prism 5 for Windows (version 5.03, Graphpad Software, San Diego, California, USA). Two-tailed unpaired Student's t tests were used to compare the characteristics of FSHD patients and healthy volunteers. Not normally distributed characteristics (according to Shapiro-Wilk test) were compared using the Mann-Whitney U test. Significance level was set to 0.05. The same test was used to compare τ, S, V_a, V_c, f_{fat}, PCSA, and σ. The relation between S and PCSA_{tot} in both the FSHD and control group was analyzed using Pearson product moment correlation analysis. We used data on specific muscle strength on 20 adult healthy subjects for use in a sample size calculation for our study because we found no sufficient information regarding specific strength variance over the FSHD population[15]. They reported specific muscle strength to be equal to (mean ± SD) 56 ± 11 N/cm². Setting a power of 0.8 and a Type I error of 0.05,
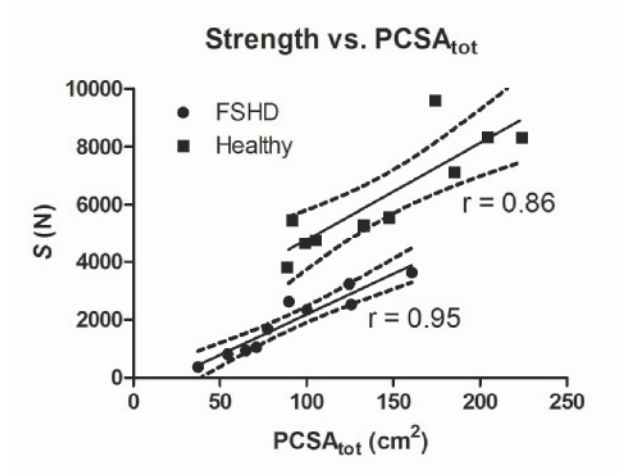
Figure 6.3 Relationship between quadriceps muscle strength (*S*) and total physiological cross-sectional area (PCSA$_{tot}$) in patients with facioscapulohumeral dystrophy (FSHD) and healthy controls.

results in a sample size of 10 patients (and 10 controls) to be able to detect a significant difference of 25 % in specific strength, which we consider to be clinically relevant. Due to the small sample size, data are presented as median [1st quartile-3rd quartile].

RESULTS

Participants characteristics

Ten FSHD patients and ten healthy controls met our inclusion criteria and were included in the analysis. Both groups were comparable in age, height, weight, and BMI (Table 6.1). Four out of the ten FSHD patients included in this study performed the muscle strength on the same day as the MRI examination. In the other six patients the examinations took place between thirty days and eleven weeks apart. The examinations in healthy controls were completed no more than two months apart.

Table 6.2 Maximum voluntary isometric contraction (MVIC) torque, (calculated) strength, anatomical volume, fat fraction, contractile volume, physiological cross-sectional area (PCSA) and (calculated) specific strength of quadriceps muscles in patients with facioscapulohumeral dystrophy (FSHD) and healthy controls.

	FSHD (n = 10)	Controls (n = 10)	*p*-value	
MVIC				
Measured torque (Nm)	63.8 (28.5, 91.3)	185.4 (146.1, 286.2)	<0.001	***
Strength (N)	2011 (905.4, 2775)	5510 (4727, 8321)	<0.001	***
Anatomical volume				
Total (cm^3)	1046 (755.3, 1361)	1515 (1049, 2039)	0.029	*
Rectus femoris (cm^3)	107.2 (44.1, 144.7)	203.5 (139.5, 322.4)	0.005	**
Vastus lateralis (cm^3)	408.8 (346.6, 489)	535.4 (329.0, 697.0)	0.393	n.s.
Vastus intermedius (cm^3)	322.0 (218.1, 368.3)	346.6 (317.9, 510.6)	0.123	n.s.
Vastus medialis (cm^3)	212.1 (103.2, 326.4)	358.7 (272.4, 497.9)	0.029	*
Fat fraction				
Total (%)	12.2 (9.3, 19.2)	7.3 (7.2, 7.3)	0.001	**
Rectus femoris (%)	17.3 (8.2, 45.0)	8.4[a]	0.020	*
Vastus lateralis (%)	10.5 (8.7, 15.5)	7.1[a]	0.011	*
Vastus intermedius (%)	10.4 (8.0, 20.9)	6.7[a]	0.002	*
Vastus medialis (%)	15.4 (8.8, 35.1)	7.5[a]	0.011	*
Contractile volume				
Total (cm^3)	862.4 (639.7, 1264)	1405 (973.4, 1891)	0.019	*
Rectus femoris (cm^3)	88.7 (24.2, 128.9)	186.4 (127.8, 295.3)	0.004	**
Vastus lateralis (cm^3)	353.1 (312.8, 456.2)	497.4 (305.7, 647.5)	0.315	n.s.
Vastus intermedius (cm^3)	284.4 (176.5, 331.6)	323.4 (296.6, 476.4)	0.043	*
Vastus medialis (cm^3)	165.9 (71.3, 302.2)	331.8 (252.0, 460.5)	0.019	*
PCSA				
Total (cm^2)	83.6 (62.3, 124.8)	140.1 (97.1, 189.9)	0.015	*
Rectus femoris (cm^2)	11.3 (3.1, 16.5)	23.8 (16.3, 37.8)	0.004	**
Vastus lateralis (cm^2)	33.7 (29.9, 43.6)	47.5 (29.2, 61.8)	0.315	n.s.
Vastus intermedius (cm^2)	28.6 (17.7, 33.3)	32.5 (29.8, 47.8)	0.043	*
Vastus medialis (cm^2)	14.9 (6.4, 27.1)	29.8 (22.6, 41.4)	0.019	*
Specific strength (N/cm^2)	20.9 (14.7, 24.0)	41.9 (38.3, 49.0)	<0.0001	***

Data are shown as median (1st quartile-3rd quartile). MVIC: maximum voluntary isometric contraction; PCSA: physiological cross-sectional area. n.s.: not significant, * p < 0.05, ** p < 0.01, *** p < 0.001
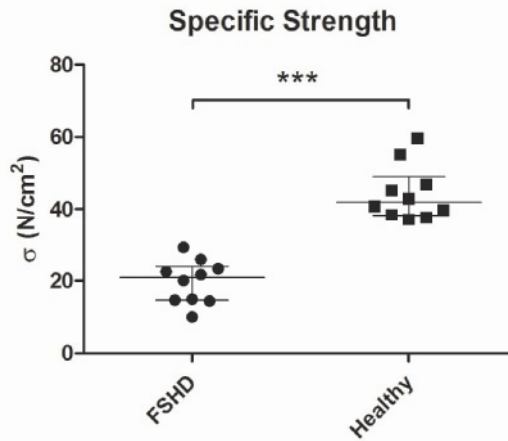[a] Fat fraction of individual muscles of healthy controls is based on unpublished experimental data.

Figure 6.4 Reduced specific strength (**σ**) of quadriceps muscles in patients with facioscapulohumeral dystrophy (FSHD) and healthy controls. Auxiliary lines indicate median [1st quartile-3rd quartile]. Asterisks (***) indicate p < 0.001.

Quantitative MRI and strength measurements

The MRI data revealed that fat fraction was significantly increased in quadriceps muscles of FSHD patients relative to normal values (p < 0.01). The *rectus femoris* and *vastus medialis* of FSHD patients had a reduced anatomical volume compared to the control group (*rectus femoris*: p = 0.005; *vastus medialis*: p = 0.029) (Table 6.2). Furthermore, the contractile volume of all quadriceps muscles, except the *vastus lateralis*, was lower in FSHD patients compared to healthy controls (*rectus femoris*: p = 0.004; *vastus intermedius*: p = 0.043; *vastus medialis*: p = 0.019, Table 6.2). Maximum voluntary isometric contraction torque was significantly lower in FSHD patients compared to healthy controls (*p* < 0.001; Table 6.2).

Musculoskeletal modeling: PCSA and specific strength calculation

Quadriceps muscle strength in FSHD patients was significantly lower than in healthy controls (FSHD: 2011 [905.4-2775] N, healthy controls: 5510 [4727-8321] N, *p* < 0.001; Table 6.2). Total PCSA, i.e. cross-sectional area perpendicular to the muscle fiber direction, of the quadriceps in FSHD

patients was significantly lower than in healthy controls (FSHD: 83.6 [62.3-124.8] cm², healthy controls: 140.1 [97.1-189.9] cm², p = 0.015; Table 6.2). Total PCSA correlated very strongly with the quadriceps muscle strength (Figure 6.3; FSHD: r = 0.95, p < 0.001; healthy controls: r = 0.86, p = 0.001). Specific muscle strength, i.e. strength per unit of PCSA, was significantly lower in FSHD patients compared to healthy controls (FSHD: 20.9 [14.7-24.0] N/cm²; healthy controls: 41.9 [38.3-49.0] N/cm², p < 0.0001; Figure 6.4). Hence, specific strength was reduced by 56 % in FSHD patients relative to controls.

DISCUSSION

Our study shows that specific muscle strength is reduced more than 50 % in our group of FSHD patients relative to healthy controls. In addition, contractile muscle volume and PCSA are significantly reduced. Therefore, it can be concluded that muscle weakness in FSHD is not only caused by a reduced amount of available contractile muscle tissue, but also by reduced function of the residual muscle tissue.

Muscle weakness in FSHD is partly caused by the reduction in the contractile muscle volume and PCSA. The smaller contractile muscle volume is firstly caused by the infiltration of fat. Furthermore, atrophy plays a role, because the anatomical muscle volume of the *rectus femoris* and *vastus medialis* is also reduced. The most important finding of our study is that the specific muscle strength is reduced in FSHD patients. This reduced specific muscle strength is not unique to FSHD, as similar results have been reported for Duchenne[16,17] and Becker[18] muscular dystrophy patients. The exact reason why specific muscle strength is reduced in FSHD is unknown. Potential explanations may be related to changes at the level of muscle fibers, energy metabolism, or in cytoarchitecture, resulting in biomechanical changes that alter force propagation.

First, reduced specific strength of the quadriceps may reflect reduced strength generation of individual muscle fibers. A pilot study by Lassche et al. found a 30 % strength reduction in demembranated FSHD type II fibers obtained from quadriceps muscle biopsies from FSHD patients, compared with healthy controls[8]. Second, the integrity of the sarcolemma can be compromised in FSHD muscle fibers, which may hamper lateral transmission of force generated by muscle fibers[19]. Third, mitochondria in FSHD quadriceps muscle

tissue might be dysfunctional[20]. Furthermore, in vivo measurement with MR spectroscopy showed that phosphocreatine to ATP ratio is reduced in moderately fat infiltrated FSHD muscles, indicating that energy metabolism is indeed altered[3,21]. Both the ATP synthesis[20] and the ratio of phosphocreatine to ATP[3] correlate positively with the force produced by the quadriceps muscles. Fourth, fatty infiltration may hamper the transfer of force to the tendon due to fatty interposition, resulting in reduced muscle strength. Advanced imaging techniques, such as ultrasound strain measurement[22-24] and diffusion-tensor imaging[25] can demonstrate muscle contraction patterns and force propagation and may characterize possible alterations in muscle fibers in FSHD. Besides fatty infiltration, FSHD muscles may suffer from increased interstitial fibrosis which would reduce the fractional muscular area. As our MRI protocol is not designed to detect fibrosis it was not taken into account in our study. As a consequence, the contractile muscle volume might have been overestimated, resulting in underestimation of the specific muscle strength in FSHD in our study. However, to explain the ± 50 % reduction of specific muscle strength in our group of FSHD patients compared to healthy controls, the remaining contractile muscle volume should consist for 50 % of fibrosis. In humans fractional fibrotic areas are rarely quantified. For the heart it has been reported that myocardial fibrosis may be present up to 15 % in coronary disease[26]. In an FSHD mouse model extreme high induction of DUX4 resulted in approximately 15 % fibrosis in the *gastrocnemius*[27]. As our patients only showed a mild to moderate fat infiltration it is unlikely that fibrosis has contributed significantly to the lower specific muscle strength observed in our study.

Quadriceps fat fraction in this study varied from normal (< 10 %) to moderately affected (46 %). This was reflected by the clinical severity scores. Three patients had no lower extremity involvement and one patient was unable to walk unaided. Thus, FSHD patients in our study show a large variability as is also seen in the FSHD population in general. Due to the retrospective nature of this study, the FSHD patients and healthy controls were recruited from two different cohorts in which a different force measurement device and MR protocol was used. Our post-hoc experiment comparing the two measurement devices in a separate group of healthy volunteers showed no systemic difference between the two devices. The MR protocol in healthy volunteers did not allow quantitative assessment of fat

infiltration. Therefore, the fat fractions for healthy controls used in this study were obtained from a separate group of healthy volunteers measured with the same 2pt Dixon protocol as the FSHD patients. For this reason, we conclude that the reduction of specific strength is not due to the different measurement set-up and MR protocol used in the FSHD patients and healthy controls. Since FSHD patients may have been fatigued or felt pain[28] more than healthy volunteers, this might have lowered their MVIC measurement. However, Bacchasson et al. found similar central and peripheral quadriceps fatigability in FSHD patients *vs.* controls, suggesting that fatigue or pain did not cause the changes in specific strength[7]. In our musculoskeletal model the pennation angle and optimal muscle fiber length were assumed to be similar in FSHD patients and healthy controls, although these may have been altered by disease processes in FSHD. However, measuring optimal fiber length and pennation angle *in vivo* is not feasible in a clinical setting, if not even impossible with the current techniques. Finally, the *rectus femoris* was included in the total quadriceps muscle PCSA, even though it has a minor contribution to force generation in the sitting position analyzed. However, in our FSHD cohort the *rectus femoris* is the most fat infiltrated quadriceps muscle. Thus, if the *rectus femoris* contribution is not taken into account the difference in specific strength between the two groups would become even larger.

This study may serve as a reference for future studies employing computer models of the musculoskeletal systems to study FSHD, as it provides values of specific muscle strength of an FSHD group in comparison to a group of healthy controls. Incorporating FSHD-specific model parameters, such as specific muscle strength, is important as the recruitment of muscles is dependent on the capacity of each muscle to generate force. To the present, it remains unclear, for instance, whether FSHD would also alter the recruitment of muscles during daily activities, which warrants further investigation.

CONCLUSIONS

Specific muscle strength of the quadriceps muscle is reduced in a group of FSHD patients compared to healthy controls, suggesting an intrinsic impairment in the force-generating capacity, energy metabolism and/or force propagation in FSHD muscles. Total contractile PCSA is also reduced in FSHD

muscles compared to healthy controls, indicating that fatty infiltration and atrophy are co-factors associated with muscle weakness in FSHD. This finding is important for two reasons. First, future studies that apply musculoskeletal models in FSHD patients should consider reduced specific muscle strength. Second, it tells us that interventions targeting muscle weakness in FSHD should focus on treating or preventing not only fatty infiltration and changes in contractile muscle volume, but also aim to restore specific muscle strength.

ACKNOWLEDGMENTS

FUNDING

REFERENCES

1. Mul, K. *et al.* What's in a name? The clinical features of facioscapulohumeral muscular dystrophy. *Pract. Neurol.* **16**, 201–207 (2016).

2. Dubowitz, V. & Sewry, C. *Muscle Biopsy: A Practical Approach. Neuropathology and Applied Neurobiology* (2007).

3. Janssen, B. H. *et al.* Distinct disease phases in muscles of facioscapulohumeral dystrophy patients identified by MR detected fat infiltration. *PLoS One* **9**, e85416 (2014).

4. Leung, D. G., Carrino, J. A., Wagner, K. R. & Jacobs, M. A. Whole-body magnetic resonance imaging evaluation of facioscapulohumeral muscular dystrophy. *Muscle Nerve* **52**, 512–520 (2015).

5. Kan, H. E. *et al.* Quantitative MR imaging of individual muscle involvement

in facioscapulohumeral muscular dystrophy. *Neuromuscul. Disord.* **19**, 357–62 (2009).

6.   Spector, S. A., Gardiner, P. F., Zernicke, R. F., Roy, R. R. & Edgerton, V. R. Muscle architecture and force-velocity characteristics of cat soleus and medial gastrocnemius: implications for motor control. *J. Neurophysiol.* **44**, 951–960 (1980).

7.   Bachasson, D. *et al.* Assessement of quadriceps strength, endurance and fatigue in FSHD and CMT: benefits and limits of femoral nerve magnetic stimulation. *Clin. Neurophysiol.* **125**, 396–405 (2014).

8.   Lassche, S. *et al.* Sarcomeric dysfunction contributes to muscle weakness in facioscapulohumeral muscular dystrophy. *Neurology* **80**, 733–7 (2013).

9.   Ricci, E. *et al.* Progress in the molecular diagnosis of facioscapulohumeral muscular dystrophy and correlation between the number of KpnI repeats at the 4q35 locus and clinical phenotype. *Ann. Neurol.* **45**, 751–7 (1999).

10.   Lund, H. *et al.* Volume estimation of extensor muscles of the lower leg based on MR imaging. *Eur. Radiol.* **12**, 2982–7 (2002).

11.   Damsgaard, M., Rasmussen, J., Christensen, S. T., Surma, E. & de Zee, M. Analysis of musculoskeletal systems in the AnyBody Modeling System. *Simul. Model. Pract. Theory* **14**, 1100–1111 (2006).

12.   Sherman, M. A., Seth, A. & Delp, S. L. What is a Moment Arm? Calculating Muscle Effectiveness in Biomechanical Models Using Generalized Coordinates. in *Volume 7B: 9th International Conference on Multibody Systems, Nonlinear Dynamics, and Control* **2013**, V07BT10A052 (ASME, 2013).

13.   Sacks, R. D. & Roy, R. R. Architecture of the hind limb muscles of cats: functional significance. *J. Morphol.* **173**, 185–95 (1982).

14.   Ward, S. R., Eng, C. M., Smallwood, L. H. & Lieber, R. L. Are current measurements of lower extremity muscle architecture accurate? *Clin. Orthop. Relat. Res.* **467**, 1074–82 (2009).

15.   O'Brien, T. D., Reeves, N. D., Baltzopoulos, V., Jones, D. A. & Maganaris, C. N. In vivo measurements of muscle specific tension in adults and children. *Exp. Physiol.* **95**, 202–10 (2010).

16.   Akima, H. *et al.* Relationships of thigh muscle contractile and non-contractile tissue with function, strength, and age in boys with Duchenne muscular dystrophy. *Neuromuscul. Disord.* **22**, 16–25 (2012).

17.   Wokke, B. H. *et al.* Quantitative MRI and strength measurements in the assessment of muscle quality in Duchenne muscular dystrophy. *Neuromuscul. Disord.* **24**, 409–416 (2014).

18.   Løkken, N., Hedermann, G., Thomsen, C. & Vissing, J. Contractile properties are disrupted in Becker muscular dystrophy, but not in limb girdle type 2I. *Ann. Neurol.* **80**, 466–71 (2016).

19.   Reed, P. *et al.* Sarcolemmal reorganization in facioscapulohumeral muscular dystrophy. *Ann. Neurol.* **59**, 289–297 (2006).

20.   Turki, A. *et al.* Functional muscle impairment in facioscapulohumeral muscular dystrophy is correlated with oxidative stress and mitochondrial dysfunction. *Free Radic. Biol. Med.* **53**, 1068–1079 (2012).

21.   Kan, H. E. *et al.* Only fat infiltrated muscles in resting lower leg of FSHD

patients show disturbed energy metabolism. *NMR Biomed.* **23**, 563–8 (2010).

22. Gijsbertse, K. *et al.* Three-dimensional ultrasound strain imaging of skeletal muscles. *Phys. Med. Biol.* **62**, 596–611 (2017).

23. Lopata, R. G. P. *et al.* Dynamic imaging of skeletal muscle contraction in three orthogonal directions. *J. Appl. Physiol.* **109**, 906–915 (2010).

24. Gijsbertse, K. *et al.* Ultrasound Imaging of Muscle Contraction of the Tibialis Anterior in Patients with Facioscapulohumeral Dystrophy. *Ultrasound Med. Biol.* 1–9 (2017). doi:10.1016/j.ultrasmedbio.2017.06.016

25. Oudeman, J. *et al.* A novel diffusion-tensor MRI approach for skeletal muscle fascicle length measurements. *Physiol. Rep.* **4**, e13012 (2016).

26. de Meester de Ravenstein, C. *et al.* Histological Validation of measurement of diffuse interstitial myocardial fibrosis by myocardial extravascular volume fraction from Modified Look-Locker imaging (MOLLI) T1 mapping at 3 T. *J. Cardiovasc. Magn. Reson.* **17**, 48 (2015).

27. Bosnakovski, D. *et al.* Muscle pathology from stochastic low level DUX4 expression in an FSHD mouse model. *Nat. Commun.* **8**, 550 (2017).

28. Kalkman, J. S. *et al.* Experienced fatigue in facioscapulohumeral dystrophy, myotonic dystrophy, and HMSN-I. *J. Neurol. Neurosurg. Psychiatry* **76**, 1406–9 (2005).

General discussion

CLINICAL RELEVANCE OF PERSONALIZED MUSCULOSKELETAL MODELING

People with musculoskeletal disorders live with profound disabilities, and see their quality of life being reduced. For diseases such as arthritis, treatments aim at reducing pain and restoring mobility of the patients, for instance, by performing a joint replacement. However, post-treatment outcomes are not always satisfactory[1], caused allegedly by current clinical assessment, which is *subjective*, *not quantitative,* and *error-prone*, and by the use of a *one-size-fits-all* approaches when formulating treatment plans, which leads to variable outcomes among different patients. Every patient suffering from a musculoskeletal disease is different, and has unique characteristics, which are difficult to comprehend when using standardized clinical protocols. It is currently believed that a more individualized approach to both diagnosis and treatment would greatly benefit the quality of healthcare services related to musculoskeletal diseases, as this would help defining better treatments, reduce errors, complaints and re-operations, and improve patient satisfaction.

Personalized musculoskeletal models can fill the gap in both diagnosis and treatment of musculoskeletal diseases, as they would provide *objective* and *quantitative* tools to ascertain the true underlying biomechanical conditions and to guide the formulation of tailored treatments. For this to occur in actuality, a paradigm shift is required to migrate from the current subjective clinical *modus operandi* to a more objective and patient-specific assessment and prediction of post-treatment outcomes. According to this approach, personalized models are created based on patient-specific data, and serve the clinicians as an objective and predictive platform to interrogate the actual patient conditions, to perform virtual simulations of alternative treatment, and on this basis, to select the optimal treatment plan to be executed.

There is a number of steps to be followed to implement personalized musculoskeletal models in clinical practice[2]. First (model preparation), the clinical outcomes that the model needs to predict have to be identified; the model complexity needs to be defined for the model to be able to accurately predict those outcomes; and the relevant patient-specific data that are necessary to create the model need to be collected. Secondly (model construction), a personalized model is constructed and its parameters

calibrated based on previously collected patient-specific data. Those model parameters, for which no patient-specific data are directly available, need to be estimated from the literature or calibrated in some other way. In this phase, possible treatment plans are also virtually incorporated into the model. Lastly (model utilization), the relevant outcome measures are predicted by the model for every virtual treatment plan, so that the best outcomes can be selected. In this stage, the outcomes of treatments that were not planned using the model can serve for model validation purposes, as well as clinical outcomes from treatments that were planned using the model.

As stressed by B.J. Fregly in his review, patient-specific calibration and validation are crucial steps for any process aiming at implementing personalized musculoskeletal models clinically[2]; the former, *calibration*, because musculoskeletal models will not be able to accurately represent individual patients unless calibrated to patient-specific data, and the latter, *validation*, because clinicians will never gain confidence in personalized model predictions until these demonstrate to accurately predict the outcomes of treatments planned without using the models. The introduction and advancement of personalized musculoskeletal models in clinical practice will depend upon a successful proof of their benefits by means of randomized controlled trials.

Personalized musculoskeletal modeling is currently undergoing a rapid development. However, very few examples exist to date implementing personalized modeling into clinical applications. In pediatric limb salvage surgery, personalized musculoskeletal models of children with a bone tumor have been used to predict the optimal rehabilitation process that would ensure adequate loading conditions on the bone allograft[3,4]. In the European TLEM*safe* project, personalized musculoskeletal models of patients with bone tumor and hip dysplasia have been used to predict the optimal surgical plan based on the evaluation of predicted post-treatment performance of activities of daily living (ADLs). The simulation platform was then linked to a surgical navigation system, in order to perform the optimally planned surgery in a safe and controlled environment[5]. Personalized models have also been used to inform the rehabilitation of post-stroke patients and above-knee amputees, in which the healthy leg kinematics served as reference for the motion of, respectively, the impaired leg and the exo prosthetic knee[6,7].

A number of requirements can be established in relation to the technical implementation of personalized musculoskeletal models. The construction of models based exclusively on patient-specific data is impractical, as this would require access to information that are not obtainable *in vivo*. For this reason, it has become common practice to use generic models and to further personalize these using patient-specific data. Generic models may come from cadaver studies, in which parameters that are inaccessible *in vivo* are measured and organized in normative datasets for re-use[8–10]. In clinical applications, which require accurate prediction of the outcomes of interest, calibration of these generic models to patient data is paramount, as simple rescaling of generic model has proven insufficient at reproducing patient-specific musculotendon lengths, muscle moment arm lengths, and joint contact forces[11–14]. For this reason, the first requirement of any musculoskeletal model devised to answer clinical questions is its ability to be customized and calibrated to geometric, kinematic, kinetic and neurologic data from the individual patient, to the extent required by the application[2]. This thesis addressed this problem, with a special focus on geometric and kinematic calibration of personalized models, as the ability to faithfully represent the skeletal anatomy, kinematics, and musculotendon morphology of individual patients (Chapters 2-5), and on kinetic calibration, as the ability to incorporate strength measurements of individual patients to predict strength-related properties of muscle tissue in muscular dystrophies (Chapter 6). Notwithstanding that each aspect of model calibration is important in terms of predicted outcomes, some model parameters, like the neuromuscular control strategy of patients with mobility impairments and several kinds of neural feedback, remain very difficult to personalize and warrants further investigation.

DEVELOPMENT OF A FRAMEWORK FOR PERSONALIZED MUSCULOSKELETAL MODELING

The first aim of this thesis was to develop a framework for the simulation of personalized knee models for use as diagnostic, pre-planning and outcome tools in total knee replacement (TKR) surgery. In Chapter 2, a methodology for generating and simulating personalized musculoskeletal models of the lower extremity was presented and validated against experimental

measurements of knee loads and kinematics. This methodology brings a few important advancements to the field of musculoskeletal modeling.

The first and most important aspect is the inclusion of a truthful anatomical representation of the lower extremity in a musculoskeletal model for the estimation of knee joint mechanics. Most previous models omitted a subject-specific representation of the musculoskeletal geometry, favoring simpler scaling methods, based on optical marker-based optimization of anthropometric parameters of generic template models[15–18].

The approach proposed in Chapter 2 used subject-specific medical images as the basis for 3-dimensional (3-D) model reconstruction, and morphing techniques for scaling muscle attachments sites from a musculoskeletal template model[10]. Image-based personalized models have already proved their superiority, when compared to rescaled generic models, in estimating subject specific muscle moment arms and musculotendon lengths[11,12], and joint and muscle loading[4,13]. For some applications (e.g., gait analysis), the use of rescaled generic models may still be acceptable, which relieves modelers of the extra efforts of an image-based personalization. However, for orthopedic applications, in which the model outcomes (e.g. joint loads and kinematics) are strongly affected by muscle forces, personalization is key. Therefore, model personalization should be attentively considered when using computational musculoskeletal models for surgical planning or clinical decision making.

A second novel aspect of the presented methodology consists in a seamless inclusion of a detailed knee joint model with discrete ligaments and contact forces into a full-body musculoskeletal model. The resultant musculoskeletal model allowed the simultaneous estimation of muscle forces, tibiofemoral and patellofemoral joint loads and kinematics using force-dependent kinematics (FDK)[19]. Force-dependent kinematics is a new approach for the solution of joint loads and kinematics for non-conforming joints, thus enhancing the paradigm of traditional inverse dynamics. Traditional inverse dynamics models oversimplify the knee joint representation, using idealized joint constraints (e.g., hinged joint) and/or prescribing the motion of secondary knee degrees of freedom (DoFs) based on previous measurements[20]. The ability, introduced by FDK, to estimate muscle forces, ligaments forces, joint loads and kinematics simultaneously in a personalized musculoskeletal model

opens up to a wide range of clinical and research applications, in which an accurate understanding of detailed joint mechanics is paramount. This is the case for pre-operative planning of orthopedic surgeries and/or evaluation of prosthetic design and alignment in TKR. Furthermore, it enables to study the effect of joint anatomy, muscle and ligament properties on knee joint kinematics and loads in a spectrum of daily activities, loading conditions and musculoskeletal pathologies, which would otherwise be impractical in traditional clinical settings.

A third aspect pertains to computational efficiency of FDK analysis of personalized musculoskeletal models. As shown in Chapter 3, an FDK solution for a normal gait cycle could be achieved in as short as 4.5 minutes using a surrogate contact model. In other words, simulations that used a surrogate tibiofemoral contact model were faster than simulations that used the reference contact model by a factor three. The acceleration of FDK analyses of ADLs did not compromise the estimation accuracy. With regard to computation time, the surrogate model presented in Chapter 3 performed better than previous studies that omitted a representation of muscles and ligaments[21], or performed comparably well as previous studies that did not include muscles at all, or prescribed some of the joint kinematics[20,22,23]. The ability to carry out FDK analyses within a few minutes is of interest to assess the effects of, for instance, ligament properties, implant alignment, different activities and loading conditions on muscle forces, ligaments forces, joint loads and kinematics, which typically requires extensive parametric analyses with many hundreds or thousands of simulations.

APPLICATION OF PERSONALIZED MUSCULOSKELETAL MODELS OF TKR

With regard to the second aim of this thesis, the personalized musculoskeletal modeling framework as presented in Chapter 2 was applied to two clinical research questions related to the sagittal alignment of the tibial (Chapter 4) and femoral (Chapter 5) component in cruciate-retaining (CR) TKR. In Chapter 4, it was shown that the tibial slope can have profound effects on the overall knee stability, depending on the surgical technique utilized. The findings of Chapter 5 support the hypothesis that flexing and downsizing the femoral component may be an interesting option to prevent anterior femoral

notching and, at the same time, achieve good reconstruction of the knee extensors mechanism and knee loading.

The use of a computational model allowed the simulation of hypothetical surgical scenarios in a very controlled study design, and to assess their impact on the mechanics of joint reconstruction during ADLs. These kinds of analysis would otherwise be impractical in clinical trials and/or *ex vivo* experiments. In clinical trials, many parameters are associated with the clinical outcomes of interest. These extra outcome-modifier parameters are difficult to control in patient cohorts, and can obfuscate the effect of the actual parameters of interest. The validity of *ex vivo* experiments is limited to the kinematics and loading patterns that can be achieved in a laboratory environment with cadaveric specimens. Particularly, the lack of physiological muscle activation and joint loading prove the findings of *ex vivo* experiments difficult to be generalized to *in vivo* conditions.

Important implant design considerations can be made, based on the findings of Chapter 4. Increasing the posterior tibial slope with anterior referencing (tibial re-cut) appears to produce detrimental effects on the overall stability of the knee, whereas increasing the slope by central referencing results in stable kinematics and reduces the loads on the patellofemoral joint. Therefore, it would be desirable, from a surgical point of view, to have a wider choice of inserts available, with variable built-in slopes that would allow surgeons to increase the tibial slope intra-operatively at need, and thus preventing dangerous re-cuts.

The findings of Chapter 4 and Chapter 5 on the effects of surgical factors are limited to a specific type of implant (CR-TKR) and patient anatomy. Therefore, they cannot be generalized to other implant types (e.g., posterior-stabilized TKR) and/or other classes of patients with severe knee deformities. Within narrower limits, it is reasonable to expect similar trends for the investigated biomechanical parameters also for a wider range of cases, which share similar characteristics to the ones of this two studies. Furthermore, for the analysis of surgical variations, the same dynamic loading conditions of ADLs as in the reference cases were used for all other simulated cases. When prosthetic parameters are changed, the way of executing a motor activity (kinematics and loading) might change as well in response. However, this event could not be taken into account with our methodology, or more

generally, with an inverse-dynamics approach, as inverse dynamics requires, notably, body-level kinematics as input to the simulation. To study how prosthetic parameters would affect the overall body kinematics, other approaches may be more suitable, like forward dynamics or inverse dynamics with motion optimization.

Albeit not validated in a clinical setting, the results of Chapter 4 and Chapter 5 provided valuable insights into the effect of surgical choices on the biomechanics of TKR, and how these can be exploited to improve the outcome of TKR surgeries. From an orthopedic surgeon's perspective, these findings do not provide an answer to the question: «What is the optimal sagittal alignment of my next patient enrolled for TKR?», but rather provide a biomechanical foundation for understanding cause-effect mechanisms involved in sagittal alignment in CR-TKR. By providing a more objective and complete picture, computational models can be used as a training tool to help orthopedic surgeons to improve the understanding of the multi-dimensional and multi-factorial effects of surgical choices.

IMAGED-BASED MUSCULOSKELETAL MODELING FOR THE STUDY OF FSHD

Chapter 6 concerned the investigation of specific muscle strength in FSHD. Specific muscle strength is a constitutive property of muscles, which accounts for the force-generating capacity of muscle tissue per unit physiological cross sectional area. Specific strength cannot be measured directly using isolated experimental techniques, and it has received little attention the study of FSHD. As shown in Chapter 6, quantitative MRI and image processing allowed for accurate discrimination between contractile muscle volume and fatty tissue content, and isometric quadriceps muscle assessment provided a way to quantitatively estimate quadriceps muscles strength. The use of these different techniques, in combination with personalized musculoskeletal modeling, allowed for the estimation of specific muscle strength on a subject- and patient-specific basis. Remarkably, specific muscle strength of quadriceps muscles was 50 % lower in FSHD patients compared to healthy controls.

This finding suggests that, besides atrophy and fatty infiltration, also the specific muscle strength is affected in patients with FSHD. This means that

differences exist in the intrinsic force-generating capacity of muscle fibers of FSHD patients and healthy subjects, and these need to be investigated further. Specific muscle strength needs, therefore, to be considered as an important co-factor of muscle weakness in FSHD. This aspect has very important implications also from a therapeutic point of view, as studies investigating potential treatment options for FSHD should also aim at restoration of specific muscle strength.

RECOMMENDATIONS FOR FUTURE RESEARCH

The applicability of personalized musculoskeletal knee modeling to larger patient groups than only one patient remains to be investigated. One possible approach could be to generate a subject-specific model for each individual, based on medical images and measurements, and perform personalized biomechanical analyses. However, the generation of personalized musculoskeletal models from medical images is time-intensive and requires a considerable amount of manual interventions. Furthermore, this approach entails also the investment of costly resources (CT and/or MRI), and its cost-effectiveness would also need to be evaluated. To accelerate and facilitate the adoption of personalized musculoskeletal models in the clinical setting using this approach, automatic algorithms for the generation of patient-specific models are needed. Such algorithms should provide either fully automated segmentation of hard and soft tissues, possibly spanning multiple image modalities, or a means to morph template musculoskeletal models to patient-specific anatomies quickly and accurately, or a combination of the two.

Another approach could be to incorporate inter-individual variability in musculoskeletal models, and perform probabilistic analyses on the entire population model. For instance, anatomical variability could be incorporated by means of statistical shape models[24]. This approach would require a large amount of input data and the generation of a dataset of probabilistic model outcomes. However, this investment is incurred only once upfront, and would allow more expedited access to model results, as the latter would be already pre-calculated. Although statistical shape models and active shape models represent an interesting approach to account for hard tissue anatomical variability, the automatic geometrical reconstruction of soft tissues like

muscles, tendons, ligaments, and cartilage remains a challenge, and requires further investigation.

In personalized musculoskeletal modeling, not only the geometry of hard and soft tissues is important, but also the underlying mechanical behavior of these structures, such as their capability of producing forces in relation to motion and deformation. The majority of current muscle-actuated models—including those presented in this thesis—represent complex muscle geometries using one-dimensional lines, via-points and wrapping objects. In future research, a transition to 3-dimensional muscle models should be explored[25], as this can account for the complex behavior of muscle tissue.

The personalization of material properties of biological materials is a very difficult task, and limited by the techniques currently available to extract relevant parameters. For instance, extracting musculotendon Hill-type musculotendon model parameters *in vivo*, for extended anatomical regions of the musculoskeletal system, remains unfeasible. However, these parameters affect the distribution of muscle forces considerably[26]. This aspects were not addressed within this thesis and warrants further investigation.

Moreover, knee kinematics are highly sensitive to ligaments' rest lengths[27], as the latter influence the laxity of joints in response to loads. Therefore, new noninvasive techniques need to be devised to quantify joint laxity and identify ligament model parameters *in vivo*. It is likely that the overall kinematics are more sensitive to a subset of very influential parameters, which can be identified based on sensitivity analyses.

There are a number of limitations in the musculoskeletal and FDK knee modeling approach that need to be considered. First, a simplified muscle model is used to represent muscles in the leg model, which uses one-dimensional line elements with via-points and wrapping surfaces. This choice provides, certainly, an efficient way to account for muscle forces in a comprehensive musculoskeletal model of the lower extremity, but may be excessively reductive when considering the anatomical complexity of muscle shapes and paths in the human leg.

An optimization criterion was chosen to compute the muscle forces distribution in 166 Hill-type muscle models in the lower extremity. This criterion minimizes the sum of the cubes of the muscle activations, weighted

by the respective muscle volumes. Although this is an efficient approach to compute muscle forces, it may not be suitable for all ADLs and/or for different types of patients or older people. Certain motor tasks may require more complex muscle control strategies e.g. to ensure additional joint stability and/or movement precision, that may not be captured fully by an effort-minimizing optimization criterion. Furthermore, whereas it is possible for the model to estimate muscle co-contraction (i.e. the concurrent activation of agonist and antagonist muscles around a joint) to balance the request for joint torque by means of contra-agonist muscles activation, phenomena like joint stiffness or pain avoidance, which may be present in patients or elderly people, are not explicitly modeled, and their effect on muscle co-contraction are, therefore, disregarded.

Making an assumption of quasi-static equilibrium in the secondary knee joint DoFs does not allow to take into account the viscoelastic behaviors of soft tissues. This aspect did not constitute a serious limitation in the present thesis, as the prosthetic materials in the artificial knee model could be represented with reasonable accuracy using elastic material properties. However, if FDK were to be used for the modeling of natural knee joint, particular attention would be required with regard to material properties of soft tissues such as articular cartilage, ligaments, menisci, and the joint capsule. To characterize the mechanical behavior of these elements in a quasi-static analysis, their material properties should be selected according to the loading rates the specific activity analyzed.

Whereas the surrogate modeling approach presented in Chapter 3 may allow the study of systematic variations in TKR, it may not be ready yet for clinical usage and/or application to patient cohorts, due to the substantial amount of time required by its generation. A possible approach to extend its usability for addressing clinical problems would be to expand the parameters space to also account for anatomical variability, thus relieving the efforts of generating a new surrogate model for each patient. Statistical shape models represent a convenient and parameterized way to account for shape variability, which may be suitable for the purposes of surrogate models generation.

For musculoskeletal models and simulations to build credibility and find their way in clinical settings as diagnostic and pre-planning tools, model predictions should be further related to clinical findings and continuously

validated. In the case of component alignment in TKR, future studies should validate model-predicted changes of knee loads and kinematics in response to surgical choices in prospective cohort studies. A corroboration process of this kind could also be useful to inform on possible important sources of uncertainty in computational models that need to be addressed and modeling aspects that require further refinement. The range of applications of personalized musculoskeletal models is wide: once a patient-specific model is generated for each new patient requiring a surgery, surgeons can test the effect of different treatment options on that patient, before actually entering the operating room, based on an *objective* biomechanical tool and *dynamic* simulation. The model-informed computer simulation platform can guide the formulation of a personalized surgical planning.

Predictive capabilities are an important aspect of musculoskeletal models. Models are most useful when they are able to predict *future* events*,* such as hypothetical *what-if* surgical scenarios, besides complying with experimental measurements that occurred in the *past* (which, nevertheless, are essential for validation purposes). An obvious challenge in predictive modeling is posed by the nearly total unavailability of input data (e.g., kinematics, ground reaction forces). In the two studies on TKA alignment presented in Chapter 4 and 5, this difficulty was overcome utilizing the same kinematic and kinetic input data in all simulation cases.

When kinematic and kinetic input data is not directly available, alternative technique should be explored. One possible approach is represented by neural data-driven musculoskeletal modeling, in which subject-specific neural data recordings (e.g., electromyography signal) are used to generate personalized musculoskeletal movement simulations[28]. This approach, potentially, also allows the inclusion of subject-specific neural strategy, which would be otherwise difficult to do using traditional optimization techniques. Another opportunity for predictive simulation is offered by motion synthesis through dynamic optimization and optimal control[29–31] and reinforcement-learning[32] techniques. In these formulations, motion is predicted based on a desired kinematic goal or a high-level description of the task. The reinforcement-learning approach is particularly appealing to clinical applications, as it would make the collection of experimental neuromuscular and/or kinematic data unnecessary, thus simplifying substantially the entire workflow for musculoskeletal simulation.

In the study of FSHD via musculoskeletal modeling, it is important to take into account take the reduction of specific muscle strength (as found in Chapter 6), as this affects directly the muscle force coordination. Particularly, in FSHD, muscle weakness progresses according to a very distinct pattern. Typically the onset is in the face, shoulder and upper arm regions, and then it progresses to the trunk and lower extremity, with early involvement of the hamstrings, the adductors and the *rectus femoris* muscle. In the leg muscles, the disease progresses from distal to proximal direction, the causes of which remains unclear. A previous musculoskeletal simulation study showed a strong correlation between fatty infiltration and eccentric muscle contraction work in Duchenne muscular dystrophy, which helps explaining selective muscle degeneration[33]. Although those findings may be specific of Duchenne dystrophy, a similar approach could be used also in FSHD, to try to understand if selective involvement of specific muscles or muscle groups in FSHD also depends on some specific parameters that can be calculated using a musculoskeletal model.

Our understanding of FSHD could benefit from the use of detailed multiscale musculoskeletal models. Multiscale modeling may bridge the body level multibody dynamics to the tissue level mechanics, or even cellular level biochemical processes, and can provide useful information on tissue stresses and strain distribution in affected muscles and the mechanical behavior of muscle fibers. A multiscale approach would allow to overcome the limitations imposed by current 1-dimensional muscle models with lumped parameters. This simplification currently hampers the study of specific muscle degenerations in FSHD. Future image-based multiscale musculoskeletal models incorporating FSHD-specific parameters have the potential to elucidate abnormal mechanisms of muscle contraction and biochemical processes in patients with FSHD.

CONCLUDING REMARKS

This thesis established a computational framework to generate personalized musculoskeletal models of the knee joint that can be used to estimate muscle forces, knee joint loads and kinematics, and ligament forces during ADLs. The proposed methodology is a step forward towards the integration of musculoskeletal modeling and simulation in the diagnostic and pre-operative

planning stages of musculoskeletal conditions. The validity of estimated knee loads and kinematics was confirmed by direct comparison with experimental measurements in a single patient, and the results were promising. Due to the complexity of the computational techniques involved, the presented personalized modeling approach was computationally expensive. Although the use of a surrogate contact model reduced the computational cost of simulations substantially, further research is required to further accelerate the model generation and simulation, and possibly make it less dependent on existing input data.

In contrast to the current clinical practice, in which static and subjective assessment tools are often utilized, the presented model-based approach provided a versatile and dynamic simulation platform to quantify the effect of surgical treatments, such as TKR, and the status of neuromuscular conditions, such as FSHD, in a personalized fashion. It is foreseen that musculoskeletal models will enter the clinical practice in the future, also considering the steadily increasing demand for healthcare services related to musculoskeletal diseases. Personalized models have the potential to improve the current diagnostic tools for musculoskeletal diseases, and to serve as an objective and reliable guide in the planning of treatments. For this to happen in actuality, future research should put efforts in simplifying and accelerating the creation process of personalized musculoskeletal models, continuously validating model predictions, and providing easy access to simulation results in the clinical settings.

Certainly, the modeling approach here presented involves still a large amount of manual work and remains computationally intensive. However, the workflow presented can be applied to more specific and relatively simpler cases, in which the biomechanical parameters of interest are limited. In this way, the dimensionality and complexity of the problem can be reduced, and thereby the application of the method becomes more practical. As an example of this approach, personalized musculoskeletal modeling has been introduced in the study of patellofemoral instability, which is object of current research. In this problem, the modeled portion of the musculoskeletal system is confined to the knee and patellofemoral joint, and a simple leg movement is simulated that does not require full-body kinematics as input data. In this ongoing study, the attention is focused on fewer anatomical and functional parameters (bony shape, muscles and ligaments properties), with the aim of

predicting the outcomes of corrective surgery for this specific pathology. For these kind of applications, a simplified modeling approach appears more feasible than modeling and simulating the whole-body musculoskeletal system, and presents important advantages in terms of computationally efficiency.

REFERENCES

1.   Bourne, R. B., Chesworth, B., Davis, A., Mahomed, N. & Charron, K. Comparing patient outcomes after THA and TKA: is there a difference? *Clin. Orthop. Relat. Res.* **468**, 542–6 (2010).

2.   Fregly, B. J., Boninger, M. L. & Reinkensmeyer, D. J. Personalized neuromusculoskeletal modeling to improve treatment of mobility impairments: a perspective from European research sites. *J. Neuroeng. Rehabil.* **9**, 18 (2012).

3.   Viceconti, M. *et al.* Multiscale modelling of the skeleton for the prediction of the risk of fracture. *Clin. Biomech.* **23**, 845–852 (2008).

4.   Taddei, F. *et al.* Femoral loads during gait in a patient with massive skeletal reconstruction. *Clin. Biomech.* **27**, 273–280 (2012).

5.   Verdonschot, N. *et al.* PATIENT-SPECIFIC MUSCULOSKELETAL MODELS TO IMPROVE PREDICTABILITY OF FUNCTIONAL RECOVERY OF PATIENTS REQUIRING SEVERE RECONSTRUCTIVE SURGERY. in *Orthopaedic Proceedings* **98–B**, 97 (2016).

6.   Vallery, H., Van Asseldonk, E. H. F., Buss, M. & Van Der Kooij, H. Reference trajectory generation for rehabilitation robots: Complementary limb motion estimation. *IEEE Trans. Neural Syst. Rehabil. Eng.* **17**, 23–30 (2009).

7.   Vallery, H. *et al.* Complementary limb motion estimation for the control of active knee prostheses. *Biomed. Tech.* (2011). doi:10.1515/BMT.2010.057

8.   Klein Horsman, M. D., Koopman, H. F. J. M., van der Helm, F. C. T., Prosé, L. P. & Veeger, H. E. J. Morphological muscle and joint parameters for musculoskeletal modelling of the lower extremity. *Clin. Biomech.* **22**, 239–247 (2007).

9.   Arnold, E. M., Ward, S. R., Lieber, R. L. & Delp, S. L. A model of the lower limb for analysis of human movement. *Ann. Biomed. Eng.* **38**, 269–279 (2010).

10.   Carbone, V. *et al.* TLEM 2.0 – A comprehensive musculoskeletal geometry dataset for subject-specific modeling of lower extremity. *J. Biomech.* **48**, 734–741 (2015).

11.   Scheys, L., Spaepen, A., Suetens, P. & Jonkers, I. Calculated moment-arm and muscle-tendon lengths during gait differ substantially using MR based versus rescaled generic lower-limb musculoskeletal models. *Gait Posture* **28**, 640–648 (2008).

12.   Scheys, L., Van Campenhout, A., Spaepen, A., Suetens, P. & Jonkers, I. Personalized MR-based musculoskeletal models compared to rescaled generic models in the presence of increased femoral anteversion: Effect on hip moment

arm lengths. *Gait Posture* **28**, 358–365 (2008).

13.   Lenaerts, G. *et al.* Subject-specific hip geometry and hip joint centre location affects calculated contact forces at the hip during gait. *J. Biomech.* **42**, 1246–1251 (2009).

14.   Scheys, L., Desloovere, K., Suetens, P. & Jonkers, I. Level of subject-specific detail in musculoskeletal models affects hip moment arm length calculation during gait in pediatric subjects with increased femoral anteversion. *J. Biomech.* **44**, 1346–1353 (2011).

15.   Kim, H. J. *et al.* Evaluation of predicted knee-joint muscle forces during gait using an instrumented knee implant. *J. Orthop. Res.* **27**, 1326–31 (2009).

16.   Hast, M. W. & Piazza, S. J. Dual-joint modeling for estimation of total knee replacement contact forces during locomotion. *J. Biomech. Eng.* **135**, 021013 (2013).

17.   Thelen, D. G., Won Choi, K. & Schmitz, A. M. Co-simulation of neuromuscular dynamics and knee mechanics during human walking. *J. Biomech. Eng.* **136**, 021033 (2014).

18.   Guess, T. M., Stylianou, A. P. & Kia, M. Concurrent prediction of muscle and tibiofemoral contact forces during treadmill gait. *J. Biomech. Eng.* **136**, 021032 (2014).

19.   Skipper Andersen, M., de Zee, M., Damsgaard, M., Nolte, D. & Rasmussen, J. Introduction to Force-Dependent Kinematics: Theory and Application to Mandible Modeling. *J. Biomech. Eng.* **139**, 091001 (2017).

20.   Bei, Y. & Fregly, B. J. Multibody dynamic simulation of knee contact mechanics. *Med. Eng. Phys.* **26**, 777–89 (2004).

21.   Lin, Y.-C., Walter, J. P., Banks, S. A., Pandy, M. G. & Fregly, B. J. Simultaneous prediction of muscle and contact forces in the knee during gait. *J. Biomech.* **43**, 945–52 (2010).

22.   Fregly, B. J., Sawyer, W. G., Harman, M. K. & Banks, S. A. Computational wear prediction of a total knee replacement from in vivo kinematics. *J. Biomech.* **38**, 305–14 (2005).

23.   Fregly, B. J., Banks, S. A., D'Lima, D. D. & Colwell, C. W. Sensitivity of knee replacement contact calculations to kinematic measurement errors. *J. Orthop. Res.* **26**, 1173–9 (2008).

24.   Aprovitola, A. & Gallo, L. Knee bone segmentation from MRI: A classification and literature review. *Biocybern. Biomed. Eng.* **36**, 437–449 (2016).

25.   Blemker, S. S. Three-Dimensional Modeling of Active Muscle Tissue. in *Biomechanics of Living Organs* 361–375 (Elsevier, 2017). doi:10.1016/B978-0-12-804009-6.00017-1

26.   Carbone, V., van der Krogt, M. M., Koopman, H. F. J. M. & Verdonschot, N. Sensitivity of subject-specific models to Hill muscle-tendon model parameters in simulations of gait. *J. Biomech.* **49**, 1953–1960 (2016).

27.   Bloemker, K. H., Guess, T. M., Maletsky, L. & Dodd, K. Computational knee ligament modeling using experimentally determined zero-load lengths. *Open Biomed. Eng. J.* **6**, 33–41 (2012).

28.   Sartori, M. & Farina, D. Neural Data-driven Musculoskeletal Modeling for Personalized Neurorehabilitation Technologies. *IEEE Trans. Biomed. Eng.* **63**, 879–893 (2016).

29.   Lee, L.-F. & Umberger, B. R. Generating optimal control simulations of musculoskeletal movement using OpenSim and MATLAB. *PeerJ* **4**, e1638 (2016).

30.   Lin, Y. C., Walter, J. P. & Pandy, M. G. Predictive Simulations of Neuromuscular Coordination and Joint-Contact Loading in Human Gait. *Ann. Biomed. Eng.* **46**, 1216–1227 (2018).

31.   De Groote, F., Kinney, A. L., Rao, A. V. & Fregly, B. J. Evaluation of Direct Collocation Optimal Control Problem Formulations for Solving the Muscle Redundancy Problem. *Ann. Biomed. Eng.* **44**, 2922–2936 (2016).

32.   Heess, N. *et al.* Emergence of Locomotion Behaviours in Rich Environments. (2017). doi:10.1177/1471301214563551

33.   Hu, X. & Blemker, S. S. Musculoskeletal simulation can help explain selective muscle degeneration in Duchenne muscular dystrophy. *Muscle Nerve* **52**, 174–82 (2015).

SUMMARY

Disorders of the musculoskeletal system are one of the primary causes of disability worldwide. With the ageing of the population, the burden of musculoskeletal disorders on the healthcare system is expected to increase dramatically. To keep healthcare sustainable, the costs of diagnosis and treatment must be reduced and the surgical outcomes optimized.

Knee arthritis is a highly prevalent condition (> 50 million aged 17 years and older in the United States) that causes pain and movement limitation. End-stage arthritis is treated with total knee replacement (TKR). The current diagnostic tools used in TKR are static and subjective, and the treatment is not tailored to each patient based on a personalized surgical planning. These facts may explain why TKR, which is considered successful, suffers still from substantial patient dissatisfaction. A new framework is needed to improve diagnostic and surgical planning in TKR surgery. This must provide *dynamic* information on patients' conditions *in vivo*, it must be *objective* and provide *personalized* surgical planning.

Facioscapulohumeral muscular dystrophy (FSHD) is a rare musculoskeletal condition (12:100,000) for which no cure currently exists. In FSHD, muscles are wasted, become fatty-infiltrated and weak. The underlying causes of muscle weakness remain unclear. Specifically, it is not known whether muscle strength per unit physiological cross-sectional area of muscle tissue (*specific strength*) is affected in patients with FSHD compared to healthy controls.

This thesis aimed at (a) developing and validating a computational framework for personalized musculoskeletal modeling that allows the estimation of internal knee loads and kinematics; and (b) can be used to address clinically relevant research questions related to TKR. Furthermore, aiming at better understanding the factors contributing to muscles weakness in FSHD, (c) this thesis combined quantitative imaging and functional muscle assessment and image-based musculoskeletal modeling to investigate whether specific muscle strength is reduced in FSHD patients compared to healthy controls.

In **Chapter 2**, a methodology was presented for the generation of a personalized musculoskeletal model of the lower extremity of a patient with TKR, and consequent estimation of muscle forces, knee joint loads and kinematics, and ligament forces during activities of daily living (ADLs). The

resulting model combined a personalized musculoskeletal morphology with a detailed representation of the artificial knee joint. The geometrical model of the leg was based on computed tomography images of the patient's leg and provided implant geometries, and the muscle morphology was scaled nonlinearly to the target patient-specific geometry from a detailed lower extremity model template using advanced morphing techniques. One hundred sixty-six musculotendon units were included in the lower extremity model, and represented by three-element Hill-type line elements, which path was defined by using either via-points or wrapping objects. A detailed 11-degree-of-freedom (DoF) knee model was created from patient-specific geometries and implants, which included discrete contact models between the articulating surfaces of the artificial joint (femoral component, tibial insert and patellar button) that were based on the elastic-foundation theory. Furthermore, tibiofemoral and patellofemoral ligaments were included and represented as discrete nonlinear spring elements. The resulting model was driven using motion-capture and force-plate data from a publicly available dataset of a patient with a telemetric knee prosthesis. Using a novel numerical method for the analysis of non-conforming joints, called force-dependent kinematics (FDK), muscle forces, medial and lateral tibiofemoral joint contact forces, ligament forces, and secondary knee kinematics were estimated simultaneously. The total, medial and lateral knee contact forces estimated during both a normal and a right-turn walking trials were in very good agreement with experimental measurements from the same subject (root-mean-square error < 0.4 body weight). Estimated sagittal-plane secondary knee kinematics compared well with kinematics measured in the same subject during a leg-swing trial under fluoroscopic examination (Sprague and Geers combined error C < 0.06).

The complexity introduced by the personalization of both knee and lower extremity models came at the expense of a high computational cost for simulating the musculoskeletal model. This problem was addressed in **Chapter 3**, in which surrogate modeling techniques were employed with the aim of accelerating the computation of FDK analyses of ADLs for the concurrent estimation of muscle, ligament and joint contact forces, and secondary knee kinematics. To that aim, artificial neural network (ANN) models were trained using samples from existing patient-specific knee model simulations. The surrogate model learned the relationships between articular

contact loads and 6-degree-of-freedom (DoF) tibiofemoral kinematics. Force-dependent kinematics analyses of several ADLs performed with the surrogate contact model produced tibiofemoral loads and kinematics that were as accurate as the one obtained using the reference contact model, but the computation time required by the surrogate model simulations were reduced by a factor three.

In **Chapters 4** and **5** a patient-specific musculoskeletal knee model was employed to address two clinical research questions related to the sagittal alignment of the tibial and femoral component in TKR, respectively. For both studies, a slightly modified version of the TKR model presented in **Chapter 2** was utilized. The main finding of **Chapter 4** was that increased posterior tibial slope with an anterior referencing technique in a patient-specific model of a patient with a cruciate-retaining (CR) TKR increased the general laxity of the knee both in flexion and extension, due to ligament slackening. It also resulted in less stable tibiofemoral kinematics during a simulated squatting motion, compared to both a reference case with neutral slope and cases with central referencing technique. In addition, patellofemoral contact forces were reduced more effectively when tibial slope was increased with a central referencing technique than with anterior referencing.

Chapter 5 showed that flexing the femoral component in a patient-specific model of a patient fitted with a CR-TKR did not alter the knee kinematics substantially during a simulated chair-rising motion, and reduced the patellofemoral contact force compared to a reference case with neutral femoral component flexion. These findings support the practice of adjusting the flexion of the femoral component intra-operatively, in order to prevent anterior notching of the femur in downsized implants, while retaining good knee extensors function and patellofemoral joint mechanics.

In **Chapter 6** it was investigated whether the specific muscle strength (maximal isometric muscle force per unit physiological cross-sectional area, PCSA, of muscle tissue) was affected in patients with FSHD compared to healthy controls. Three-dimensional magnetic resonance imaging (MRI) and maximal voluntary isometric contraction (MVIC) were employed to quantify the effective contractile volume and the strength of quadriceps muscles in ten healthy controls and ten FSHD patients. Quadriceps muscles volumes were calculated by taking fatty infiltration into account. Subsequently, a

musculoskeletal model of the lower extremity was used to estimate PCSA and specific muscle strength for each patient and for each healthy subject. The specific muscle strength was significantly lower in FSHD patients relative to controls (21 *vs.* 42 N/cm², p < 0.001). This may indicate alterations of the force-generating capacity in affected muscles at the level of muscle fibers, which cannot be explained by atrophy and/or fatty tissue infiltration alone. Therefore, specific strength alterations must be considered as an additional factor contributing to the observed muscle weakness in FSHD, and future research for possible therapies should also aim at restoration of specific muscle strength.

Although personalized musculoskeletal modeling was effectively employed to answer clinically relevant research questions using a patient-specific model, a number of limitations still need to be addressed, before such methodology can enter the clinical practice at full capacity. The process of generation and personalization of patient-specific models from medical images requires a considerable amount of time and manual intervention, which limits their applicability to larger patient cohorts or population studies. Segmentation of medical images and 3-D reconstruction of the musculoskeletal morphology remain the main time-intensive processes. Further research is required to accelerate the generation of musculoskeletal models. Two possible different solutions are: developing more (semi-)automatic segmentation algorithms, specifically targeting the structures of the musculoskeletal system; and using statistical shape models, as an alternative approach to account for geometrical variability, and/or as an aid to the segmentation process itself.

The personalization of musculotendon parameters was not addressed comprehensively in this thesis, and requires further attention, as these parameters considerably affect the joint mechanics estimated by the model, and the musculotendon forces distribution itself. This is important especially when studying pathologies that may affect the characteristics of muscles, and may therefore have an important effect on the model outcomes. However, estimating musculotendon parameters directly *in vivo* is not feasible, but calibration of these parameters is possible using muscle strength measurements and optimization techniques.

The increased computational expense of simulating personalized models can be addressed by means of surrogate modeling, as shown in **Chapter 3**, which

replaces *costly* processes of the musculoskeletal model (in terms of computation) with inexpensive one. However, the generation of surrogate models is, in itself, very time-demanding and depends on existing simulation data. Further research should also aim at accelerating the generation of surrogate models, possibly by incorporating anatomical variability with statistical shape models, for a more expedited application to different patients, and making it independent from existing simulation data.

Finally, thanks to their predictive capabilities and possibilities of analyzing *what-if* scenarios, personalized musculoskeletal models, showed their great potential as tools to improve the formulation of surgical planning for musculoskeletal disorders. It is foreseeable that, when applied to larger patient groups, this approach will help clinicians formulating more optimized clinical decisions on the basis of each patient's needs. For this to occur, personalized models need to be further developed, become easier to generate and operate, and build their credibility in the clinical setting by continuous validation.

NEDERLANDSE SAMENVATTING

Aandoeningen van het bewegingsapparaat zijn wereldwijd een van de belangrijkste oorzaken van invaliditeit. De verwachting is dat met de vergrijzing van de bevolking de belasting van musculoskeletale aandoeningen op het gezondheidszorgsysteem dramatisch zal toenemen. Om de gezondheidszorg duurzaam te houden, moeten de kosten van diagnose en behandeling worden verlaagd en de chirurgische resultaten worden geoptimaliseerd.

Knieartrose is een veel voorkomende aandoening (> 50 miljoen van 17 jaar en ouder in de Verenigde Staten) die pijn en bewegingsbeperkingen veroorzaakt. End-stage artrose wordt behandeld met totale knievervanging (TKR). De huidige diagnostische hulpmiddelen gebruikt in TKR zijn statisch en subjectief, en de behandeling is niet op maat gemaakt voor elke patiënt op basis van een persoonlijke chirurgische planning. Alhoewel TKR als erg succesvol wordt beschouwd, heerst er hierdoor nog steeds een substantiële ontevredenheid bij patiënten. Een nieuwe aanpak is nodig om de diagnostische en chirurgische planning bij TKR-chirurgie te verbeteren. Deze aanpak moet *dynamische* informatie verschaffen over de condities van de patiënt *in vivo*, moet *objectief zijn* en een *gepersonaliseerde* chirurgische planning bieden.

Facioscapulohumerale spierdystrofie (FSHD) is een zeldzame musculoskeletale aandoening (12:100.000) waarvoor momenteel geen genezing bestaat. Bij FSHD worden neemt de spiermassa af en ontstaat er vet infiltratie, waardoor de spieren zwak worden. De onderliggende oorzaken van spierzwakte blijven onduidelijk. Het is met name niet bekend of de spierkracht per fysiologisch dwarsdoorsnede van het spierweefsel (*specifieke sterkte*) verminderd is bij patiënten met FSHD in vergelijking met gezonde controles.

Dit proefschrift is gericht op (a) het ontwikkelen en valideren van een simulatiemethode voor gepersonaliseerde musculoskeletale modellering dat de berekening van interne kniekrachten en kinematica mogelijk maakt; en (b) kan worden gebruikt om klinisch relevante onderzoeksvragen met betrekking tot TKR aan te pakken. Daarnaast (c) combineerde dit proefschrift kwantitatieve beeldvorming en functionele spierbeoordeling en beeld

gebaseerde musculoskeletale modellering om te onderzoeken of specifieke spierkracht is verminderd bij FSHD-patiënten in vergelijking met gezonde controles, om zodoende een beter beeld te krijgen van de factoren die bijdragen aan de spierzwakte bij FSHD.

In **Hoofdstuk 2** werd een methodologie gepresenteerd voor het genereren van een gepersonaliseerd musculoskeletaal model van de onderste extremiteit van een patiënt met TKR, waarmee een schatting van spierkrachten, kniegewrichtskrachten, kinematica ligament krachten is gemaakt tijdens verschillende activiteiten van het dagelijks leven (ADLs). Het model combineerde een gepersonaliseerde musculoskeletale morfologie met een gedetailleerde weergave van het gereconstrueerde kniegewricht. Het geometrische model van het been was gebaseerd op computertomografiebeelden van het been van de patiënt, met daarin het implantaat gemodelleerd. De spiermorfologie werd niet-lineair geschaald naar de patiënt-specifieke geometrie van een gedetailleerd model van de onderste extremiteiten met behulp van geavanceerde morphingtechnieken. Honderdzesenzestig spier-pees-eenheden werden opgenomen in het onderste extremiteitsmodel, ieder weergegeven door drie Hill-type lijnelementen, met werklijnen gedefinieerd door via-punten of wrapping surfaces. Een gedetailleerd 11-degree-of-freedom (DoF) kniemodel werd gecreëerd op basis van patiënt-specifieke geometrieën en implantaten, waaronder afzonderlijke contactmodellen tussen de articulerende oppervlakken van het kunstmatige gewricht (femorale component, tibiale insert en patella-knop) die waren gebaseerd op de theorie van de elastische fundering. Bovendien werden tibiofemorale en patellofemorale banden opgenomen en gerepresenteerd als discrete niet-lineaire veerelementen. Het resulterende model werd aangedreven met behulp van motion-capture en force-plate data van een openbare dataset van een patiënt met een telemetrische knieprothese. Gebruik makende van een nieuwe numerieke methode voor de analyse van gewrichten, force-dependent kinematics (FDK), zijn de spierkrachten, mediale en laterale tibiofemorale contactkrachten, ligament krachten en de secundaire kniekinematica berekend. De totale, mediale en laterale knie contactkrachten zijn berekend tijdens een normale loopbeweging en een rechtsdraaiende loopproef. Deze waren in zeer goede overeenstemming met de experimentele metingen (RMS-error <0,4 lichaamsgewicht). De berekende kinematica in het sagittale vlak hadden een goede overeenkomst met de

kinematica van een flexiebeweging gemeten in een fluoroscopisch onderzoek (Sprague en Geers gecombineerde fout C <0,06).

De complexiteit geïntroduceerd door de personalisatie van zowel knie- als onderste extremiteitsmodellen ging ten koste van hoge rekenkundige kosten voor het simuleren van het musculoskeletale model. Dit probleem kwam aan de orde in **Hoofdstuk 3**, waarin technieken voor surrogaatmodellering werden gebruikt, met als doel het versnellen van de berekening van FDK-analyses van ADLs voor de gelijktijdige schatting van spier-, ligament- en gewrichtscontactkrachten en secundaire knie-kinematica. Hiertoe werden artificial neural networkmodellen (ANN-modellen) getraind met behulp van data van bestaande patiënt-specifieke knie-modelsimulaties. Het surrogaatmodel werd getraind om de relaties tussen gewrichtscontactbelastingen en tibiofemorale kinematica van 6 graden van vrijheid (DoF) te leren. Krachtafhankelijke kinematische analyses van verschillende ADL's uitgevoerd met het surrogaat-contactmodel produceerden tibiofemorale belastingen en kinematica die even nauwkeurig waren als die verkregen met behulp van het referentiecontactmodel, maar de rekentijd die vereist was voor de surrogaat-modelsimulaties was met een factor drie verminderd.

In de **Hoofdstukken 4** en **5** werd een patiënt-specifiek musculoskeletaal kniemodel gebruikt om het effect van de sagittale uitlijning van de tibiale en femorale component in TKR te onderzoeken. Voor beide studies werd een gemodificeerde versie van het TKR-model gebruikt die in **Hoofdstuk 2** is gepresenteerd. De belangrijkste bevinding van **Hoofdstuk 4** was dat meer posterior tibial slope met een anterior referencing-techniek in een patiënt-specifiek model van een patiënt met een cruciate retaining (CR) TKR de laxiteit van de knie zowel in flexie als extensie verhoogde, als gevolg van een verhoogde laxiteit in de ligamenten. Daarnaast resulteerde meer posterior slope ook in een vermindering van de stabiliteit in de tibiofemorale kinematica tijdens een diepe kniebuiging. Bovendien namen de patellofemorale contactkrachten af met een toenemende tibial slope, zowel met central referencing en anterior referencing.

Hoofdstuk 5 liet zien dat het meer in flexie plaatsen van de femorale component de knie-kinematica niet substantieel veranderde gedurende een simulatie van opstaan uit een stoel, maar dat de patellofemorale contactkracht

werd verlaagd vergeleken met een neutrale oriëntatie van de femorale component. Deze bevindingen ondersteunen de praktijk van het intra-operatief aanpassen van de flexie van de femorale component, om anterior notching in kleinere maten implantaten te voorkomen, terwijl een goede kniestrekkingsfunctie en patellofemorale gewrichtsmechanica behouden blijven.

In **Hoofdstuk 6** werd onderzocht of de specifieke spierkracht (maximale isometrische spierkracht per eenheid fysiologisch dwarsdoorsnede, PCSA) was aangetast bij patiënten met FSHD in vergelijking met gezonde controles. Driedimensionale magnetische resonantie imaging (MRI) en maximale vrijwillige isometrische contractie (MVIC) werden gebruikt om het effectieve contractielvolume en de sterkte van de quadriceps-spieren te kwantificeren in tien gezonde controles en tien FSHD-patiënten. De volumes van de quadriceps-spieren werden berekend door rekening te houden met de vetinfiltratie. Vervolgens werd een musculoskeletaal model van de onderste extremiteit gebruikt om de PCSA en specifieke spierkracht voor elke patiënt en voor elk gezond individu te schatten. De specifieke spierkracht was significant lager bij FSHD-patiënten ten opzichte van de controles (21 *versus* 42 N/cm², p <0,001). Dit kan wijzen op veranderingen in het vermogen om kracht te genereren in de getroffen spieren op het niveau van spiervezels, wat niet kan worden verklaard door alleen atrofie en/of vetinfiltratie. Daarom moeten specifieke veranderingen in sterkte worden beschouwd als een bijkomende factor die bijdraagt tot de waargenomen spierzwakte bij FSHD. Toekomstig onderzoek naar mogelijke therapieën moet ook gericht zijn op herstel van specifieke spierkracht.

Hoewel gepersonaliseerde musculoskeletale modellering effectief werd gebruikt om klinisch relevante onderzoeksvragen te beantwoorden met behulp van een patiënt-specifiek model, moet nog een aantal beperkingen worden aangepakt voordat dergelijke methodologie klinisch geïmplementeerd kan worden. Het genereren en personaliseren van patiënt-specifieke modellen uit medische beelden vereist een aanzienlijke hoeveelheid tijd en handwerk, waardoor de toepasbaarheid ervan op grotere patiëntcohorten of populatieonderzoeken wordt beperkt. Segmentatie van medische beelden en 3D-reconstructie van de musculoskeletale morfologie blijven de belangrijkste tijdsintensieve processen. Verder onderzoek is nodig om het genereren van musculoskeletale modellen te versnellen. Twee mogelijke oplossingen zijn de

ontwikkeling van meer (semi-)automatische segmentatie-algoritmen, specifiek gericht op de structuren van het bewegingsapparaat en het gebruik van statistical shape modellen, als een alternatieve benadering om geometrische variabiliteit te analyseren of als een hulpmiddel voor het segmentatieproces zelf.

De personalisatie van spier-pees-parameters werd niet uitgebreid behandeld in dit proefschrift en vereist verdere aandacht, omdat deze parameters de door het model geschatte gewrichtsmechanica en verdeling van de krachten aanzienlijk beïnvloeden. Dit is vooral belangrijk bij het bestuderen van pathologieën die de eigenschappen van spieren kunnen beïnvloeden en kan daarom een belangrijk effect hebben op de uitkomsten van het model. Het direct *in vivo* schatten van spier-pees-parameters is niet haalbaar, maar kalibratie van deze parameters is mogelijk met behulp van spierkrachtmetingen en optimalisatietechnieken.

De toegenomen rekenkundige kosten van het simuleren van gepersonaliseerde modellen kunnen worden verminderd met surrogate modelling, zoals aangetoond in **Hoofdstuk 3**. Het genereren van surrogate models is op zich echter zeer tijdrovend en afhankelijk van bestaande simulatiegegevens. Verder onderzoek moet daarom ook gericht zijn op het versnellen van het genereren van surrogaatmodellen, mogelijk door het opnemen van anatomische variabiliteit in statistical shape models, voor een snellere toepassing bij verschillende patiënten en om deze onafhankelijk te maken van bestaande simulatiegegevens.

Tot slot hebben gepersonaliseerde musculoskeletale modellen hun grote potentieel aangetoond als hulpmiddelen om de formulering van chirurgische planning voor musculoskeletale aandoeningen te verbeteren, dankzij hun voorspellende mogelijkheden en mogelijkheden om *what-if-* scenario's te analyseren. Het is te voorzien dat, indien toegepast op grotere patiëntengroepen, deze aanpak clinici helpt om meer geoptimaliseerde klinische beslissingen te formuleren op basis van de behoeften van de individuele patiënt. Om dit mogelijk te maken, moeten gepersonaliseerde modellen verder worden ontwikkeld, eenvoudiger te genereren en te bedienen zijn en moet hun geloofwaardigheid in de klinische omgeving vergroot worden door continue validatie.

ACKNOWLEDGMENTS

I would like to express my sincere gratitude to everyone who, through these last 5 and a half years, helped me completing my PhD. Without your help, this thesis could have not been finished. First of all, I thank my PhD supervisors, Nico Verdonschot, Bart Koopman, and co-supervisor, Dennis Janssen.

Nico, I have been so inspired by you, through all these years, and from you I learned so much about science, the passion for research, and your very human touch. I cannot remember a single meeting with the two of us that, at the end, has not left me more positive and energized than before I entered your door. Truly, your optimism and challenging spirit have positively influenced my work and my life. I had just finished my PhD project at the ORL, under your supervision, that you soon became my new mentor at the UT. You are the person I can certainly turn to when I need a boost! Thank you for believing in me; without you, I would have not had the chance to do all of this.

Bart, during my PhD, I thought coming to Enschede for our 1-hour supervision meetings was not so efficient, and I did that only once a month. At that time, I did not know this was to become my new daily routine! In retrospect, I wish we had more meetings. Your deep biomechanical insight was always very useful, and you often came up with original ideas on how to solve a though problem. Thank you very much for your support.

Dennis, working with you could have not been more enjoyable. Through our many weekly meetings—in which sometimes I could not make any sense of my results—you had always a smart way to untie a difficult knot. Thank you very much for supporting me since my very first day at the ORL till the *Nederlandse samenvatting* of my thesis ☺

I wish to thank the members of the manuscript committee of my thesis, Prof. dr. Geurts, Prof. dr. Veeger, and Dr. Jutte, for being available and for investing their time to read and evaluate the manuscript.

A word of thanks also to Wouter Akkerman (Livit Orthopedie) and Dr. Beat Gasser (RMS Foundation) for kindly sponsoring this thesis.

To the Biomechanics Research Group at Aalborg University, particularly, Michael Skipper Andersen, John Rasmussen, Morten Lund, and to Michael Damsgaard from AnyBody Technology, a big big thank you! I spent two

wonderful months with you at the very beginning of my PhD, and that has been the best thing to do at the rightest moment, because I learned the ABC's of musculoskeletal modeling very quickly. Thank you for your support!

Michael (Skipper), you have been a constant reference point for me when it came to difficult questions related to AnyBody and musculoskeletal modeling. Oftentimes, you were the only person who could help me out with that, and you did it. Thank you so much for your hospitality in Aalborg, and for being available every time I needed your help.

A warm thanks to Ate Wymenga and Petra Heesterbeek from the Sint Maartenskliniek. Working with you has been so stimulating, and I learned a lot from your in-depth explanations about complicated matters of total knee arthroplasty. Thank you for being so welcoming to me.

I wish to express my appreciation to Marc Vogels, Michelle Zawadzki and Chuck Perrone from Zimmer Biomet (Warsaw, IN) for their kind assistance in providing technical files useful for this thesis.

Special thanks to all collaborators from the Radiology department and Neurology department of the Radboudumc for their precious contributions. Many thanks also to Sebastiaan van de Groes from the Orthopedics department for his input throughout the project.

I wish to thank all my former fellow PhD students and colleagues from the BioMechTools project, all master students and research assistants I supervised during my PhD, and all my former colleagues, technicians, and secretaries at the ORL. I enjoyed very much working with you! Even though I changed my job, I visit the lab every now and then, and it still feels like home. Hamid and Kaj, thank you so much for being my paranymphs!

To my parents, family and friends who have always been present and supported me, even though from a long distance for more than ten years now, a big big thanks! Who I am today, I owe a lot to you.

Dear Anna, my beloved, thank you for being always there with me. With both the two of us pursuing a PhD, our Dutch adventure could not have been more challenging... or maybe it could, that is why we had our little wonder, Amalia, who fills our everyday lives with colors! Thank you for being supportive, whenever I needed your help.

LIST OF PUBLICATIONS

Peer-reviewed journal articles

Leijendekkers, R.A., **Marra, M.A.**, Ploegmakers, M.J.M., Van Hinte, G., Frölke, J.P., Van De Meent, H., Staal, J.B., Hoogeboom, T.J., and Verdonschot, N. (2018) "Magnetic-resonance-imaging-based three-dimensional muscle reconstruction of hip abductor muscle volume in a person with a transfemoral bone-anchored prosthesis: A feasibility study.," *Physiotherapy Theory and Practice*, doi: 10.1080/09593985.2018.1453902.

Marra, M.A., Strzelczak, M., Heesterbeek, P.J.C., van de Groes, S.A.W., Janssen, D.W., Koopman, B.F.J.M., Verdonschot, N.J.J., and Wymenga, A.B. (2018) "Flexing and downsizing the femoral component is not detrimental to patellofemoral biomechanics in posterior-referencing cruciate-retaining total knee arthroplasty.," *Knee Surgery, Sports Traumatology, Arthroscopy*, **26**(11), p. 3377–3385.

Niu, K., Anijs, T., Sluiter, V., Homminga, J., Sprengers, A., **Marra, M.A.**, and Verdonschot, N. (2018) "In situ comparison of A-mode ultrasound tracking system and skin-mounted markers for measuring kinematics of the lower extremity.," *Journal of biomechanics*, **72**, p. 134-143.

Leijendekkers, R.A., **Marra, M.A.**, Kolk, S., van Bon, G., Schreurs, B.W., Weerdesteyn, V., and Verdonschot, N. (2018) "Gait symmetry and hip strength in women with developmental dysplasia following hip arthroplasty compared to healthy subjects: A cross-sectional study.," *PloS one*, **13**(2), p. e0193487.

Marra, M.A.[*], Heskamp, L.[*], Mul, K., Lassche, S., van Engelen, B.G.M., Heerschap, A., and Verdonschot, N. (2017) "Specific muscle strength is reduced in facioscapulohumeral dystrophy: An MRI based musculoskeletal analysis.," *Neuromuscular Disorders*, **28**(3), p. 238-245.

Marra, M.A., Strzelczak, M., Heesterbeek, P.J.C., van de Groes, S.A.W., Janssen, D.W., Koopman, B.F.J.M., Wymenga, A.B., and Verdonschot, N.J.J. (2018) "Anterior referencing of tibial slope in total knee arthroplasty considerably influences knee kinematics: a musculoskeletal simulation study.," *Knee Surgery, Sports Traumatology, Arthroscopy,* **26**(5), p. 1540-1548.

Marra, M.A., Andersen, M.S., Damsgaard, M., Koopman, B.F.J.M., Janssen, D., and Verdonschot, N. (2017) "Evaluation of a Surrogate Contact Model in Force-Dependent Kinematic Simulations of Total Knee Replacement.," *Journal of Biomechanical Engineering*, **139**(8), p. 81001.

Oudeman, J., Mazzoli, V., **Marra, M.A.**, Nicolay, K., Maas, M., Verdonschot, N., Sprengers, A.M., Nederveen, A.J., Strijkers, G.J., and Froeling, M. (2016) "A novel diffusion-tensor MRI approach for skeletal muscle fascicle length measurements.," *Physiological Reports*, **4**(24), p. e13012.

Marra, M.A., Vanheule, V., Fluit, R., Koopman, B.H.F.J.M., Rasmussen, J., Verdonschot, N., and Andersen, M.S. (2015) "A subject-specific musculoskeletal modeling framework to predict in vivo mechanics of total knee arthroplasty.," *Journal of Biomechanical Engineering*, **137**(2), p. 20904.

Conference abstracts

Marra, M., Bisognano, A., van de Groes, S., Janssen, D., Koopman, B., Verdonschot, N. (2018) "Effect of trochlear dysplasia on patellar tracking and patellofemoral contact pressure. A musculoskeletal analysis using an efficient cartilage contact model.," *8th World Congress of Biomechanics*, Dublin, Ireland, 8-12 July 2018.

Heskamp, L., **Marra, M.A.**, Mul, K., van Engelen, B., Verdonschot, N., and Heerschap, A. (2017) "P.345 - Specific strength is reduced in facioscapulohumeral dystrophy muscles. An MRI-based musculoskeletal analysis," *Neuromuscular Disorders*, **27**(Supplement 2), p. S200 (presented at *22nd International Congress of the World Muscle Society*, St Malo, France, 3-7 October 2017).

Marra, M.A., Strzelczak, M., van de Groes, S., Heesterbeek, P.J.C., Janssen, D., Koopman, B.F.J.M., Verdonschot, N., and Wymenga, A.B. (2017) "The effect of flexion of the femoral component in TKA: A musculoskeletal simulation study.," *European Knee Society Arthroplasty Conference*, London, UK, 20-21 April 2017.

Marra, M.A., Strzelczak, M., Heesterbeek, P.J.C., van de Groes, S., Janssen, D., Koopman, B.F.J.M., Wymenga, A.B. and Verdonschot, N. (2017) "The effect of posterior tibial slope on simulated laxity tests in cruciate-retaining total knee arthroplasty.," *European Knee Society Arthroplasty Conference*, London, UK, 20-21 April 2017.

Marra, M.A., Strzelczak, M., Heesterbeek, P.J.C., van de Groes, S., Janssen, D., Koopman, B.F.J.M., Wymenga, A.B. and Verdonschot, N. (2017) "The effect of tibial slope in cruciate-retaining total knee arthroplasty: A musculoskeletal simulation study.," *European Knee Society Arthroplasty Conference*, London, UK, 20-21 April 2017.

Marra, M., Strzelczak, M, Heesterbeek, P., Van de Groes, S., Janssen, D., Koopman, B., Wymenga, A., and Verdonschot, N. (2017) "The effect of tibial slope on the biomechanics of cruciate-retaining TKA: a musculoskeletal simulation study.," *63rd Annual Meeting Orthopaedic Research Society*, **42**, Paper no. 1981, San Diego, USA, 19-22 March 2017.

Marra, M., Strzelczak, M, Heesterbeek, P., Van de Groes, S., Janssen, D., Koopman, B., Wymenga, A., and Verdonschot, N. (2017) "The effect of posterior tibial slope on simulated laxity tests in cruciate-retaining TKA.," *63rd Annual Meeting Orthopaedic Research Society*, **42**, Paper no. 1013, San Diego, USA, 19-22 March 2017.

Marra, M., Heesterbeek, P., van de Groes, S., Janssen, D., Koopman, B., Wymenga, A., and Verdonschot, N. (2017) "Effect of referencing technique for the tibial slope in cruciate-retaining total knee arthroplasty.," *The Bone & Joint Journal*, **99-B**(SUPP 4), 139 (presented at *International Society for Technology in Arthroplasty Congress*, Boston, USA, 5-8 October 2016).

Verdonschot, N., **Marra, M.A.**, Heesterbeek, P., van de Groes, S., Janssen, D., Koopman, B., and Wymenga, A. (2016) "Effect of Referencing Technique for the Tibial Slope in Cruciate-Retaining Total Knee Arthroplasty.," *Combined Members Meeting of the European Knee Society and the American Knee Society*, Paris, France, 8-9 September 2016

Marra, M. A., Vanheule, V., Fluit, R., Koopman, B. H. F. J. M., Rasmussen, J., Verdonschot, N., and Andersen, M. S. (2016) "A subject-specific musculoskeletal modeling framework to predict in

vivo mechanics of total knee arthroplasty.," *22nd Congress of the European Society of Biomechanics*, Lyon, France, 10-13 July 2016 (**top-5 nominee for the Mimics Innovation Awards 2016**).

Marra, M.A., Strzelczak, M, Van de Groes, S., Heesterbeek, P.J.C., Wymenga, A., Koopman, B., Janssen, D., and Verdonschot, N. (2016) "Biomechanical effects of femoral component flexion in TKA; a musculoskeletal modeling analysis.," *62nd Annual Meeting Orthopaedic Research Society*, **41**, Paper no. 1882, Orlando, USA, 5-8 March 2016.

Marra, M.A., Andersen, M.S., Koopman, B., Janssen, D., and Verdonschot, N. (2016) "Evaluation of a surrogate contact model of TKA.," *62nd Annual Meeting Orthopaedic Research Society*, **41**, Paper no. 278, Orlando, USA, 5-8 March 2016.

Marra, M.A., Strzelczak, M., van de Groes, S., Heesterbeek, P., Wymenga, A., Koopman, H.F.J.M., Janssen, D., and Verdonschot, N. (2015) "Evaluation of laxity tests with a musculoskeletal model of total knee arthroplasty.," *21st Congress of the European Society of Biomechanics*, Prague, Czech Republic, 5-8 July 2015.

Marra, M., Vanheule, V., Fluit, R., Koopman, B., Rasmussen, J., Verdonschot, N., and Andersen, M. (2015) "A patient-specific musculoskeletal model of total knee arthroplasty to predict in vivo knee biomechanics." *5th Dutch Bio-Medical Engineering Conference*, Egmond aan Zee, The Netherlands, 22-23 January 2015.

Andersen, M. S., **Marra, M.A.**, Vanheule, V., Fluit, R., Verdonschot, N., and Rasmussen, J. (2014) "Patient-specific musculoskeletal modelling of total knee arthroplasty using force-dependent kinematics.," *7th World Congress of Biomechanics,* Boston, USA, 6-11 July 2014 (**Winner of the 5th Grand Challenge Competition to Predict In Vivo Knee Loads**).

---

[*] Authors contributed equally to this work

PHD PORTFOLIO

Institute for Health Sciences
Radboud umc

Name PhD student:	M.A. Marra
Department:	Orthopaedic Research Lab
Graduate School:	Radboud Institute for Health Sciences

PhD period:	1 October 2013 – 1 October 2017
Promotor(s):	Prof. dr. ir. N. Verdonschot
	Prof. dr. ir. H.F.J.M. Koopman
Co-promotor(s):	Dr. ir. D. Janssen

TRAINING ACTIVITIES

		Year(s)	ECTS
a)	**Courses & Workshops**		
	RIHS Introduction Course for PhD students	2014	1.4
	2-day course Scientific Integrity for RIHS and RIMLS PhD students	2015	0.7
	2-month training at the AnyBody Research Group, Aalborg, Denmark	2013	15
	Introduction: Careers in industry - what's possible and how do I get hired	2017	0.1
b)	**Symposia & congresses**		
	WCB, World Congress of Biomechanics, Boston, MA, USA	2014	1.5
	CMBBE, International Symposium Computer Methods in Biomechanics and Biomedical Engineering, Amsterdam, The Netherlands	2014	0.75
	RIHS PhD Retreat, Wageningen, The Netherlands (oral)	2014	0.75
	BME, Dutch Bio-Medical Engineering Conference, Egmond aan Zee, The Netherlands (oral)	2015	0.75
	ISMRM Benelux Chapter meeting, Ghent, Belgium	2015	0.25
	ESB, Congress of the European Society of Biomechanics, Prague, Czech Republic (poster)	2015	1.5
	ORS, Annual Meeting of the Orthopedic Research Society, Orlando, FL, USA (2 posters)	2016	2
	ESB, Congress of the European Society of Biomechanics, Lyon, France (oral)	2016	1
	RIHS PhD Retreat, Wageningen, The Netherlands	2016	0.5
c)	**Other**		
	Journal club - Orthopaedic Research Lab	2013-2016	4
	Lab Presentations - Orthopaedic Research Lab	2014-2017	4
	Research Meetings - Orthopaedic Department	2014-2015	2
	'Spiegeluur' - Orthopaedic Department	2016-2017	2
TEACHING ACTIVITIES			
d)	**Lecturing**		
	MSc course 5HM02 (Radboudumc) – Tissue: Biomechanics and engineering	2014-2016	4.8
	BSc course MIN05 (Radboudumc) – Moving Questions: an introduction to Clinical Human Movement Sciences	2015-2016	0.85
	MSc course (Politecnico di Milano, Milan, Italy) Computer modeling in Orthopaedic Biomechanics	2017	0.15
	MSc course BMS53 (Radboudumc) – Orthopaedic Biomechanics in Motion	2017	1.6
e)	**Supervision of internships / other**		
	Research assistant (Marta Strzelczak)	2014-2016	4.33
	MSc students from University of Twente, Enschede (Thomas Anijs, Floris Bloembergen, Niala den Braber, Dieuwke van Dartel, Job Stoks)	2015-2016	10
	MSc student, Politecnico di Milano (Antonino Bisognano)	2016-2017	3
	TOTAL		**63**

Radboud University   Radboud umc
university medical center

CURRICULUM VITAE

Marco Antonio Marra was born in Galatina, in the province of Lecce, Puglia (Italy) on 13 June 1989. He obtained his gymnasium diploma in 2003 from the Science and Technology school in Lecce. In 2008, he moved to Turin, in northern Italy, where he studied Biomedical Engineering at the Polytechnic University of Turin. In 2011, he obtained his bachelor degree with an original thesis on a telemedicine service in prisons. During his master's program, he spent one year at the Royal Institute of Technology (Stockholm, Sweden), where he specialized in human movement and neural trauma biomechanics, modeling of biological systems, and bioinformatics. There, he also carried out his master's thesis project on the study of osteoporotic fractures of the upper spine using computational biomechanics. Upon graduation, in 2013, he moved to the Orthopaedic Research Lab (Radboudumc, Nijmegen, the Netherlands) to pursue a doctoral degree in orthopedics biomechanics, joining the EU-funded project *BioMechTools* led by Prof. dr. ir. Nico Verdonschot.

Within the BioMechTools project, he developed advanced computational knee joint models to aid in the preoperative planning of total knee arthroplasty surgery. In 2014, together with Prof. Michael Skipper Andersen (Aalborg University, Denmark), he was part of the winning team of the 5th *Grand Challenge Competition to Predict In Vivo Knee Loads*, held at the 7th World Congress of Biomechanics (Boston, USA). During his PhD project, he established fruitful collaborations with clinical institutions and different research groups, he attended national and international scientific symposia, and he (co-)authored nine articles in international peer-reviewed scientific journals. In 2018, his research led to the completion of the present doctoral dissertation.

Marco has taught biomechanics courses at both bachelor's and master's degree programs. He supervised more than twelve students from (inter-)national universities. In November 2017, he joined as an Assistant Professor the Biomechanical Engineering group led by Prof. dr. ir. Bart Koopman in the Faculty of Engineering Technology of the University of Twente (Enschede, the Netherlands). His current research focuses on personalized musculoskeletal modeling, predictive simulation and clinical implementation thereof.

Marco is a passionate musicophile and computer geek. In the *good* season, he is also a recreational inline skater. He currently lives in Beuningen (Gld), together with his better half, Anna Greco, and their beloved daughter, Amalia.

Institute for Health Sciences

Radboud umc